Experimental and Numerical Investigation into the Sand/Geotextile Shear Interaction Behaviour

by

C.C.Wise
B.Sc. Eng (Civil)
University of Cape Town

A thesis submitted to the University of Cape Town in partial fulfilment of the requirements for a degree of Master of Science in Civil Engineering.

Department of Civil Engineering
University of Cape Town
September 1997

Dedication

I dedicate this thesis to my
νυμφιοζ

He is truly the Alpha and Omega, being with me from the beginning to the end and beyond. He is the one true absolute and my source.

Declaration

I, Chris Wise hereby declare that the thesis work presented here is essentially my own work, except were otherwise indicated, and has not been submitted for a degree at any other university.

Signed by candidate

September 1997 Signature Removed

Acknowledgements

It would be most appropriate to first thank my supervisor, Dr Scheele. His invaluable advise and guidance, commitment to the research, professionalism, engineering excellence and encouragement cannot be overestimated. I sincerely appreciate all his time and assistance. He was ready to listen to my ideas, but still always kept me on track. It has been of tremendous benefit for me to work under him.

Many thanks go to Eike von Guerard, Charles Nicholas and the rest of the workshop staff, who helped develop and manufactured the pull-out test equipment. Without their precision and ingenuity, this thesis would definitely not have been possible. I can only say "German engineering where you need it most".

Special thanks go to Tony Howe of Kaymat who so generously provided the geotextile used in the investigation and who helped with the literature search.

I would also like to thank the laboratory staff, namely Noor Hassen and Chris Temmers who were always there to lend a helping hand with the equipment.

To the Ninham Shand geotechnical laboratory goes much appreciation for the use of their stress path machine. I would like to express special appreciation to Rowede for her patience, technical advise and training on the stress path machine. How she managed to put up with me, I really don't know.

Thanks also goes to the staff and students at CERECAM for their frequent input into the finite element analysis.

I also would like to express my appreciation to the FRD for their financial support over the two years of this degree.

Then to my family who put up me on the bad days and helped in so many ways. I know that they will reap what they have sown and many rewards are waiting for their patience and encouragement.

To my friends who always believed in me and gave me encouragement at precisely the right time, thank you so much.

Synopsis

Geotextiles are planar polymeric textile materials which are utilised in geotechnical engineering in various applications, including the reinforcement of soils which is achieved by laying geotextile sheets horizontally to carry the induced horizontal stresses. The behaviour of such reinforced soil structures (e.g. retaining walls) is determined primarily by the shear interaction between the soil and individual geotextile sheets. This dissertation presents an investigation into the shear interaction behaviour between a locally manufactured non-woven geotextile and Cape Flats sand.

The literature review exposed a certain lack in understanding of the displacement and shear stress mechanisms involved in the pull-out of geotextiles from sand. Also, the prediction of either rupture or slippage failure was unclear. The shear stress at slippage failure has not previously been determined for confinements greater than 100kPa. The applicability of using direct shear tests (specified by the BS8006) to determine the friction parameters for design, is uncertain. Numerical techniques have been shown to be an adequate tool to analyse the pull-out mechanism of a geotextile in soil.

In-isolation tensile tests were initially performed on the non-woven geotextile and the material was found to have a linear stress-strain relationship. The primary experimental work was then undertaken involving pull-out test of the non-woven geotextile (150mm long by 200mm wide) confined in Cape Flats sand at pressures from 25 kPa to 250 kPa, applied uniformly over the sand. The geotextile remained in contact with the soil throughout the loading. It was shown that three characteristic zones in the displacement of the geotextile during pull-out exist and are defined by the displacement of the free end. In the first zone the free end does not displace and the front end displacement is due entirely to stretch of the fabric within the front 25mm of the sample. The second zone, identified from the initial movement of the free end until failure, is characterised by the geotextile both stretching and slipping. With the aid of the finite element analysis it is shown that the slip in this zone is elastic slip, i.e. it is due to deformation of the geotextile and sand surfaces in contact. At failure, the interface shear stresses across the geotextile has attained the critical shear stress value and the entire geotextile sample slips relative to the sand, which characterises the third zone.

In the pull-out tests, rupture failure of the samples occurred at confining pressures above 140 kPa and slippage failure at confinements below this defining value. It was shown that the tensile strength of the geotextile is 23% greater than the in-isolation tensile strength and is not influenced by confinement. The relationship between the maximum average interface shear stress and confinement was shown to be bi-linear. It was noted that the maximum average interface shear stress is attained only once the front end had undergone a certain displacement and this should be considered in the design.

A finite element model was developed to verify the friction parameters obtained from the pull-out experiments and evaluate the shear stress and displacement mechanisms involved in pull-out. The results showed that the mobilisation of the interface shear stress initiates from the front of the sample and the critical shear stress is progressively developed along the sheet until slippage failure occurs. The finite element model adequately simulates the load transfer between the sand and geotextile but fails to predict the geotextile

displacements, due to a limitation in the friction model and an apparently high Young's Modulus defining the geotextile. An improvement of the friction model was suggested incorporating a delay in the initial displacement of the free end, but the implementation of this modification was beyond the scope of this research project.

From direct shear tests it was found that the development of the shear stress with displacement occurs over a significantly shorter displacement compared with pull-out tests. These tests were also found to over predict the interface shear stresses at failure by approximately 25% to 40% and it was thus concluded that the direct shear test is not an adequate test method to determine the friction parameters for design.

This project provides a reliable understanding into the displacement and shear stress mechanisms associated with a sand/geotextile interface and can form the basis of future research into a variety of sand/geotextile reinforcement applications.

Table of Contents

List of Figures

List of Tables

Chapter 1
Introduction

How can a cloth strengthen soil? This might have been the response of a few cynics when the principle of geotextile reinforced earth was first introduced in the late 1960's. The idea of using a fibrous material to strengthen soil can be dated as far back as 4000 BC, when the Hebrew nation was in slavery in Egypt. In Exodus 5: 6-9 there is a record of the use of straw fibres to reinforce clay building blocks. It was, however, only in 1966 that a Frenchman by the name of Henri Vidal (Vidal, 1966) developed the modern theory behind the technique to strengthen soils using reinforcing elements. He developed the theory for what is known today as "Reinforced Earth", using steel strips placed in soil which act as the reinforcing.

Separate to this development, a fabric was developed for use in geotechnical engineering, originally designed to act as a filter to allow water drainage in soil. This fabric was later termed geotextile by Dr. J.P. Giroud in a paper presented at the "International Conference on the Use of Fabrics in Geotechnics", held in 1977 (IGS, 1994). Ever since, geotextiles have had many applications in civil engineering, including filtration, separation and drainage. It was however, soon discovered that this material could be used in the same way as Henri Vidal's steel strips as a soil reinforcement (i.e. geotextile reinforced soil).

Geotextile reinforced soil has many applications in civil engineering including retaining walls and earth slopes. It is in fact becoming a more popular alternative to the traditional retaining wall. This type of retaining wall has three components, the facing (cladding), the backfill material and the reinforcing elements. Many types of materials can be used for the reinforcing elements, but this investigation is focused on the use of geotextiles. The geotextile sheets are placed horizontally in the backfill material behind the wall and are either wrapped around the face to form a cladding, or are fixed to a concrete facing. The reinforcement has the effect of reducing the lateral earth pressure exerted on the facing, thus, increasing the stability of the soil structure (Jones, 1985).

The behaviour of a geotextile reinforced earth wall is a function of the behaviour of the individual reinforcement sheets. It was for this reason that it was felt that a geotextile reinforced earth wall could be better understood once the behaviour of a single sheet was investigated. The behaviour of a geotextile sheet acting as a soil reinforcement is determined primarily by the frictional behaviour between the soil and geotextile since this influences the internal stability of the reinforced structure (Murray, 1981). The primary aim of the thesis was thus to investigate the displacement behaviour and shear stress transfer associated with a geotextile sheet confined in sand. The research was limited to the investigation of a locally manufactured non-woven geotextile interacting with Cape Flats sand.

Initially a literature review was undertaken in order to determine to what extent this type of problem has been investigated. Once it was discovered that there was scope for a more in-depth study, the following procedure was followed. Tensile tests on the non-woven geotextile were first undertaken to determine the material properties. Small scale pull-out

experiments on geotextile sheets confined in a Cape Flats sand were then performed in order to determine the soil-geotextile frictional and confined geotextile stiffness parameters. In parallel, a numerical investigation was started. Finite element models of pull-out tests were developed using ABAQUS, a multi-purpose finite element package. The frictional and stiffness parameters determined from the experiments were applied to the finite element simulations in order to calibrate the results and verify the friction and material models which characterised the soil-geotextile interface. The frictional parameters obtained from the pull-out tests were also compared with those obtained from direct shear box tests, a more common test used to evaluate soil-geotextile friction parameters (BS 8006, 1995).

This dissertation initially explains the applications and technical background to geotextile reinforced soil. A review of available literature is then followed by a summary of the objectives of the research. Tensile tests performed on the geotextile to determine the material parameters are described. The small scale pull-out tests and results are then presented. This is followed by a description of the direct shear tests and the finite element analysis of the pull-out tests. Finally, the results are summarised and conclusions are drawn.

Chapter 2
Geotextiles in Geotechnical Applications

Geosynthetics is a term which describes a wide range of products, including geomembranes, geogrids, geotextiles and geomatresses, which are man made from chemical materials. These materials are primarily manufactured for the use in civil and geotechnical engineering. Although relatively new, having only been around for about 25 years, these materials are finding increased applications in all construction industries since they can be used in many functions and generally provide an economic and technically reliable solution to problems. Geotextiles are a specific class of the geosynthetic group of materials. A geotextile is defined by the International Geosynthetics Society as: "A planar, permeable, polymeric (synthetic or natural) textile material which may be non-woven, knitted or woven, used in contact with soil/rock and/or any other geotechnical material in civil engineering applications." (IGS Secretariat, 1996)

In this chapter a brief overview of geotextiles and their applications is given. Initially, the manufacturing process is explained. The basic functions and applications of geotextiles are then described and the basic principles of design using geotextiles are presented. The chapter is concluded with a brief review of the advantages of the use of geotextiles in geotechnical structures.

2.1 Manufacturing process

Although a very large range of geotextile products are available on the market, there are generally two broad categories, namely woven and non-woven geotextiles. These two classes of geotextiles differ only in the manner in which they are manufactured.

Woven geotextiles are woven on a loom, in the same manner as normal clothing textiles, forming a woven sheet. The individual strands are usually made of polyester or polypropylene. These strands can either be drawn threads or extruded flat tapes. The thickness of the threads vary from 0.5 mm to 3mm, while the flat tapes can be as wide as 20mm.

In the case of non-woven geotextiles, on the other hand, the polyester or polypropylene beads are heated, extruded and drawn into very thin threads. These threads are then sprayed randomly, at high speed, via a vibrating disc onto a conveyor belt, as is schematically shown in Figure 2-1. The high speed random spraying causes the threads to interlock with one another, forming a continuous textile sheet. A vacuum is applied beneath the conveyor belt to aid the interlocking process. The sheet is then rolled. Finally, to increase the bond between the strands, the sheet is either heat bonded or needle punched. This increases the overall strength of the geotextile sheet. Either the sheet is heated causing the strands to melt slightly and bond together. This processes produces what is known as heat bonded non-woven geotextiles. Alternatively, the sheet is punched with barbed needles, which draws the lower strands upward to entangle with the upper strands. This is shown schematically in Figure 2-2. The result is a needled punched non-woven geotextile.

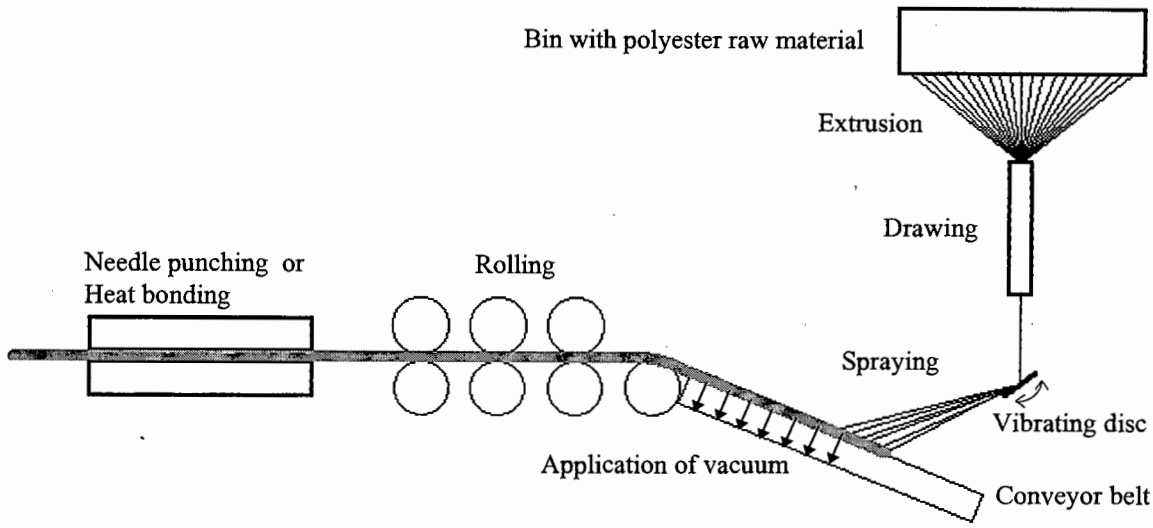

Figure 2-1: ***Schematic of the manufacturing process of non-woven geotextiles***

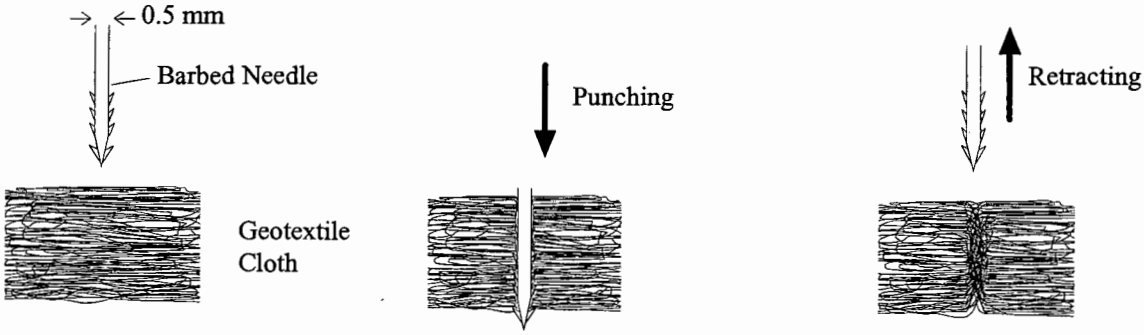

Figure 2-2: ***Needle punching process of non-woven geotextiles***

2.2 Basic functions and applications

The numerous applications of geotextiles in geotechnical engineering can be grouped into six basic modes of operation (IGS Secretariat, 1996):

1) Filtration : To allow the passage of fluids
2) Separation : To prevent intermixing of dissimilar geotechnical materials
3) Protection : To reduce localised stresses or prevent damage to a surface
4) Drainage : To collect and transport fluids
5) Erosion control : To prevent surface erosion due to water run-off
6) Reinforcement : To resist stresses or contain deformations in geotechnical structures

It is the reinforcement function that is of interest in this research study.

To briefly indicate the basic principle of soil reinforcement, a schematic is shown in Figure 2-3. If a vertical stress, σ_1, is applied to a confined soil cube, horizontal stresses, σ_3, associated with horizontal strains, ε_3, are induced. However, if horizontal reinforcing elements (e.g. geotextiles) are placed in the soil at various levels, a portion of the induced horizontal stresses will be taken up by the stiffer reinforcing element, thus reducing the horizontal strains. This soil-reinforcement interaction is obviously only possible if there is sufficient frictional contact between the soil and reinforcements to allow the stress transfer to take place (Jones, 1985).

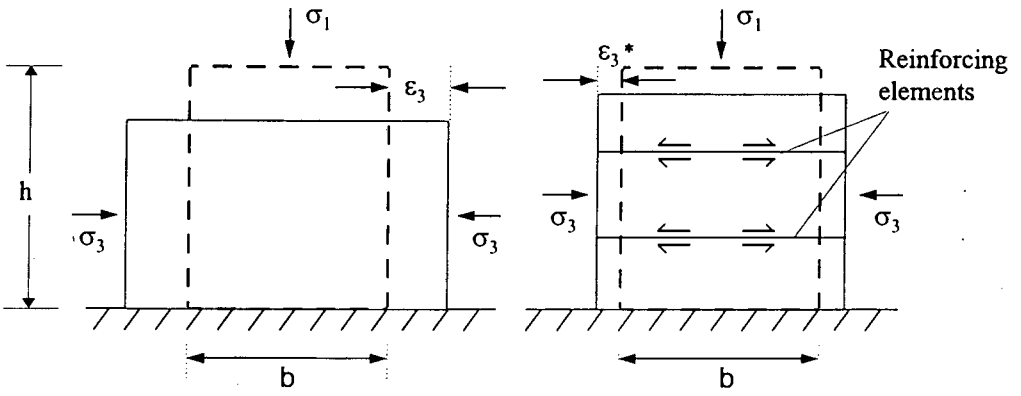

Figure 2-3: ***Principle of reinforced soil***

Typical applications of geotextiles used for their reinforcement function are shown in Figure 2-4. These applications include geotextile reinforced soil walls, slopes and reinforced soil below shallow foundations. Geotextile reinforced soil walls have three components:

1) Facing (concrete panels, blocks, timber and geosynthetic)
2) Backfill (usually granular, free draining material, clay in certain situations)
3) Reinforcement (geotextile sheeting, steel strips and geogrids)

Generally, there are two classes of geotextile reinforced soil walls, differing only in the construction of the cladding. The first type is shown in Figure 2-4(a), where the geotextile reinforcing sheets are connected to a light, but fairly stiff retaining wall, usually made of concrete. The second class involves the sheets being wrapped around the face to form the cladding. This type of geotextile reinforced earth wall is known as a "wrapped" wall and is shown in Figure 2-4(b). With both types, the reinforcing sheets serve to reduce the horizontal earth pressures on the face and thus increase the stability and stiffness of the structure as a whole.

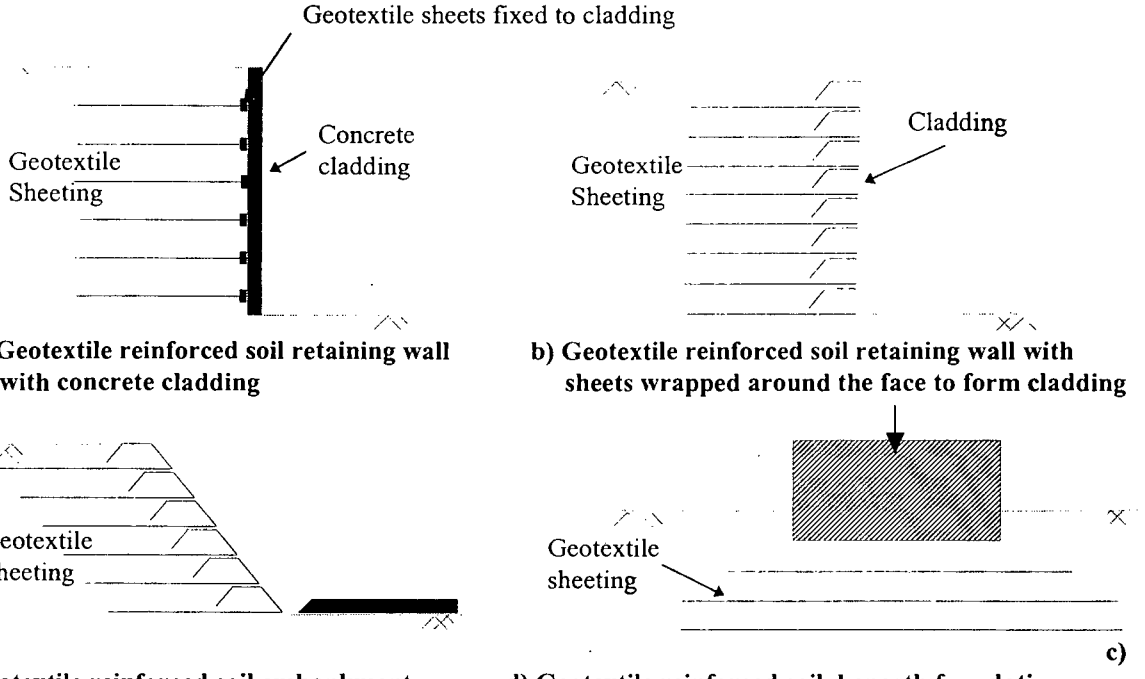

a) Geotextile reinforced soil retaining wall with concrete cladding

b) Geotextile reinforced soil retaining wall with sheets wrapped around the face to form cladding

Geotextile reinforced soil embankment

d) Geotextile reinforced soil beneath foundation

Figure 2-4: ***Geotextile reinforced soil applications***

Another typical application is the geotextile reinforced soil embankment which is shown in Figure 2-4(c). The geotextile reinforcement reduce the horizontal strain in the slope and increases the stability against slip failure. The sheets also provide surface protection against erosion. This system has the added advantage over other slope stabilisation systems in that the soil can be hydroseeded, which will allow vegetation to grow through the geotextile sheets at the surface, forming an attractive grass bank.

The fourth application of geotextile reinforced soil, shown in Figure 2-4(d), is under shallow foundations and the like. Geotextile sheets are placed horizontally, in the ground prior to the installation of the foundation, to form an improved base on which the foundation rests. This increases the bearing capacity of soil and reduces settlements.

2.3 Basic design principles of geotextile reinforced soil structures

In the design of geotextile reinforced soil structures, both the internal and external stability need to be considered (Jones, 1985). The external stability is concerned with the failure of the entire reinforced structure (wall or embankment) acting as a monolithic block. Global horizontal sliding, bearing capacity failure at the base, global tilting and global slippage along a slip plane, should be checked in the design (BS 8006, 1994).

Internal stability failure, on the other hand, addresses the failure of a single geotextile sheet within the structure. Because of the tensile loading on the geotextile sheets, failure can take place when either the geotextile tears, known as rupture failure or when the geotextile pulls out of the soil, known as slippage failure. Another aspect of internal stability is the serviceability design, where the displacement of the face of the wall or embankment (which is dependant on the displacement of the geotextile sheets) is to be within acceptable limits.

A wide range of design theories as well as design codes (BS 8006, 1994) and recommendations (Thaum, 1997) are available to undertake internal design of geotextile reinforced structures. However, in terms of internal stability considerations, certain basic assumptions are common amongst all these methods. For slippage failure, the basic assumption is always that the geotextile's resistance to slippage (termed pull-out resistance) is a function of:

- the overburden pressure of the sheet
- the area of contact between the sheet and the soil
- the friction coefficient between the sheet and the soil

It appears that a constant friction coefficient, independent of the overburden pressure, is a standard presupposition throughout the design methods in practice.

In terms of rupture failure, it is always assumed that the load which causes tearing of the fabric is a function of the tensile strength of the geotextile. When serviceability is considered, the stiffness and area of contact between soil and geotextile are assumed to influence the displacement of the front end of the sheet.

This research project is focused on investigating the interaction mechanisms associated with the internal stability and will concentrate on a single geotextile sheet in pull-out.

Chapter 3
Review of Previous Research

Research into the field of geotextile earth reinforcement has been performed in a large and varied scope of research directions. These range from investigations of full scale geotextile reinforced structures (Rowe and Gnanendran, 1994) to the behaviour of a single geotextile sheet undergoing transverse shear (Atmatzidis and Athanasopoulos, 1994).

Prior to understanding the interface behaviour between sand and a geotextile, research into the tensile behaviour of the geotextile material, either unconfined or confined in soil, was first required and is thus initially be presented. In the study of the actual sand-geotextile interface, two primary streams of research exist, namely the pull-out behaviour and the direct shear behaviour of geotextiles in sand. Generally, the research has been performed with two very different laboratory apparatus, which produce very different loading and displacement mechanisms. Experimental research into both of these tests are discussed. Numerical modelling of the interface between sand and geotextiles has previously been undertaken and this research is also reviewed.

3.1 Unconfined tensile behaviour of geotextiles

The in-isolation tensile behaviour of a geotextile is defined as the material response when loaded with a tensile force, without any form of confinement being applied normal to the direction of tensile loading. Experimental programs have been undertaken in various laboratories, to determine the in-isolation tensile behaviour of various geotextile products. Other than a description of the deformation characteristics of non-woven geotextiles, the research projects reviewed here were focused mainly on establishing accepted test parameters to obtain consistent results in terms of tensile stress and strain at failure. The influence of aspect ratio and strain rate on these results have been investigated. The aspect ratio is the ratio of the width to the length of the test sample. The strain rate is the rate at which the tensile strain is applied to the sample, to produce a tensile load in a strain controlled manner. The studies reviewed here are those undertaken on only non-woven geotextiles tested in-isolation and disregard quality the control type of research.

3.1.1 Characteristic deformation of non-woven geotextiles under in-isolation conditions

Based on in-isolation tensile tests, Boudonnel et al. (1982) explained that non-woven geotextiles, under in-isolation tensile conditions, are characterised by very high axial and lateral strains. This is because of the loose structure which allows the individual threads to re-orientate relatively freely into the direction of the tensile load. At the clamps, lateral strain is prevented from occurring, thus, the lateral strain increases away from the clamps to a maximum strain at the centre. This gives rise to the typical deformed shaped shown in Figure 3-1 (Boudonnel et al., 1982). This characteristic deformed shape of non-woven geotextiles is termed necking.

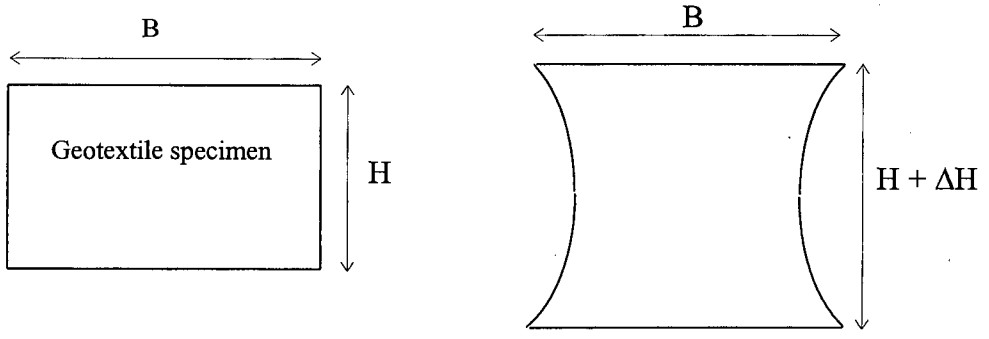

Figure 3-1 : ***Typical deformation of a non-woven geotextile during in-isolation tensile testing (after Baudonnel et al., 1982)***

The axial strains at failure (i.e. ΔH/H) are typically in the order of 50% to 80% depending on the specific product. It was also shown by Baudonnel et al. (1982) that lateral strains are greatly influenced by the aspect ratio (B/H). As the aspect ratio increases, the magnitude of necking decreases.

3.1.2 Influence of aspect ratio on the in-isolation tensile strength and strain

The in-isolation tensile strength of non-woven geotextiles is defined as the maximum tensile load that can be carried by a 1 meter wide geotextile sample (IGS secretariat, 1995). The in-isolation tensile strength of non-woven samples was found to vary significantly with the aspect ratio (Baudonnel et al., 1982; Wang et al., 1990). It was determined from both these research projects, that the tensile strength decreases as the sample width decreases below 200mm or as the length increases above 100mm, yielding unrealistic strengths in tension. This was attributed to necking effects which are significant for aspect ratios of less than 2.

Shrestha and Bell (1982) also established that the tensile strains at failure vary significantly for aspect ratios less than two.

It was therefore suggested by Wang et al. (1990) and Shrestha and Bell (1982) that a minimum aspect ratio of 2 be utilised to obtain realistic in-isolation tensile strength and strain results for non-woven geotextiles. Based on this research, the ASTM consequently specify a width of 200 mm and a length of 100 mm for the in-isolation tensile testing of non-woven geotextiles (ASTM D4595-86).

3.1.3 Influence of strain rate on the in-isolation tensile strength and strain

Baudonnel et al. (1982), Shrestha and Bell (1982) and Lai Sang et al. (1995) indicated that a change in strain rate from 1% per minute to 100% per minute has no significant influence on the ultimate tensile strength. Furthermore, Lai Sang et al. (1995) showed that the load versus strain behaviour is also not influenced by the strain rate. A strain rate of 10% has been suggested by most researchers and as a result, has been specified by ASTM (ASTM D4595-86).

In summary, the necking behaviour of non-woven geotextiles has been introduced and can be said to be a distinct characteristic of non-woven fabric. The aspect ratio of in-isolation test samples has been found to influence the tensile test results due to this necking effect. Therefore to obtain reproducible results, in terms of tensile stress and strain at failure, it has been suggested to employ an aspect ratio of 2. Generally, a strain rate of 10% per minute is accepted.

3.2 In-soil confined tensile behaviour under fixed end conditions

Although it is important to interpret the in-isolation tensile behaviour of geotextiles, geotextiles in geotechnical applications are embedded in soils under confinement when tensile loading is applied. Thus, an understanding of the response of geotextiles to tensile loading when confined in soil is required. This section briefly discusses the research, to this date, of confined tensile behaviour of geotextiles.

McGown et al. (1982) manufactured a test apparatus specifically for the investigation of load extension behaviour of geotextiles confined in soil. A schematic of this apparatus is shown in Figure 3-2. Samples are sandwiched between two 10 mm thick soil layers. Air pressurised bellows applied a required normal pressure to the soil layers. The upper end of the sample was fixed, while the lower end was displaced, thereby applying the tensile load to the specimen. The geotextile specimens were cut according to the ASTM suggested sample size (for in-isolation conditions) of 200 mm in width and 100 mm in length (ASTM 4595-86).

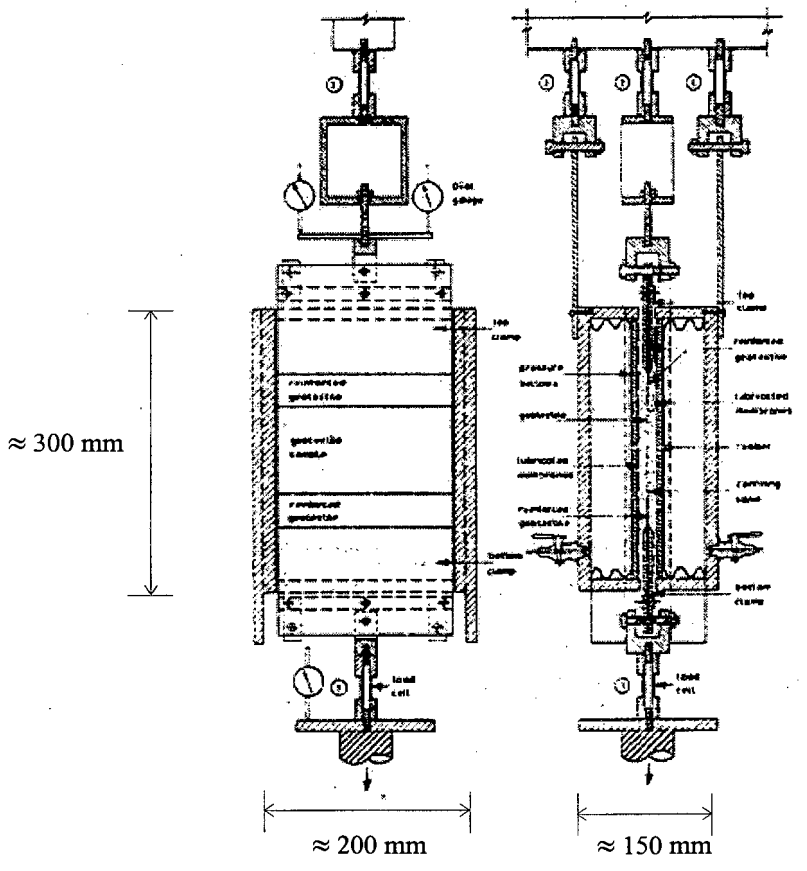

Figure 3-2: ***Confined geotextile tensile testing apparatus used by McGown et al. (1982)***

The relationships between load and axial strain were found to be significantly different for in-soil confined tensile tests of geotextiles compared to unconfined in-isolation tensile tests of the same products. The ratio between load and axial strain is defined as the load-strain modulus. In Figure 3-3, a typical example is shown demonstrating the influence of confinement on the load-strain modulus of a geotextile. A difference in the initial load-strain modulus of up to 270% was recorded. The tensile strength of geotextiles, when confined in soil, was also found to increase.

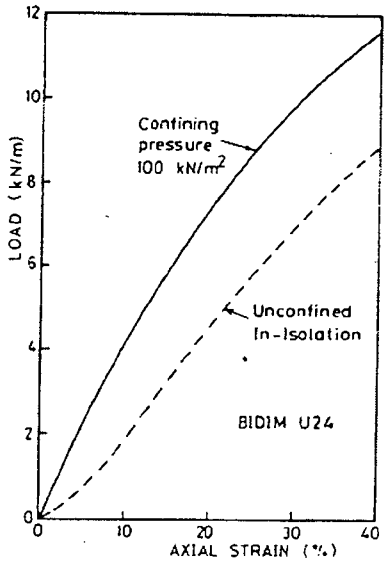

Figure 3-3: ***Load-axial strain behaviour of a confined and unconfined in-isolation geotextile sample (after McGown et al., 1982)***

Leshchinsky and Field (1987) modified a standard direct shear box apparatus to perform confined tensile tests on a geotextile. A schematic of the test apparatus is shown in Figure 3-4. The one end of the geotextile was fixed to a clamp and load cell while the other end was attached to the lower half of the shear box which was free to displace. The soil was confined in the upper half of the shear box, which was fixed. As the lower half of the box was displaced, the geotextile elongated while being confined on the one side by the sand in the upper frame.

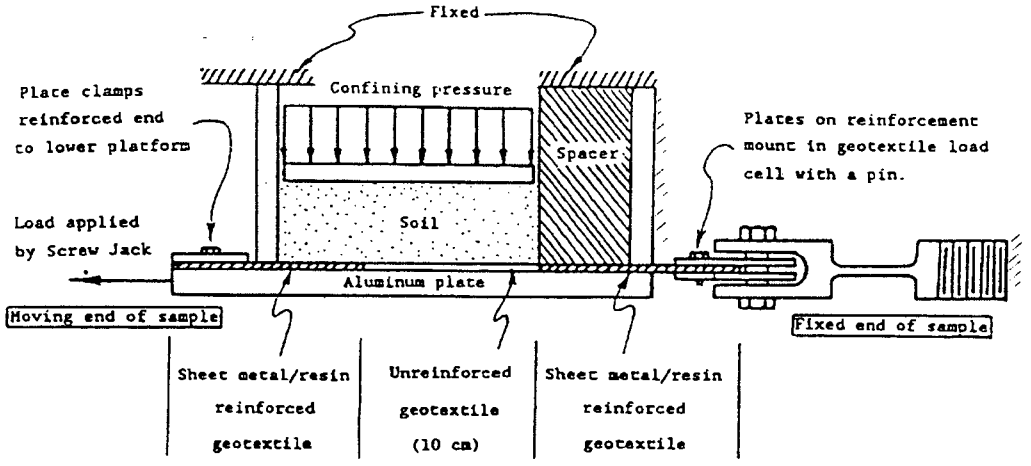

Figure 3-4: ***Modified shear box apparatus used by Leshchinsky and Field (1987)***

The load-strain modulus was found to increase as the normal pressure increased. It is interesting to note that the tensile strength, T_f,was found to increase linearly with normal pressure, as is shown in Figure 3-5.

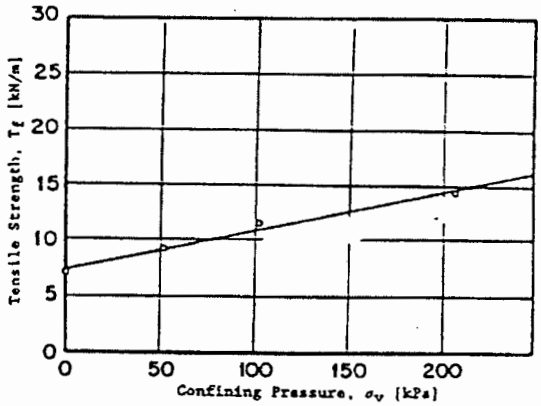

Figure 3-5: ***Tensile strength versus normal pressure for a geotextile (Leshchinsky and Field, 1987)***

Research undertaken by Kokkalis and Papacharisis (1989) in a similar apparatus to the one developed by Leshchinsky and Field (1987) and by Wu and Lin (1994) with equipment similar to McGown et al. (1982) also investigated the confined tensile behaviour of non-woven geotextiles. Both studies confirmed the significant increase in load-strain modulus with an increase in confinement.

In addition to this, Wu and Lin (1994) also presented the distribution of the geotextile deformation along the test specimen, during confined tensile loading. This is shown in Figure 3-6. The ratio of the local displacement to the total displacement of the sample, R_d, is a normalised measure of the local displacement at various confinements.

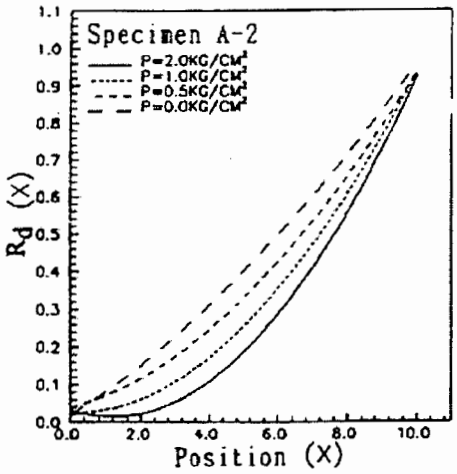

Figure 3-6: ***Deformation distribution along a geotextile sample during a confined tensile test (Wu and Lin, 1994)***

This non-uniform distribution indicates that the tensile force applied to the geotextile is not evenly distributed along the length of the sample. From Figure 3-6 it would appear that the tensile load distribution is not linear when there is no lateral confinement. This is

probably due to a certain amount of friction which occurred along the geotextile sample during the so called "zero confinement" test. Unlike the work by Leshchinsky and Field (1987), these results indicated that the confined tensile strength increases non-linearly with increased confining pressure.

In summary, research has shown that the tensile strength and load-strain modulus of geotextiles both increase significantly with confinement for a particular soil, although there is no relationship which captures the magnitude of this change. It is also not known whether it is dependent on the type of geotextile product and/or the type of soil. In a confined tensile test, the tensile load appears to be distributed in a non-linear fashion along the geotextile specimen.

3.3 Pull-out tests of geotextiles

Pull-out tests, which will be discussed in this chapter, have predominantly been the test chosen by researchers to investigate soil-reinforcement interface behaviour. It has been used successfully to determine friction parameters of steel and geogrid reinforcements and many attempts have been made to do the same with geotextiles. However, this has proven to be more difficult because of the extensibility of geotextiles. The interpretation of geotextile pull-out tests (Kharchafi and Dysli, 1993) was found to be complex and therefore the determination of a friction coefficient for the soil/geotextile interface was an intricate procedure.

The research work reviewed here is limited to pull-out tests performed in sand material. Granular materials are traditionally the preferred fill material in reinforced earth applications.

Since any result is a function of the test arrangement, the various arrangements employed by the researchers will first be discussed. This is followed by a description of the manner of failure of geotextiles during the tests and an introduction of the calculation of the friction angle. Findings related to the development of shear stress and the influence of normal pressure on the maximum shear stress are then presented. Finally other aspects including the displacement distribution along the pull-out sample and the effect of geotextile stiffness is discussed.

3.3.1 Test arrangements

Many variations of the geotextile/soil pull-out test are published, but the basic set-up is as follows. A geotextile sheet is sandwiched between two soil layers. A pressure is then applied at the outer boundaries of the soil layers. This is usually done by means of an air bag and generally, the confinement is applied to the soil on only one side of the geotextile. The interface is thus normally loaded via the confined soil. A tensile force is then applied to the geotextile sheet which interacts with the soil. The load is increased until failure of the geotextile is achieved. In the past, researchers have chosen one of three test arrangements, the differences being in the boundary conditions at the clamped end of the geotextile. These three set-ups are shown schematically in Figure 3-7.

The first type of test arrangement is also the most basic one. The geotextile protrudes from the pull-out box and is attached directly to the loading device (Figure 3-7a) as used by Palmeira and Milligan (1990).

Tzong and Cheng-Kuang (1987), however, contended that it was necessary for the whole geotextile specimen to be confined throughout the test to ensure that the necking (see Section 3.2.1) and the failure took place within the soil confinement. Therefore, in the second test set-up the geotextile is attached to a thin, rigid plate which, in turn, is attached to the load application (Figure 3-7b). The plate is embedded some distance into the soil, thereby ensuring that the entire geotextile length remains confined throughout the test. The third variation involved constructing a sleeve which extends into the soil mass (Figure 3-7c) . The purpose of the sleeve is to reduce boundary effects at the end of the box through which the geotextile sheet is being pulled.

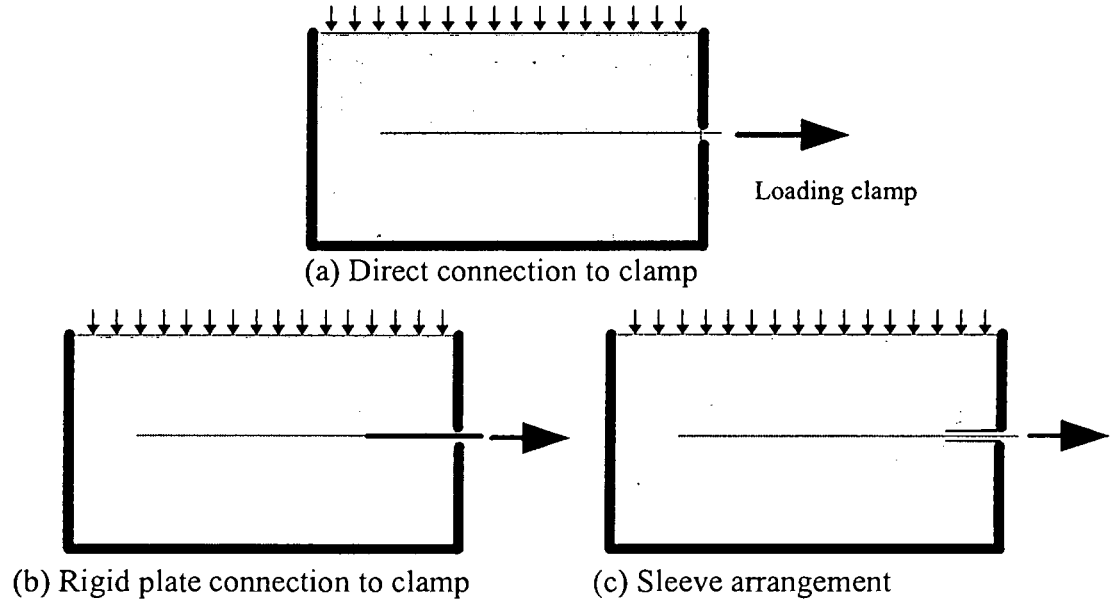

(a) Direct connection to clamp

(b) Rigid plate connection to clamp (c) Sleeve arrangement

Figure 3-7: A *schematic of typical pull-out test arrangements*

A common addition to these test set-ups are thin wires which are attached at various points along the geotextile sheet. These wires extend out of the pull-out box and are connected to displacement measuring devices. This facilitates the measurement of displacements at various locations on the sheet as the load increases. This arrangement of displacement measuring devices are termed extensometers. In Table 3-1 a summary of the pull-out tests found in literature is presented, showing the use of the three test arrangements.

Author	Test * set-up	Size of pull-out box (Length,Width, Height) (mm)	Size of geotextiles (Length,Width) (mm)	Soil type	Confining pressures (kPa)	Studied influences of ...
Forsman & Slunga , 1994	Plate (b)	1800, 1000, 800	300-1350, 300	Sand, crushed rock, clay	15-70	Normal pressure, length, soil type
Tzong & Cheng-Kuang, 1987	Plate (b)	1219,610, 1448	305, 460	Sand	30	(only 1 test performed)
Bourdeau et al., 1990	Plate (b)	2900, 1100, 3000	1500, 850	Sand	40	Geotextile type
Khachafi & Dysli, 1992	Plate (b)	800, 200, 550	500-800, 200	Sand , silt	24 & 34	Geot. stiffness, soil type, normal pressure
Palmeira & Milligan, 1990	Direct (a)	1000, 1000, 1000	500, 1000	Sand	25 - 100	Geotextile type, normal pressure
Abramento & Whittle, 1995	Direct (a)	450,152,520	420, 133	Sand	24.5	Pull-out strain rate
El-Mogahzy et al., 1994	Sleeve (c)	915, 610, 457	915, 102	Sand	5 - 16	Geotextile type, normal Pressure
Bonczkiewicz et. al. , 1988	Sleeve (c)	1350, 690, 460	1350, 610	Sand, gravel, silt, clay	14-103	Geotextile type, normal pressure, soil type

* Description of the test set-up refers to the various arrangements described in Figure 3-7

Table 3-1: *Summary of reviewed pull-out tests*

The pull-out tests have previously provided results to investigate a variety of parameters. These include the failure modes of geotextiles in tension, the friction coefficient, the change in interface shear stress with displacement and confining pressure, the displacement distribution along the geotextile and the influence of geotextile stiffness. These aspects are discussed below.

3.3.2 Failure modes

Using a pull-out box of the type shown in Figure 3-7c , Bonczkiewicz et al. (1988) observed two different failure modes for woven and non-woven geotextiles. These were rupture and slippage failure. The occurrences of rupture failures increased as the applied normal pressure increased. However, the author stated that the rupture failures took place at a point on the geotextile located outside the box (i.e. at the unconfined tensile rupture load). This is, however, not representative of the situation in the field, where rupture failure takes place in confinement. At lower confining stresses (less than 17 kPa), slippage failure was predominant. This failure mode was identified when, after the attainment of the maximum pull-out load, no tearing of the fabric sample was observed. This indicated that the drop in the pull-out force was due to a reduction in the friction between the geotextile and the soil (i.e. slippage). The two failure modes were also identified by Forsman and Slunga (1994).

El Mogahzy et. al. (1994) performed pull-out tests at low confining pressures (smaller than 16 kPa), with a test arrangement similar to the one shown in Figure 3-7a. The mechanism of slippage failure was described as follows: The shear resistance along the geotextile sample builds up as the geotextile sample is pulled out of the box, until the pull-out force is large enough to overcome the shear resistance. This point is termed the maximum shear force. Beyond this point the sample slides continuously through the soil while a residual shear resistance is developed. During this residual sliding, the geotextile sample experiences a negligible axial strain. In Figure 3-8, the two failure modes in terms of pull-out force versus pull-out displacement behaviour are shown (El Mogahzy et al., 1994). The distinct difference in the post failure behaviour, the gradual decrease in the pull-out force in the case of slippage failure compared with the abrupt change for rupture failure, is evident. For this material (a woven fabric) the rupture failure occurred at a confinement of 16.4 kPa and slippage at a confinement of 5.1 kPa. The point of failure occurred at a lower pull-out displacement for slippage failure (about 60mm) as opposed to rupture failure (at about 120mm).

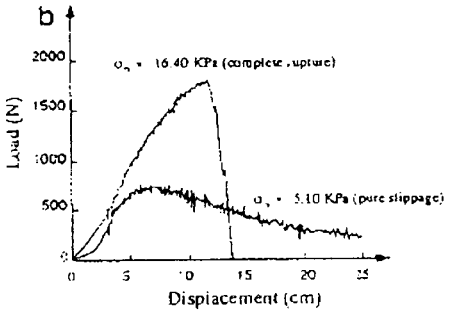

Figure 3-8: ***Pull-out load versus displacement relationship for slippage and rupture failure (El Mogahzy et al., 1994)***

From these studies it is not clear whether it is possible to predict at what normal pressures slippage or rupture failure would occur, or whether there is a clear transition pressure when this might occur. There is also the question of whether it is possible to obtain a combination of both, tearing and pull-out failure. Also, the effects of the geotextile stiffness, soil type and density on the failure mode is not addressed.

3.3.3 Calculation of the friction angle

The traditional equation, used by Kharchafi and Dysli (1993) and Palmeira and Milligan (1990), to determine the soil/geotextile friction angle is given as:

$$\tan\phi_g = \frac{\tau}{\sigma_n} = \frac{P}{A_r \cdot \sigma_n} \qquad \text{.....(3. 1)}$$

where

τ = interface shear stress between soil and geotextile
ϕ_g = soil/geotextile friction angle
P = maximum pull-out load (pull-out resistance)
A_r = area over which the shear stress is distributed (shear area)
σ_n = applied normal pressure

However, because geotextiles generally exhibit large strains when loaded, the shear area is constantly changing as the pull-out test progresses. This traditional equation does therefore not take into consideration the change in area associated with the large strains.

Leshchinsky and Field (1987) used a modified method for calculation the maximum shear stress, as follows:

$$\tan\phi_g = \frac{P}{2\,w(L_o + u)\sigma_n} \qquad \text{.....(3. 2)}$$

where

ϕ_g = soil/geotextile friction angle
P = maximum pull-out load (pull-out resistance)
w = width of the geotextile sheet
L_o = initial length of geotextile embedded in the soil
u = extension of the geotextile sheet in loading direction
σ_n = applied normal pressure

In this equation, changes in the shear area are taken into account and provisions must therefore be made to measure the extension of the geotextiles. However, slippage of the geotextile samples is not accounted for in the calculation. This method was also used by Forsman and Slunga (1994) and Bonczkiewicz et al. (1988).

Another method was proposed by Solomone et al. (1980) which incorporates the shear stress mobilisation. They assumed that up to the point of failure, the shear stress is distributed over only a certain portion of the sample near the front end. This length of geotextile was termed the mobilised length. Thus, for a specific pull-out force, only a certain length of geotextile is mobilised and the shear area should be calculated from this

length. The pull-out force versus mobilised length relationship, which is assumed to be linear, is defined by the constant, K_r, as follows:

$$K_r = \frac{P}{L^*} \qquad \text{.....(3. 3)}$$

where

K_r = interaction parameter
P = pull-out force
L^* = mobilised length

Thus, the friction angle is expressed as:

$$\tan \phi_g = \frac{K_r}{2 \cdot w \cdot \sigma_n} \qquad \text{.....(3. 4)}$$

with w and σ_n as defined in (Equation 3.2).

Bonczkiewicz et al. (1988) compared these three different methods using the results from the pull-out test data. The comparison of the various friction angle (ϕ_g) calculation methods is listed in Table 3-2 below. Results are also compared with a commonly used design assumption which states that the soil/geotextile friction angle is two thirds of the internal angle of friction, ϕ_s , of the respective soil (Steward, 1977). The tests were performed in a poorly graded sand with an angle of internal friction of 35 degrees.

Reinforcement	Elongation at P_{max}	2/3 ϕ_s	Traditional Area Method (Eq. 3.1)	Corrected Area Method (Eq. 3.2)	K_r Method (Eq. 3.4)
Coarse woven	20 %	22	28	29	23-27
Smooth woven	26 %	22	31	34	21-29
Needle punched non-woven	94 %	22	14	27	28
Heat-bonded non-woven	60 %	22	37	37	25-31
Extruded grid	12 %	22	33	33	11-23
Steel strip	0 %	22	63	N/A	N/A

Table 3-2: ***Calculation of a sand/geotextile friction angle using various equations (after Bonczkiewicz et al., 1988)***

This shows that a wide range of values for the friction angle can be obtained, depending on the equation used. Thus, the method chosen to calculate the friction angle is very important. Clearly, more extensible materials exhibit greater variance between methods. The needle punched, non-woven geotextile was the most extensible (94% at failure) geotextile and displayed a very large difference (100%) between the traditional (Eq. 3.1) and corrected area (Eq. 3.2)methods. The K_r -method is highly dependant on a correct assumption for the K_r value. Therefore, if a better method is to be found, this would have to arise out of a better understanding of the actual shear stress mobilisation as well as the shear stress distribution at failure. None of these methods, however, make provision for slippage of the geotextile.

3.3.4 Development of shear stress

It is of interest to determine how the average shear stress across the entire geotextile develops as failure is approached. Palmeira and Milligan (1990) produced plots comparing various geosynthetic materials and steel in terms of the bond coefficient versus displacement. The bond coefficient (f_b) is the relationship between the sand/geotextile friction angle and the sand/sand friction angle and is defined as follows:

$$f_b = \frac{\tan\phi_g}{\tan\phi_s} = \frac{P}{A\sigma_n \tan\phi_s} = \frac{\tau_{ave}}{\sigma_n \cdot \tan\phi_s} = \frac{\tau_{ave}}{C} \qquad \text{.....(3. 5)}$$

where

ϕ_g = sand/geotextile friction angle
ϕ_s = sand/sand friction angle
P = pull-out load
A = area of contact between sand and geotextile
σ_n = confining pressure
τ_{ave} = average shear stress along the sand/geotextile interface
C = constant when the confining pressure remains the same throughout the test

As can be seen in this equation, the bond coefficient is proportional to the average shear stress across the whole geotextile sheet, for a test performed at a constant confining pressure. In Figure 3-9, the bond coefficient (f_b) versus displacement results for a low normal pressure of 25 kPa are shown. The corresponding average shear stress is shown on the second scale.

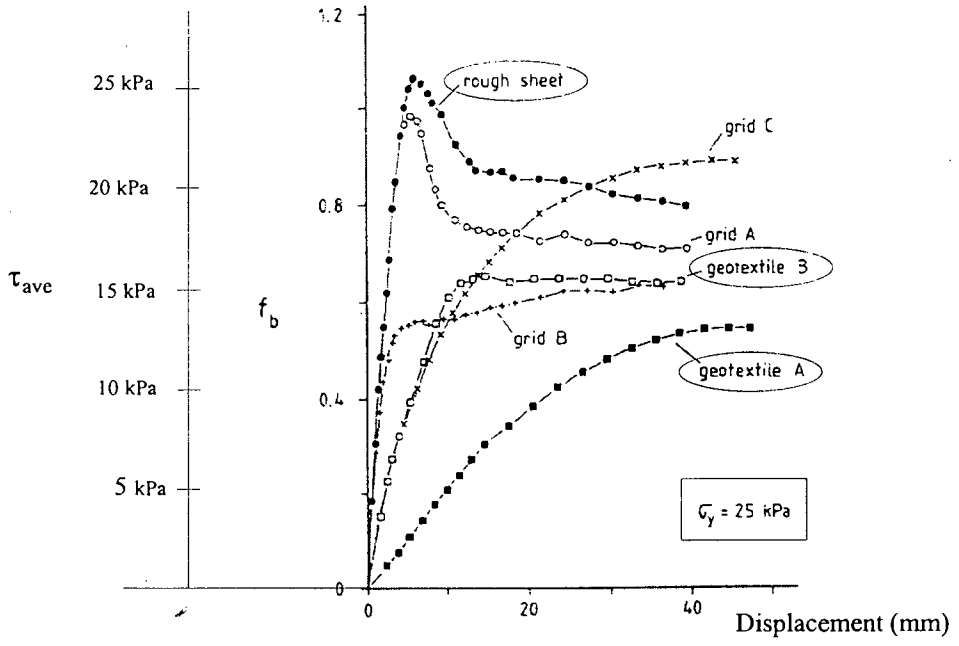

Figure 3-9: ***Bond coefficient versus displacement results (after Palmeira and Milligan, 1990)***

The shear stress increases as the displacement of the clamped end of the geotextile increases. The metal sheets (described in the figure as "rough sheet") displayed a sharp peak in the bond coefficient (shear stress), followed by a drop-off to a residual value. The geosynthetics, on the other hand, did not exhibit the same behaviour, showing a gradual increase and levelling-off to the maximum shear stress. This gradual increase was also

observed by other researchers (Forsman and Slunga, 1994; Tzong and Cheng-Kuang,1987; Bonczkiewicz et al., 1988; Kharchafi and Dysli, 1993 ; El Mogahzy et al., 1994, Juran and Chen, 1988). A similar difference in pull-out behaviour of steel compared with a geotextile was recorded by Bourdeau et al.(1990). This difference in shear displacement patterns is a clear indication that the soil/geotextile interface behaviour is very different to the soil/steel interface behaviour.

Forsman and Slunga (1994) addressed the post peak interface shear stress behaviour of geotextiles in soil. At low normal pressures, a gradual shear stress drop-off after peak was observed. This drop-off became steeper as the normal pressure increased.

El-Fermaoui and Nowatzki (1982) proposed the following explanation of the shear stress mobilisation. The shear stress is distributed along a certain front portion of the geotextile. This is termed the mobilised length. As the pull-out force increases, the mobilised length increases until the shear stress is carried over the entire length of the geotextile. At this point the peak shear stress has been reached (the pull-out force is also at a maximum) and the entire sample begins to slip. In the post peak failure state, the shear stress is distributed uniformly over the whole length of the sample because of a re-orientation of the soil particles.

3.3.5 Maximum shear versus normal pressure relationship

The relationship between the maximum shear and normal pressure is important as it determines the restraining force offered by a geotextile sheet under a certain overburden pressure. This relationship determines when slippage of the geotextile occurs and thus has implications for the design assumptions (Section 2.3).

The maximum shear stress, τ_{max} , is defined by the following equation:

$$\tau_{max} = \frac{P_{max}}{A_s} \qquad \text{.....(3. 6)}$$

where .....

P_{max}= maximum pull-out force measured during the pull-out test
A_s= shear area - determined using one of the three methods described in Section 3.3.3.

With respect to the literature reviewed here, the normal pressure, σ_n, was defined as the pressure which is applied perpendicular to the geotextile on the soil surface (i.e. at the boundary). However, this is not what is ultimately required in design, as is would be desirable to know the maximum shear stress in relation to the normal pressure, specifically at the interface.

Forsman and Slunga (1994) observed a linear τ_{max} - σ_n relationship for a sand/geotextile pull-out test at normal pressures up to 60 kPa. Both woven and non-woven geotextiles were tested. The tests were performed in a pull-out box of the type in Figure 3-7b in highly compacted as well as in loose sands. For the loose sand, the gradient of the τ_{max} - σ_n relationship was only 50% of that for the dense sand. Palmeira and Milligan (1990) observed a linear τ_{max} - σ_n relationship for a woven geotextile in sand at confining pressures of up to 100 kPa. The shear stress was calculated assuming that the area

remains constant (i.e. Equation 3.1 in Section 3.3.3). The pull-out box used was of the type shown in Figure 3-7a. It is, however, believed that this set-up induces errors into the results as the geotextile sample does not remain in the sand throughout the test and there is therefore uncertainty as to the magnitude of area of contact between the geotextile and the soil. This affects the calculation of the maximum shear stress and little confidence was thus placed on the results from this study.

Bonczkiewicz et al. (1988) performed pull-out tests in sand at normal pressures up to 35 kPa. The τ_{max} - σ_n relationship was found to be non-linear for both woven and non-woven geotextiles. Generally, the maximum shear stress increased with an increase in the normal pressure until a limiting stress value was attained. After this, the increase in shear stress dropped significantly. Ingold (1985) also observed a non-linear τ_{max} - σ_n relationship for woven and non-woven geotextiles (see Figure 3-22). El Mogahzy et al. (1994) obtained a highly non-linear τ_{max} - σ_n relationship for a non-woven geotextile in sand at low normal pressures (< 16 kPa).

Leshchinsky and Field (1987) attempted to determine a friction coefficient from a confined tensile test apparatus which was discussed in Section 3.2 (see also Figure 3-4). Tests were performed under pressures of up to 200 kPa and friction angles of between 24.2 ° and 28.8 ° were calculated.

In Figure 3-10 a summary of the τ_{max} - σ_n relationships in various sands and types of geotextile, obtained by various researchers, is presented.

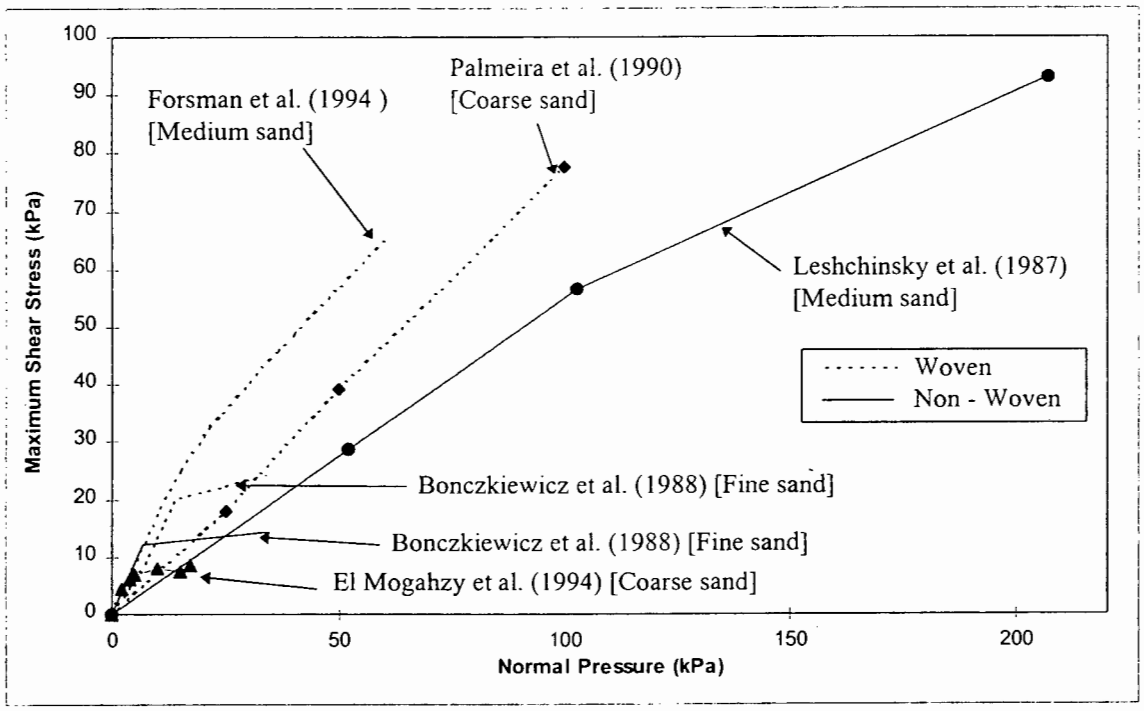

Figure 3-10: ***τ_{max} - σ_n relationships of geotextiles in sand observed in pull-out tests by various researchers***

It is evident that the combination of sand and geotextile used has a significant influence on the τ_{max} - σ_n relationship. The data from Leshchinsky and Field (1987) indicates a non-linearity in the τ_{max} - σ_n relationship at normal pressures above 100 kPa. However,

no other information is available on pull-out tests of non-woven geotextiles in highly confined sand.

3.3.6 Kinematics of the geotextile during pull-out

Extensometers have been used by many researchers to measure the displacement of points along a geotextile sample during pull-out tests. From these measurements, three relationships were determined. These are the distribution of the displacement along the geotextile sample, the change in elongation (or stretch) of the geotextile as the pull-out load increases and the displacement of the free end in relation to the pull-out force. The displacement of the free end is termed slippage.

By plotting the displacement measurements of various points along the geotextile, the displacement distribution was determined by Kharchafi and Dysli (1993) for non-woven geotextiles in a sand. The research showed that the displacement was distributed linearly along the sample at low pull-out forces. As the pull-out force increases, the displacement was found to be re-distributed hyperbolically along the sample. A similar pattern was obtained by Juran and Christopher (1989) in tests performed on an instrumented geotextile reinforced model wall.

The elongation of various points along the geotextile as the pull-out load increased were determined by Tzong and Cheng-Kuang (1987) for a non-woven geotextile placed in Ottawa sand. They observed that the geotextile initially begins to elongate at the front end. As the pull-out load increases, the elongation progresses along the sample to the free end. The observation was confirmed by experimental data from Forsman and Slunga (1994). This behaviour results in the greatest elongation occurring at the clamped end and becoming less towards the free end.

From displacement measurements, researchers were also able to determine the manner in which the free end displaces (slips) during pull-out. Tzong and Cheng-Kuang (1987) and Forsman and Slunga (1994) presented data for low confining pressures, indicating that the free end did not move throughout the duration of the test. Kharchafi and Dysli (1993), however, found that at a similar pressures the free end displaced before the peak pull-out force was attained.

Abremento and Whittle (1995) presented a different approach to interpret the elongation in an extensible reinforcing element, which was termed the shear lag analysis.

Initially, the zone of sliding was said to progress from the clamped end of the geotextile. However, this analysis differs for Tzong and Cheng-Kuang (1987) in that prior to slippage of the entire sample, a slippage front propagates from the free end. Failure then takes place when these two slippage fronts meet. After the peak pull-out force has been attained, a "snap-back" is observed. This occurs immediately when the whole length of geotextile is mobilised and the sheet rapidly shortens as the pull-out force decreases. This analysis was confirmed with pull-out tests. It must be noted that the test samples were nylon sheets of relatively narrow width (133 mm) and may not be representative of geotextiles in general.

3.3.7 Effect of geotextile stiffness on pull-out behaviour

Kharchafi and Dysli (1993) investigated the effect of the geotextile stiffness on the pull-out behaviour. The geotextile stiffness was defined as the ratio between the in-isolation tensile load and the elongation of the geotextile during in-isolation tensile tests of the geotextile. Three grades of the same geotextile product were tested. Each had the same surface texture, but a different stiffness. Tests were performed under identical conditions (σ_n=24 kPa, sample length = 500 mm). The configuration of the pull-out box was similar to that shown in Figure 3-7b. The pull-out load versus clamp displacement results from these three tests are shown in Figure 3-11.

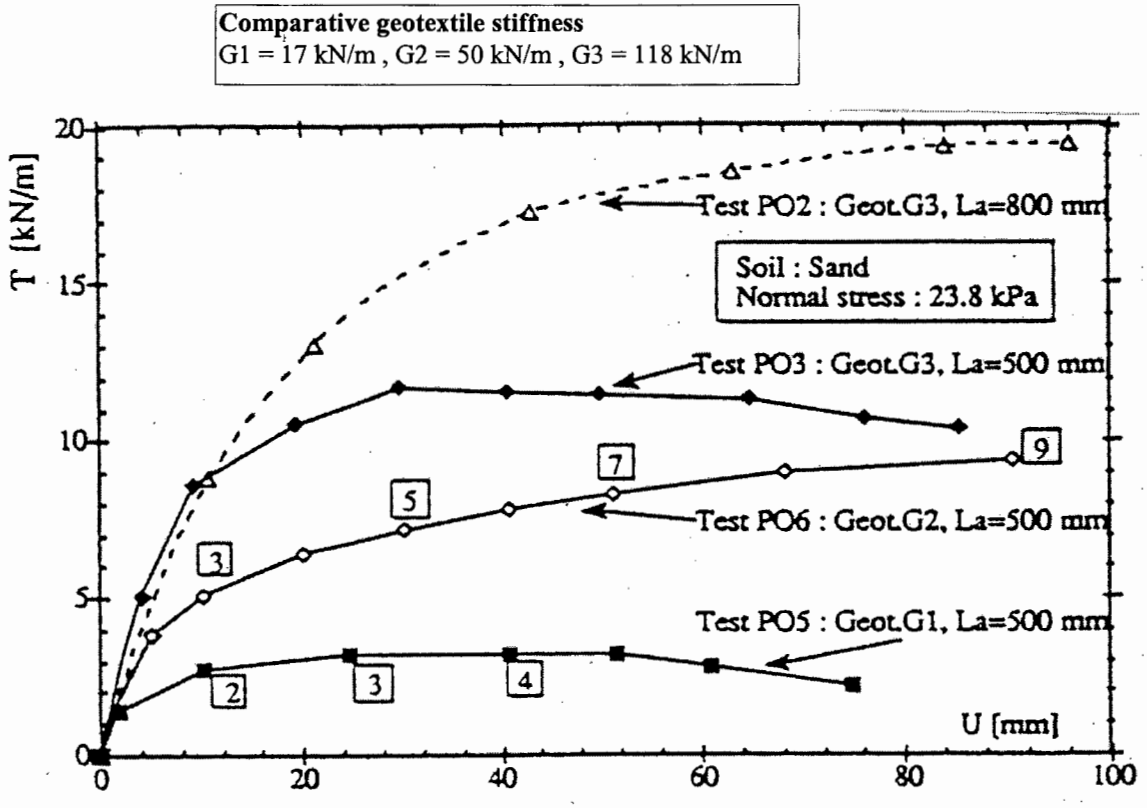

Figure 3 - 11: ***Effect of geotextile stiffness on the load versus clamp displacement relationship***

The sample with the lowest stiffness failed by rupture, while the two stiffer samples exhibited slippage failure. The research showed that an increase in stiffness increases the initial ratio between the pull-out load and clamp displacement. The influence of the stiffness on the strain along the sample is shown in Figure 3-12. As the stiffness increases, the strain is distributed more linearly. The strain in the stiffer geotextile extends further along the sample. This indicates that the shear stress is distributed over a larger area for the more rigid geotextiles. The maximum pull-out force increases with an increase in stiffness. However, the friction angle (calculated with the corrected area method, Equation 3.2) was not influenced by the stiffness. Although the stiffer geotextile exhibits a greater pull-out force, the greater geotextile stiffness causes the force to be distributed over a larger area.

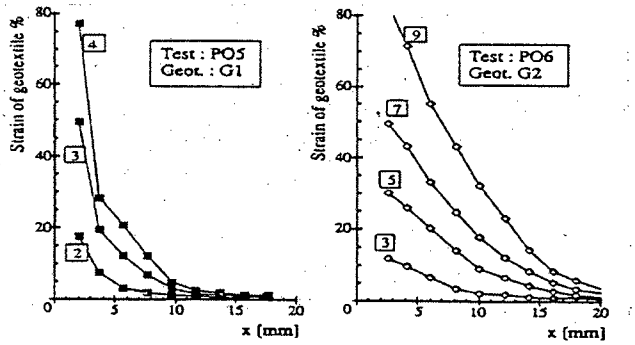

Figure 3 - 12: ***Influence of stiffness on the strain distribution along a geotextile (Kharchafi and Dysli, 1992)***

3.3.8 Summary

Since no investigation could produce a repetition of results from another investigation, it appears that the overall pull-out behaviour is highly influenced by the combination of soil and geotextile. Rupture and slippage failure modes are both possible during pull-out tests, however no clear understanding exists of the effects of the confinement on the respective failure modes.

There were three different methods quoted for determining the friction angle and the shear area of a geotextile sheet from a pull-out test. These methods, however, are valid only if the free end does not move during the test.

With the exception of the work by Bonczkiewicz et al. (1988) and El Mogahzy (1988), it would appear that the majority of soil/geotextile combinations exhibit a linear τ_{max} -σ_n relationship below 100 kPa. It was found (see Section 2.3) that most designs methods recommend that the maximum shear stress is directly proportional to the normal stress (i.e. the soil/geotextile friction angle is constant). However, it was shown that the relationship is more likely to be non-linear at confinements greater than 100 kPa and it is thus advisable to reconsider the assumptions made in these design methods for these greater confinements.

No pull-out tests were performed at pressures above 100 kPa. It is therefore not clear whether the τ_{max} -σ_n relationship remains linear above this pressure. Also, no attempts have been made to measure the confining pressure at the soil/geotextile interface, but it has been assumed that the pressure at the interface is the same as the applied pressure at some distance away from the geotextile.

From the data available, the shear stress mobilisation and actual movement along the geotextile is not clearly understood. Research is needed to help understand the mechanism involved in this process.

A certain amount of progress has been made in understanding the displacement distribution along the length of a geotextile sheet in pull-out. Yet, it is still unclear at what rate the displacement propagates along the sample. Also, the nature of the displacement of the free end has not been explained or quantified. The influence of the geotextile stiffness is significant and therefore, in order to compare pull-out test results, the same soil and geotextile should be employed.

3.4 Direct shear tests on sand / geotextile interfaces

This test is an adaptation of the standard direct shear box test originally devised to determine the internal angle of friction of soils. The test has been adopted by previous researchers to investigate the soil/geotextile interface behaviour and is a standard test specified by the British design code (BS 8006) for geotextiles to determine the sand/geotextile friction angle. It is an attractive test set-up because very little modification is required to standard equipment. Primarily, the function of the test is to determine the maximum shear stress (i.e. failure shear stress) at the soil/geotextile interface for various normal pressures, but has also been used to assist in investigating the shear stress mobilisation. This is a measure of the amount of displacement required at the interface for a specific interface shear stress to develop. The test arrangement, as described below, is typical of what was employed in all the research studies reviewed in this section. The size of the test equipment and the type of materials tested varied amongst the investigations.

The test, in essence, entails moving a soil mass, which is under a specific normal pressure, relative to a geotextile sheet which is in contact with the soil. The equipment, typically consisting of two frames, is shown in Figure 3-13. The geotextile is attached to the lower frame and the soil compacted into the upper frame. A confining pressure is then applied to the soil in the upper frame by applying a vertical load. The two frames are then displaced at a constant rate, relative to one another, thereby inducing shear stresses at the sand/geotextile interface. In some cases, the geotextile remains stationary (Myles, 1982; Makiuchi and Miyamori, 1988) while in others, the soil mass does not displace while the geotextile is moved (Saxena and Budiman, 1985). In all the tests reviewed, the area of soil in contact with the geotextile was less than the area of the geotextile itself.

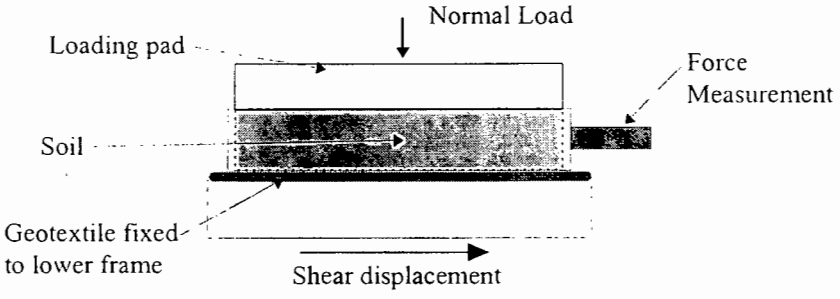

Figure 3-13: ***Schematic of a typical soil/geotextile direct shear test arrangement***

The shear stress developed across the interface is calculated from the measured reaction force exerted on the frame. By ignoring the friction between the frames, the shear stress is calculated as:

$$\tau = \frac{F}{A} \qquad \text{.....(3. 7)}$$

where....

F = shear force acting along the sand/geotextile interface (the measured force)
A= shear area (updated to account for the reduction in area due to the relative displacement of the frames)

To calculate the maximum shear stress, τ_{max} the maximum shear force experienced is substituted into this equation.

Table 3-3 presents a summary of the relevant published work for direct soil/geotextile interface testing using the direct shear box test. Clearly, a full range of pressures and test rates have been covered by the researchers.

Author	Box Size	Soil type	Pressure range	τ_{max} -σ_n curve	Test rate	Displ. to peak τ	Friction angle ratio
Saxena et al., 1985	250 mm x 250 mm	Sandy clay	69 kPa-207 kPa	Linear (up to 207 kPa)	0.76 mm/min	15 mm	2.18 (Non-woven)
Myles, 1982	310 mm x 310 mm	Sand	50 kPa - 200 kPa	Linear	10,25,75 mm/min	Not reported	0.86-0.97 (Non-woven)
Makiuchi et al., 1988	316mm x 316mm	Sand & clay	50 kPa - 200 kPa	Linear	0.5 mm/min	2 - 6mm	0.75-0.9 (Woven)
Fourie et al., 1987	60mm x 60mm	Clay	50kPa - 350kPa	Linear (up to 150kPa)	0.9 mm/min	3 - 6mm	0.52-1.65 (Non-woven)

Table 3-3: ***Summary of reviewed work on interface testing in the direct shear box***

3.4.1 Maximum shear stress versus normal pressure relationship

The emphasis in shear box testing has been placed by most researchers on determining the relationship between the maximum shear stress, τ_{max} and the normal pressure, σ_n.

Saxena and Budiman (1985) investigated the maximum shear stress versus normal pressure relationship using a 254 mm x 254 mm shear area. The soil material was a sandy clay which was normally loaded from 69 kPa to 276 kPa. Soil interface with both woven and non-woven geotextiles was investigated. The maximum shear stress was found to be directly proportional to the normal pressure, up to a normal pressure of 207 kPa. This applied for both woven and non-woven geotextiles. However, at normal pressures above this value, the relationship became non-linear for the non-woven geotextile. For the linear part, a friction coefficient (the tangent slope of the τ_{max} -σ_n relationship) was determined. Values of 0.52 for a non-woven geotextile and 0.4 for a woven geotextile was evaluated.

Myles (1982) also obtained a linear τ_{max} -σ_n relationship in tests involving a 0.1m^2 shear area with both woven and non-woven geotextiles. Leighton Buzzard sand was used at normal pressures of 50 kPa to 200 kPa. Tests were done at various displacement rates to investigate the rate dependence of the τ_{max} -σ_n relationship. Three relatively fast test rates (compared to Saxena and Budiman,1985) were used, namely 10 mm/min, 25 mm/min and 75 mm/min. It was clearly shown that for this range of displacement rates, there was no significant influence on the friction coefficient.

3.4.2 Friction angle ratio

The friction angle ratio is the ratio between the sand/geotextile friction angle and the internal friction angle of the soil. It has been investigated by many researchers in an attempt to determine if this ratio is constant for a specific geotextile product, irrespective of the soil in which it is confined.

The ratio is a common parameter used in many design methods and is the same quantity defined as the bond coefficient by Palmeira and Milligan (1990).It is calculated as:

$$\eta = \frac{\tan\phi_g}{\tan\phi_s} \qquad \text{.....(3. 8)}$$

where

η = Friction angle ratio
ϕ_g = Friction angle of the soil/geotextile interface
ϕ_s = Internal friction angle of the soil

Friction angle ratios have been calculated in sand from the work done by Myles (1982), Makiuchi et al. (1988) for sand and clay and Fourie et al. (1987) in clay. The respective friction angle ratios are shown in Table 3-4. These values apply for the specific geotextile product employed by the researchers. The specific conditions of these tests are described in Section 3.4.1.

Myles (1982) (Three soil types compared: a fine sand, a coarse sand and fly ash)		
Heat bonded non-woven 0.81 - 0.93	Needle punched non-woven 0.86 - 0.98	Woven 0.89 - 0.98
Makiuchi et. al.(1988) (A loose dry sand, a dense dry sand, a wet sand and a clay were used)		
Heat bonded non-woven 0.83 - 1.1	Needle punched non-woven 0.75 - 1.05	Woven 0.75 - 0.90
Fourie et al. (1987) (A clay at three moisture contents was tested)		
Non-woven 0.52 - 1.65	Woven 0.89 - 1.08	

Table 3-4: ***Range of published friction angle ratios***

For the geotextile products and sands used by Myles (1982), the friction angle ratios fall within a fairly narrow range of 0.81 to 0.98. However, the range of values is greater for the soils used by Makiuchi et al. (1988) and Fourie et al. (1987).

3.4.3 Mobilisation of shear stresses

Observations have shown that the peak shear stress obtained in the shear box test only occurs after a certain amount of displacement has taken place at the interface. This development in the attainment of the maximum shear stress is known as shear stress mobilisation.

Makiuchi et al. (1988) investigated this mobilisation in shear box tests in various clays and sands, using woven and non-woven geotextiles. The results from this work are presented as friction angle versus displacement plots for a number of geotextile and soil combinations in Figure 3-14. Since the Coulomb friction model assumes that the friction angle is proportional to the shear stress, for a constant normal pressure, these plots are a direct reflection of the development of the shear stress. The tests were performed at a shear displacement rate of 0.5 mm/min at a normal pressure of 50 kPa.

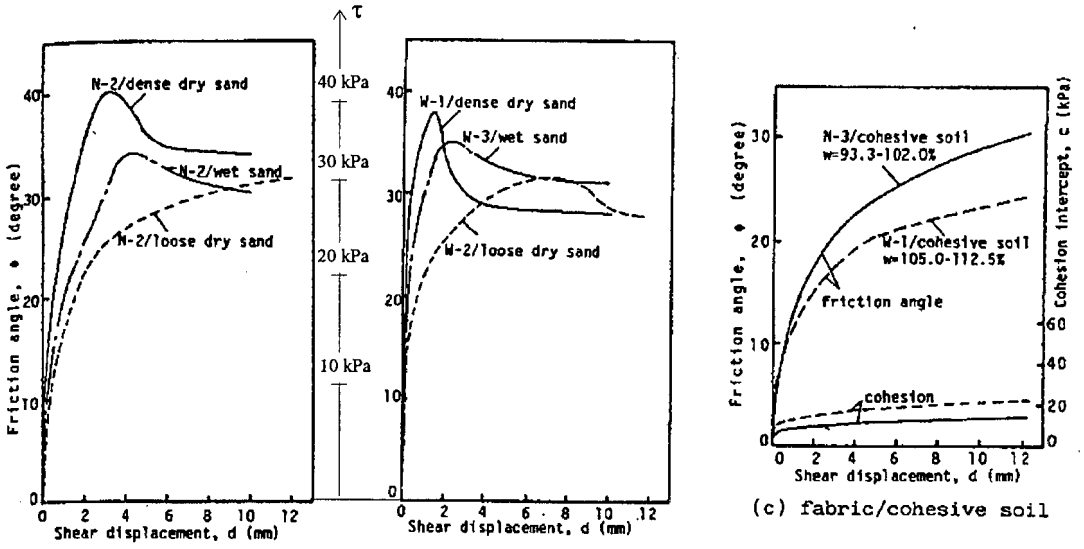

(a) Non-woven in sand **(b) Woven in sand** **(c) Woven & non-woven in clay**

Figure 3-14: ***Friction angle versus shear displacement relationships for various geotextiles in sand and clay (after Makiuchi et al., 1988)***

In loose dry sands the shear stress develops gradually with shear displacement and a large relative displacement is needed before the maximum shear stresses are achieved. The mobilisation of the shear stresses occurs over a small shear displacement in dense dry sands and wet sands and the peak shear stress is distinct. After the peak shear stress has been reached, there is a drop-off to a residual shear stress. There was also evidence that an increase in moisture content of sand causes the shear stress to develop over a larger shear displacement. In cohesive soils, there is a gradual increase in shear stress with no clear peak apparent for woven and non-woven geotextiles.

Saxena and Budiman (1985) observed a slower shear stress development in relation to clamp displacement, for both woven and non-woven geotextiles compared with Makiuchi et al. (1988). Here the peak shear stresses occurred at about 15 mm shear displacement compared with 7 mm measured by with Makiuchi et al. (1988). For a woven geotextile, Saxena and Budiman (1985) did not detect a distinct peak in shear stress followed by a lower residual value, as was the case with Makiuchi et al. (1988). The results obtained by Myles (1982) indicated that the behaviour after the attainment of the peak shear stress was highly dependant on the displacement rate. This however, does not explain the differences between the results obtained by Saxena and Budiman (1985) and Makiuchi et al. (1988) as the test rates were similar. It therefore appears that the shear stress development is greatly dependant on the soil/geotextile combination used in the test.

3.4.4 Summary

It would appear as if shear box tests for soil/geotextile interfaces produce linear τ_{max} -σ_n relationships for normal pressure of up to about 200 kPa. This relationship has been shown not to be influenced by the displacement rate.

Despite the apparent variability in friction angle ratios, it is however clear that the soil/geotextile friction angle is generally lower than the respective soil friction angle.

The rate of shear stress mobilisation with shear displacement can vary greatly depending on the type of geotextile and soil material. The post peak behaviour has been found to be influenced by the test rate.

3.5 Numerical modelling of soil/geotextile interaction problems

Numerical modelling techniques have been employed by various researchers to investigate the interface behaviour between soil, geogrids and geotextiles. The predominant method of analysis is by means of the finite element technique. Much attention has been placed on finite element modelling of geosynthetic reinforced walls and embankments. However, only a few researchers have modelled the interface behaviour of individual sheets in soil and it appears that this has been done only in terms of pull-out tests. Consequently, this review is limited to examining the various finite element models used to simulate pull-out tests and summarises a few relevant results obtained from these simulations. Also some results from an investigation using another numerical method of analysis are reviewed.

3.5.1 Finite element models and results

Geogrids as well as geotextiles in pull-out situations have been modelled with the finite element method of analysis. Since, there is little difference in the numerical simulation of these two geosynthetics, both will be reviewed.

Yogarajah and Yeo (1993) used the mesh, as shown in Figure 3-15 to model a pull-out test involving a geogrid. The soil was modelled using quadrilateral elements with a Mohr-Coulomb soil material model (friction angle = $0.9\phi_s$). Bar elements idealised the geogrid and the geogrid / sand interface was modelled using interface elements proposed by Goodman et al. (1968).

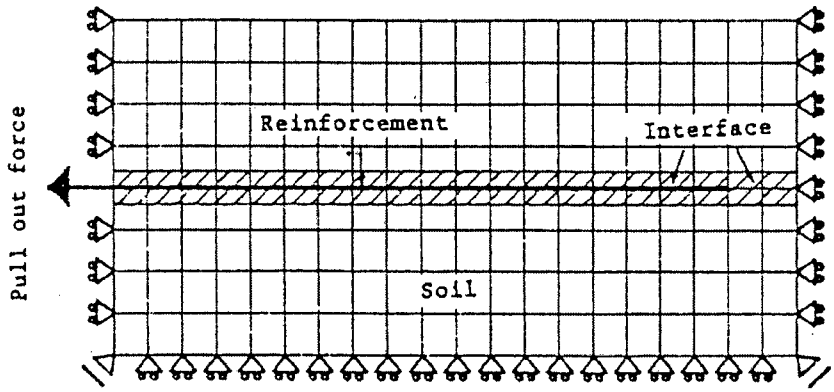

Figure 3-15: ***Finite element mesh to model a geogrid pull-out test (after Yogarajah and Yeo, 1993)***

Results from the finite element investigation for the strain and load distributions along the geotextile matched the experimental data well. This research indicated that a Mohr-Coulomb model is adequate to simulate this pull-out test.

A simple thin interface element with a Mohr-Coulomb friction model was developed by Handel et al. (1990) to model a geotextile pull-out test. Although the numerical results were not compared with any experimental data, the pull-out load versus displacement curve reflected a similar shape as the results discussed earlier in Section 3.3.4. The distribution of the shear stress along the interface was plotted for four pull-out loads and is shown in Figure 3-16.

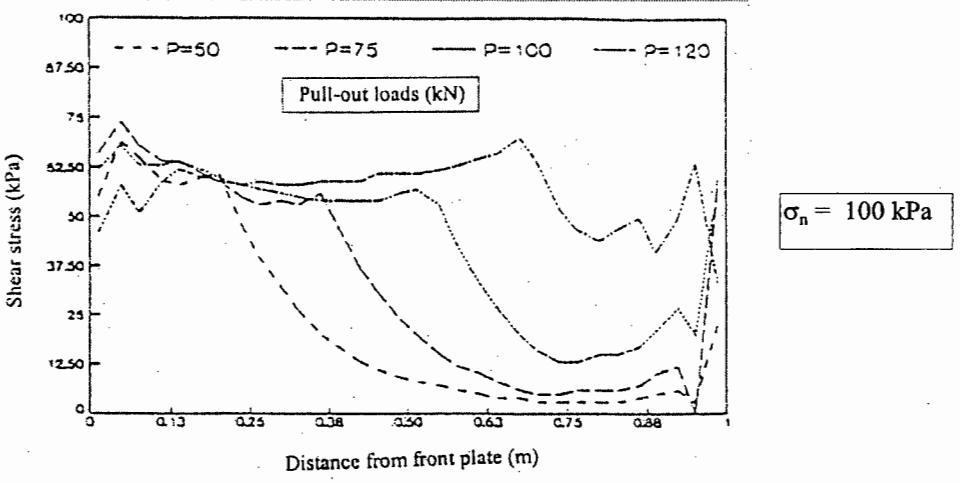

Figure 3-16: ***Shear stress along the interface at various pull-out loads (after Handel et al., 1990)***

The ultimate shear stress of about 70kPa is developed from the front which progressively translates towards the free end of the geotextile with increased loading. Stress concentration were noticed at the free end, and are attributed to the sensitivity of the interface element to the choice of the "stiffness" of the interface (i.e. ratio of interface stress response to the interface strain). Similar results were obtained by Hohberg and Schweiger (1992) in terms of the nature of the shear stress development and the stress concentrations at the free end.

An interface element with zero thickness was proposed and employed by Jianchao and Victor (1994), which was implemented in the simulation of a geogrid pull-out test. The soil was modelled as a hyperbolic continuum material. Quadrilateral soil elements were used. Bar elements and an isotropic hardening material model was utilised to model the geogrid. Figure 3-17 shows the comparison of finite element model predictions with the actual experimental results in terms of pull-out load versus clamp displacement.

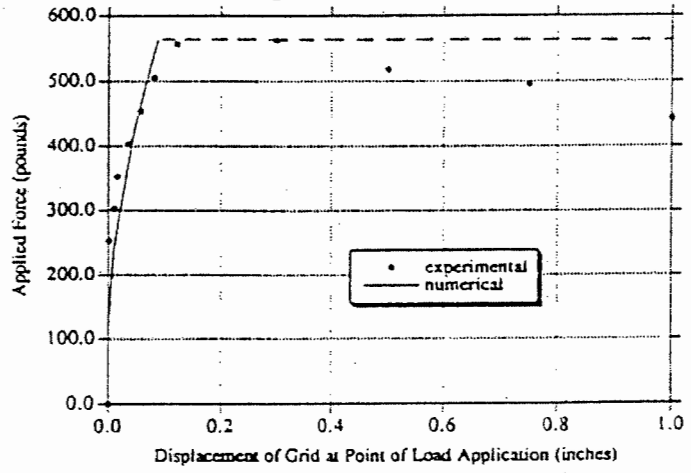

Figure 3-17: ***Experimental and numerical results of pull-out force versus clamp displacement (Jianchao and Victor, 1994)***

The numerical simulation results match those from the experiment in the initial part fairly well, although the finite element model initially under-predicts the pull-out force. In the interpretation of the analysis, it was then assumed that after the maximum pull-out load is reached a constant residual pull-out force is maintained. This analysis thus only simulated the pull-out behaviour up to the point of failure.

3.5.2 Non-finite element methods

Juran and Chen (1988) proposed a load transfer model for soil reinforcements as well as a numerical technique to interpret pull-out test results. This numerical technique is based on the finite difference method. The load transfer model was calibrated with experimental pull-out tests on geotextiles and a parameter study was undertaken varying the Young's modulus of the geotextile. It was found that an increase in the Young's modulus of the geotextile, resulted in increased pull-out resistance (see Figure 3-18). The measure of displacement at points along the geotextile decreased and became more uniformly distributed as the Young's modulus increased, as is shown in Figure 3-19. This can be verified by the findings of Kharchafi and Dysli (1993) (see Section 3.3.7).

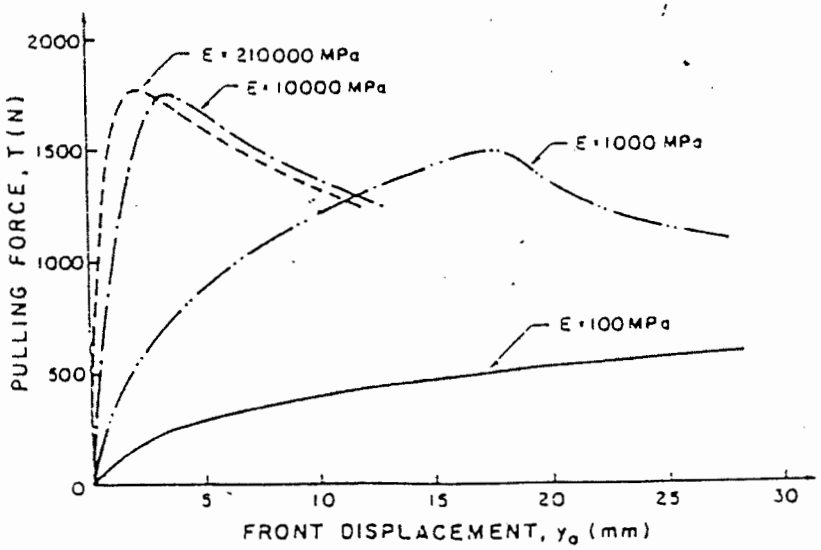

Figure 3-18: ***Influence of stiffness on pull-out load and front end displacement (Juran and Chen, 1988)***

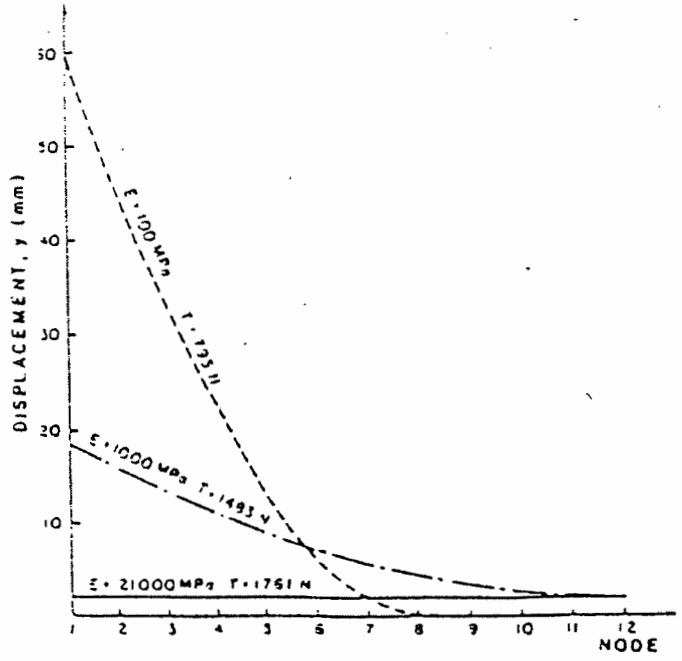

Figure 3-19: ***Influence of stiffness on displacement distribution (Juran and Chen, 1988)***

3.5.3 Summary

It would appear that the finite element method can be used to successfully simulate pull-out tests. Bar elements for the geotextile sheets and four-noded quadrilateral elements for the soil seem to be adequate to simulate the problem. Based on the work by Yogarajah and Yeo (1993), a Mohr-Coulomb model seems to be sufficient for the interface modelling between geogrids and geotextile in sand.

The shear stress along the soil/geotextile interface appears to develop at the front end and progress towards the free end. Finite element simulations generated stress concentrations at the free end of the geotextile due to an abrupt change in the interface stiffness at the free end.

Juran and Chen (1988) showed that an increase in the Young's modulus of the geotextile increases the pull-out resistance and causes the displacement of the geotextile to be more uniformly distributed along the sample.

Chapter 4
Objectives and Outline of the Research

The review of literature in the previous chapter highlighted certain areas were there is a need for additional research. This scope for investigation gave rise to the objectives of this research project which are described in this chapter. Also, the investigative procedure followed to meet these objectives is briefly outlined.

4.1 Objectives of the research project

The main theme of the research work is the investigation of the shear interface behaviour between a particular non-woven geotextile and Cape Flats sand. From the literature review, it became clear that researchers have pursued this task by consideration of either the pull-out or direct shear situation. It was decided that the pull-out condition will be the primary emphasis of the investigation, since it is felt that the sand/geotextile behaviour in the field situation is more realistically represented. The direct shear interface behaviour was, however, also investigated since direct shear tests are in general recommended (BS 8006). It would thus be possible to assess the applicability of direct shear test results in design by means of comparison with the pull-out test results. The specific objectives that were identified are:

1.) to determine the pull-out mechanisms of non-woven geotextiles in sand.
Here, the primary aim was to determine how the strains and stresses of a non-woven geotextile sample propagate in a confined pull-out situation in Cape Flats sand. It was hoped that this would lead to a better understanding of the actual load transfer mechanism as well as the shear stress mobilisation for the sand/geotextile interface. The effect of the confining pressure on these mechanisms could also be determined in the same context.

2.) to ascertain the confining pressure conditions at which slippage and rupture failure occur.
In the pull-out situation two failure modes are possible, namely slippage and rupture failure and it is well established that the type of failure is a function of the confining pressure. This investigation will focus on the conditions of the respective failure modes. The confining pressures which govern the failure modes will thus be quantified for the sand/geotextile combination. It will also be assessed whether transitional stages of failure between slippage and rupture failure occur during pull-out.

3.) to quantify the effect of the confining pressure on the maximum interface shear stress.
Another important objective was to determine the relationship between the confining pressure and maximum shear stress at failure for the sand/geotextile interface in both the pull-out and the direct shear situation. As described earlier, a linear relationship between the maximum interface shear stress and confining pressure is assumed in design methods, irrespective of the soil/geotextile combination in question (see Section 2.3). The research work is expected to shed some light on whether this is a satisfactory assumption for the specific sand-geotextile interface being investigated.

Also, most researchers have performed pull-out tests at confinements below 100 kPa and little attention has been placed on the investigation of the interface behaviour above this pressure. It is thus of interest to ascertain the relationship between the maximum pull-out shear stress and the confining pressure at pressures above 100kPa.

In the previous chapter, it was mentioned that no work was done where the confining pressure readings were taken at the actual soil/geotextile interface during pull-out tests. Therefore, this research project also aims to obtain maximum shear stress values which correspond to the actual confining pressures acting at the interface and not simply for pressure applied at the soil surface, some distance apart from the geotextile.

4.) to compare the pull-out with direct shear test results.
As was stated earlier, direct shear tests are generally the substitute for the more representative pull-out test (see Section 3.4). However, it is a matter of debate whether direct shear tests produce results which are adequately realistic. This research project will thus compare the maximum shear stress versus confining pressure relationship and shear stress mobilisation results observed in pull-out tests and in the direct shear tests. Again, in all tests, the same type of non-woven geotextile in Cape Flats sand will be investigated.

5.) to make recommendations concerning design methods.
From the results obtained in this study an attempt will be made to come up with recommendations to modify the current design approach for the purpose of improved stability and economy of geotextile reinforced structures.

4.2 Outline of the research project

To fulfil these above objectives, the following approach was undertaken. The research program involved combining results from experimental work and numerical simulations. The experimental work began with in-isolation tensile tests on the locally manufactured non-woven geotextile product used in this study. These tests provided information on the tensile behaviour of the product.

The emphasis of the experimental work involved performing pull-out tests on the specific geotextile confined in Cape Flats sand. In order to carry out the pull-out testing, a sophisticated test apparatus was developed in the Civil Engineering Department at the University of Cape Town. This equipment was manufactured with the aim of performing highly controlled pull-out tests with well defined boundary conditions and to take highly accurate measurements during experimentation. The measurement of the following quantities was therefore allowed for:

- the pull-out force, which was applied in a displacement controlled manner
- local displacements along geotextile sample
- the confining pressure at the soil-geotextile interface

The non-woven geotextile was embedded in dense Cape Flats sand. A wide range of confining pressures, from 25 kPa to 250 kPa, were employed in the pull-out test program.

A secondary experimental program was carried out in a direct shear apparatus again involving the same geotextile and Cape Flats sand. A standard shear box was slightly

modified in order to perform the direct shear tests. The confining pressure was varied from 50 to 350 kPa.

A third thrust of this project was the numerical investigation program in which a finite element model was developed to simulate a pull-out test. The model was developed using ABAQUS, a multi-purpose finite element program. To obtain the parameters for constitutive model of the soil, stress path tests were performed on the Cape Flats sand. These tests were undertaken with the sand compacted to the same density as was measured in the pull-out tests. The in-isolation tensile test results were used to determined suitable constitutive parameters for the geotextile. Results from the finite element simulations were then compared with the laboratory experiments. In this way, it was envisaged that a better understanding of the load transfer mechanism, in terms of stresses and strains, reflected by the interface behaviour between the non-woven geotextile and Cape Flats sand, could be obtained.

Finally, all the results are collated and summarised and compared with previous research. Also, a number of comments are made on the consequences of this research for the design of geotextile reinforcement applications in geotechnical engineering.

Chapter 5
In-Isolation Tensile Tests on Geotextiles

In this research project, the focus was placed on a typical non-woven geotextile which is applied in the Cape Flats environment. The geotextile tested was a non-woven geotextile product known as "Kaymat" which is manufactured in Atlantis in the Western Cape. It was, at the time, the only product of its kind available on the South African market. It is a relatively heavy, non-woven, needle punched, continuous filament geotextile which is manufactured in the manner as described in Chapter 2.

It was shown in the literature review that the tensile behaviour of a geotextile (woven or non-woven) has a significant influence on the geotextile pull-out behaviour (Karchafi and Dysli, 1992). The tensile properties which are important in describing this pull-out behaviour, are the tensile strength and load-elongation modulus (Wang et al., 1990; Baudonnel et al., 1982 ; Shestha and Bell, 1982). A tensile strength of a geotextile is defined as the breaking load of a 1m wide geotextile sample (International Society of Geosynthetics Secretariat, 1996). The load-elongation modulus, on the other hand, is the increase of tensile load per unit strain increment in a 1m wide geotextile sheet. Both of these parameters were determined for this particular product from in-isolation tensile tests. These tests served a four fold purpose, namely:

1) To determine the ultimate in-isolation tensile strength of the geotextile product which would be investigated in the pull-out tests. This could then be compared with the tensile strength of the material when confined in Cape Flats sand.

2) To determine the in-isolation load-elongation modulus of the geotextile. A suitable material model could then be adopted to simulate the fabric.

3) The tests served as a quality control check to ensure that the material exhibited the tensile strength quoted by the manufacturers.

4) A variation in the thickness of the geotextile was observed and thus the influence of the thickness on the tensile strength and load-elongation modulus of the geotextile was established.

In this chapter the geotextile under consideration is first described by means of the specifications published by the manufacturer. The in-isolation tensile test apparatus and clamping mechanism is explained. Each tensile test sample was prepared in a very specific manner to reduce inconsistencies in strain measurement. The procedure for preparing these samples is also explained. Relevant results from the in-isolation tensile tests are then presented. These results include the influence of thickness on the tensile strength and load-elongation modulus. Typical failure patterns are described and the respective stress strain relationships shown and discussed. To conclude, a summary of the important findings from the in-isolation tensile tests are given.

5.1 Manufacturer's specifications of the tested geotextile

The manufacturer, Kaytech Industrial Fabrics, grade their non-woven geotextile products according to the weight per square metre. For this investigation, it was decided to use a fairly heavy grade of 340g / m^2 (U34) with a specified tensile strength of 18 kN/m. It is standard practice to specify strength in units of kN/m since geotextiles are generally manufactured and installed in relatively wide sheets of 2 to 5m width. Tensile tests, however, are performed on samples which are only 200 mm wide (according to ASTM D4595-86). It is therefore necessary to convert the tensile test results to a strength per meter width of geotextile so that the quoted strength value can be related to a full scale application.

The list of the manufacturer's specifications related to the mechanical properties as well as the standards used for determining these specifications is presented in Table 5-1.

Property	Unit	U34	Standard
Mass per unit surface	g/m^2	340	SABS 79
Thickness under 0.5 kPa	mm	2.3	SABS 85
Thickness under 200 kPa	mm	1.05	EDANA 30074
One-directional tension (50 x 200 mm)	kN / m	14	SABS 93
One-directional tension (100 x 200 mm)	kN / m	18	DIN 53857

Table 5-1: ***Properties specified by the manufacturer of U34 non-woven geotextile (Kaytech Industrial Fabrics, 1995)***

A microscopic view of the structure of a typical non-woven geotextile is shown in Figure 5-1. The fibres of the fabric are randomly interlocked due to the manufacturing process (see also Chapter 2). The material has a loose structure and the holes created by the needle punching process are easily discernible.

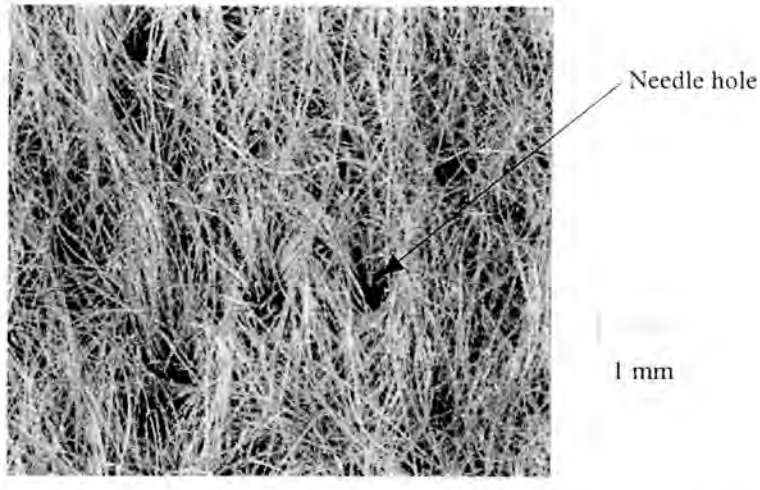

Figure 5-1: ***Micrograph of non-woven geotextile (after Kaytech Industrial Fabrics, 1995)***

5.2 Test apparatus and clamping device

The tensile testing was carried out on a computer controlled Zwick universal material testing machine. A tensile load was applied to the geotextile specimens in a strain controlled manner. A personal computer carries out the machine control and displays the measurement values, load and clamp displacement in numerical and graphical format.

Wide width clamps were manufactured to clamp the geotextile samples according to the ASTM D4595-86 specifications. In Figure 5-2 these clamps are shown. Their dimensions are such that test fabric samples of up to 200 mm width could be tested. A swivel connection between the load cell and clamp was introduced to ensure an even distribution of the tensile force across the width of the sample.

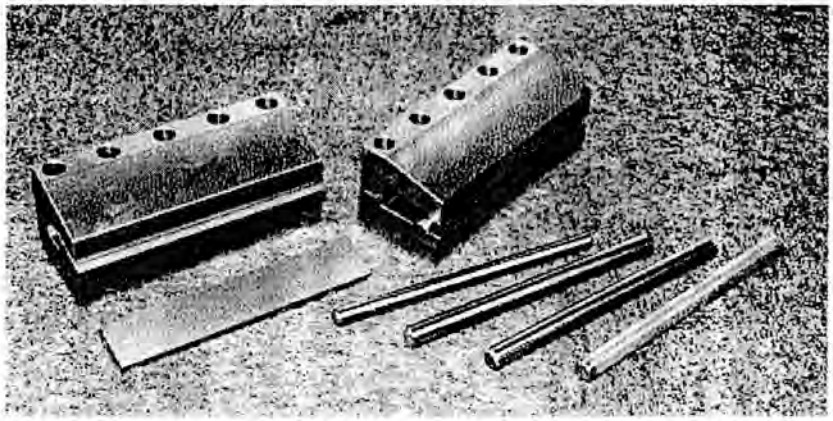

Figure 5-2: ***Wide width tensile test clamps***

The geotextile is wrapped around a steel rod which clamps itself in the narrowing gap of the clamp when a load is applied. It was noted that the clamping mechanism significantly influences the load-elongation behaviour due to slippage of the geotextile specimen at the clamps. Tests with various clamps are described in Section 5.3.3.

5.3 Test procedure

The in-isolation tensile tests were performed on samples of a width of 200 mm and a length of 100 mm, in accordance with ASTM D5495-86. All geotextile specimens were tested only in the direction of manufacture. A displacement rate of 10 mm per minute was selected after tests with slower rates showed no significant difference in load-displacement behaviour (Lai Sang, 1995).

5.3.1 Cutting and thickness measurements of test samples

Samples were cut at random from a standard roll of Kaymat U34. Test specimens were trimmed with an accuracy of 0.5 mm to a width of 200 mm and to a length of 300 mm. An extra length of 75 mm was allowed for clamping purposes. The thickness of each sample was measured according to the ASTM D1777-64 standard at a confinement of 2kPa.

The thickness of the roll of Kaymat U34 was found to vary significantly across the width and length. It ranged from 2.10 mm to 2.35 mm. For a total number of 30 specimens the average thickness was 2.209 mm, with a standard deviation of 0,0659 mm.

5.3.2 Preparation of test samples

Seven specimens were tested. The specimen number and thickness of each sample is given in Table 5-2. A range of the specimens with varying thickness were tested to determine the influence of thickness on the load-elongation and stress-strain response.

Specimen number	Thickness
TSA4	2.19 mm
TSA5	2.19 mm
TSA6	2.35 mm
TSA7	2.31 mm
TSB3	2.11 mm
TSB4	2.14 mm
TSC2	2.19 mm

Table 5-2: ***Measured thickness of each sample***

Before testing, each sample was trimmed and the test length of 100 mm was marked on the sample with two parallel lines. The ends of each sample were then sandwiched and bonded with polyester resin on either side between two brass sheets (see Figure 5-3). Weights were placed on top of the sheets during the drying period of the resin, to ensure a perfect bond between the geotextile and brass. A minimum of twenty four hours was allowed for the resin to dry before testing.

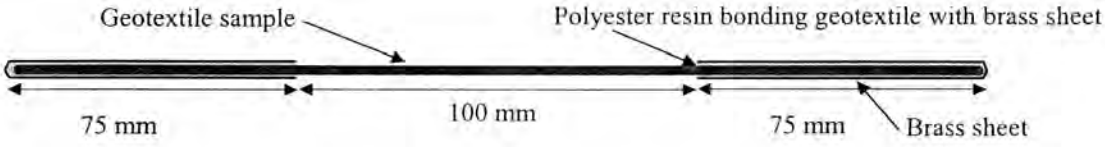

Figure 5-3: ***Schematic of the brass sheet arrangement on a geotextile sample***

5.3.3 Clamping of test samples

Lai Sang (1995) performed in-isolation tensile tests on the same geotextile product used in this investigation and compared different methods of clamping the geotextile. Based on that study, it was decided to clamp the brass sheets in the wide width clamps with knurled rods (see Figure 5-2). Before testing took place, the two rods were attached to one another with straps and a 1 kN tensile load was applied to embed the rods in the brass sheets, while the geotextile remained unloaded (as shown in Figure 5-4). This significantly reduce initial slippage.

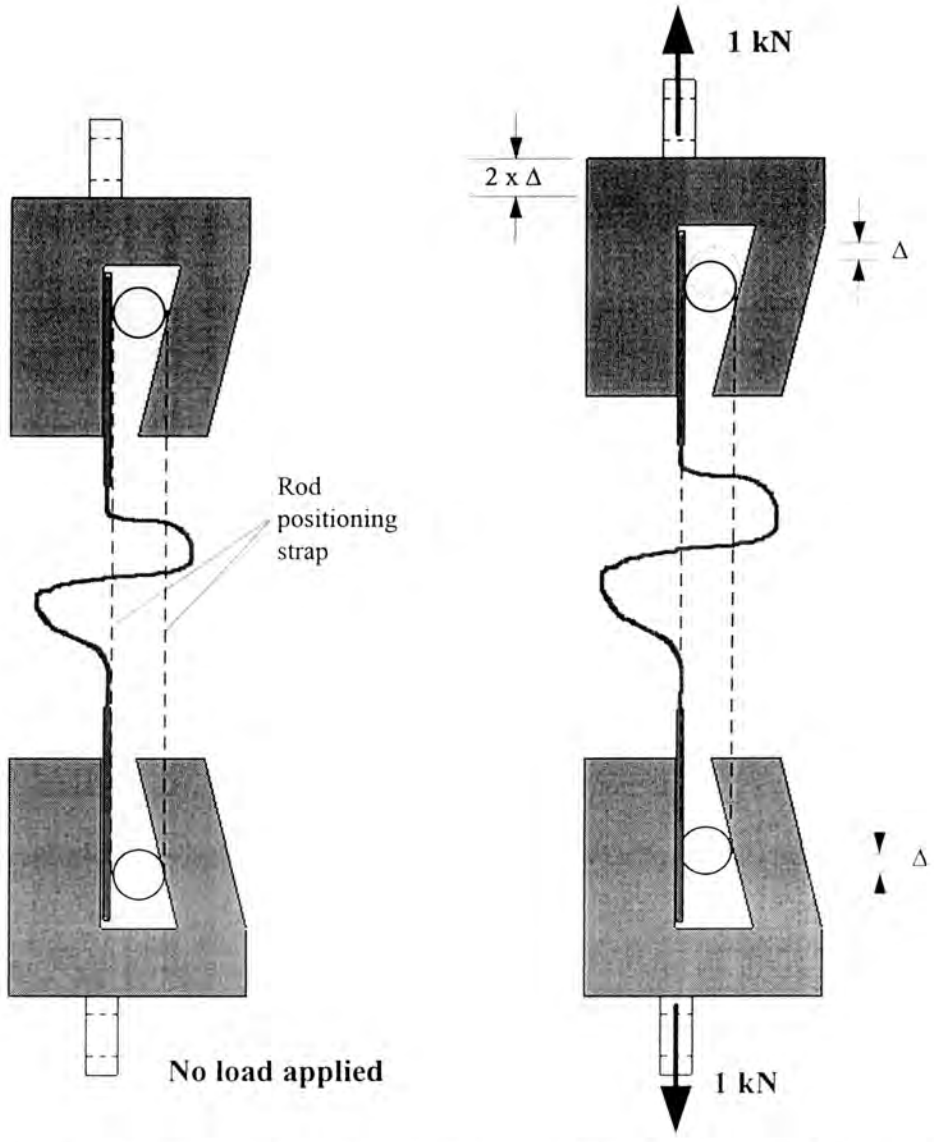

Figure 5-4: ***Clamping procedure of a geotextile sample in the in-isolation tensile tests***

5.3.4 In-isolation tensile tests

Seven in-isolation tensile tests were performed on Kaymat U34. The specimen size was 200 mm by 100 mm. The displacement rate applied was 10 mm/min for all tests. Load and elongation was automatically monitored and stored for further analysis.

5.4 In-isolation tensile test results

The load-elongation results are presented in graphical format. The influence of the sample thickness on the load-elongation modulus and tensile strength is discussed and the respective stress-strain relationships evaluated.

5.4.1 Influence of sample thickness on load-elongation behaviour

The load-elongation curves for 5 of the 7 tests are presented in Figure 5-5, along with an additional test performed by Lai Sang on the same product (1995). Two tests (TSB4 and TSC2) were discarded due to excessive slippage which occurred at the clamps during these tests.

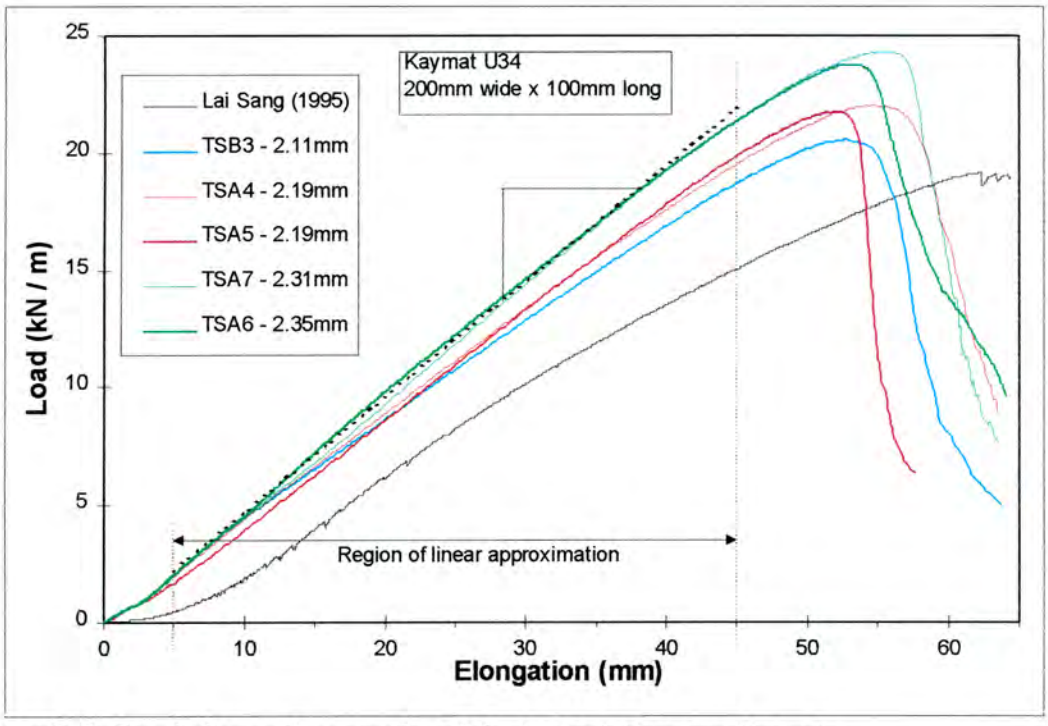

Figure 5-5: ***Load elongation results of the in-isolation tensile tests***

It was observed that up to 5 mm elongation, the load elongation behaviour is influenced by an initial "seating-in" deformation. This is followed by a similar rate of increase of tensile load with elongation for the tests. After about 12mm elongation, the influence of the sample thickness on the load-elongation modulus (i.e. slope of the load-elongation curve, E_{LE}) became evident. The thinnest sample (blue line) exhibited the lowest load-elongation modulus. In turn, the two thickest samples (green) displayed a steeper slope than the 2.19 mm thick (red) specimens. It is thus clear that a thicker geotextile specimen has a higher load-elongation modulus under in-isolation tensile loading.

The data obtained by Lai Sang (1995) in Figure 5-5 demonstrates the effect of the clamping procedure (as described above) on reducing the slip at the clamps. The initial pre-tensioning to place the rod was not undertaken by Lai San, so that in the initial phase of the test, a high measure of displacement was observed.

In Figure 5-6, the influence of the thickness of geotextile sample on the load-elongation modulus, E_{LD}, is quantitatively demonstrated. The load-elongation relationship appeared

to be linear between elongations of 5 mm and 45 mm which allowed a linear regression analysis to be undertaken. A least squares approach was implemented. The load-elongation modulus was calculated for each test in the approximate linear portion of the load-elongation curves. The values are shown in Figure 5-6.

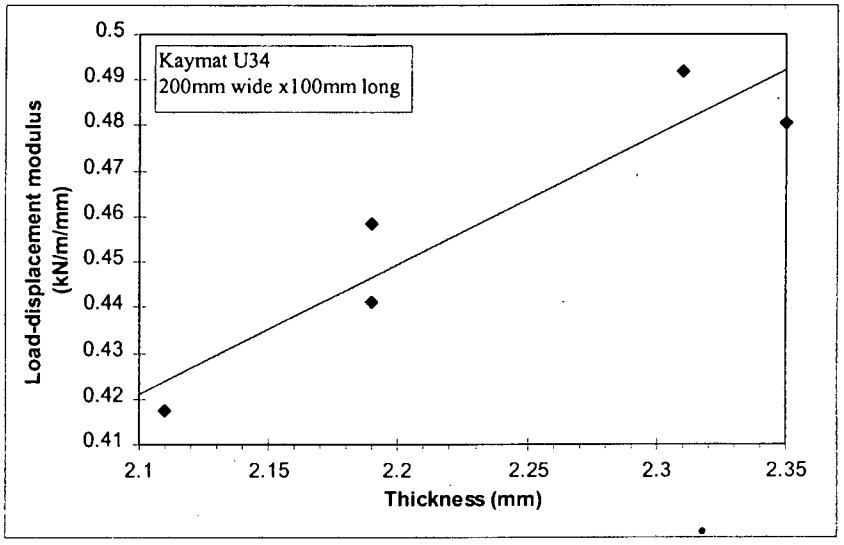

Figure 5-6: ***Influence of the sample thickness on the load-elongation modulus***

A clear trend is obvious which again indicates an increase of load-elongation modulus as the geotextile thickness increases. A straight line was fitted to this data. The results of this regression analysis denote that the load-elongation modulus increases, on average, by 0.0284 kN/mm per meter width, for every 0.1 mm increase in thickness. This result was implemented to determine a thickness tolerance for geotextile samples tested in the pull-out tests (see Section 6.3). It was done so that the influence of the geotextile thickness could be eliminated from the pull-out test results.

5.4.2 Influence of thickness on the tensile strength

In-isolation tensile strength for each sample was determined and also plotted against the sample thickness, shown in Figure 5-7. The in-isolation tensile strength of geotextiles is commonly defined as the maximum load per meter width of sample which is carried by the geotextile sample during in-isolation testing (International Geosynthetics Society Secretariat, 1996).

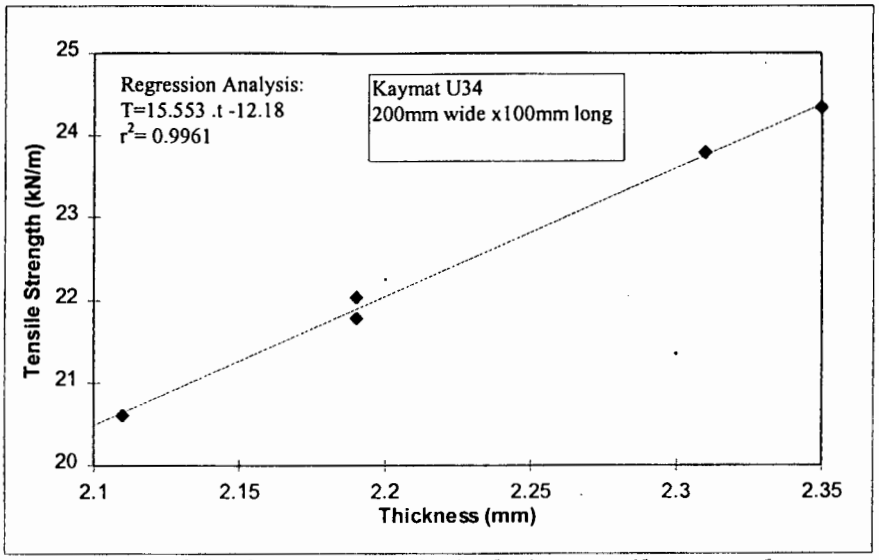

Figure 5-7: ***Influence of thickness on the in-isolation tensile strength***

The ultimate strengths experienced in the tests were greater than 20 kN/m, approximately 10 % to 30% higher then the manufacturer's specifications. Furthermore, it was noted that the tensile strength increases with sample thickness in a linear manner as is seen in Figure 5-7. Again, based on a regression analysis ($r^2 = 0.996$), the tensile strength was found to increase, on average, by 1.55 kN/m for every 0.1 mm increase in thickness of the geotextile. The expected in-isolation tensile load at rupture can thus be predicted for a specific sample thickness, provided it is measured according to ASTM D1777-64 at 2kPa confining pressure (see Section 5.3.1).

The rupture of the samples did not occur instantaneously, but progressively propagated primarily from the clamps towards the centre of the sample. All samples, besides TSA6, displayed tearing diagonally across the sample. Test number TSA6, however, tore orthogonal to the direction of load application. The picture in Figure 5-8 shows failed samples displaying the typical failure patterns.

The geotextile material did undergo very large lateral strains during tensile stretching, which is termed necking. This has previously been attributed the ability of the individual fibres to freely re-orientate and displace laterally during testing (Baudonnel et al. 1982). Lateral strains of 25% were recorded during testing. This excessive necking can also be seen in Figure 5-8. No attempt was made to investigate this phenomenon in further detail.

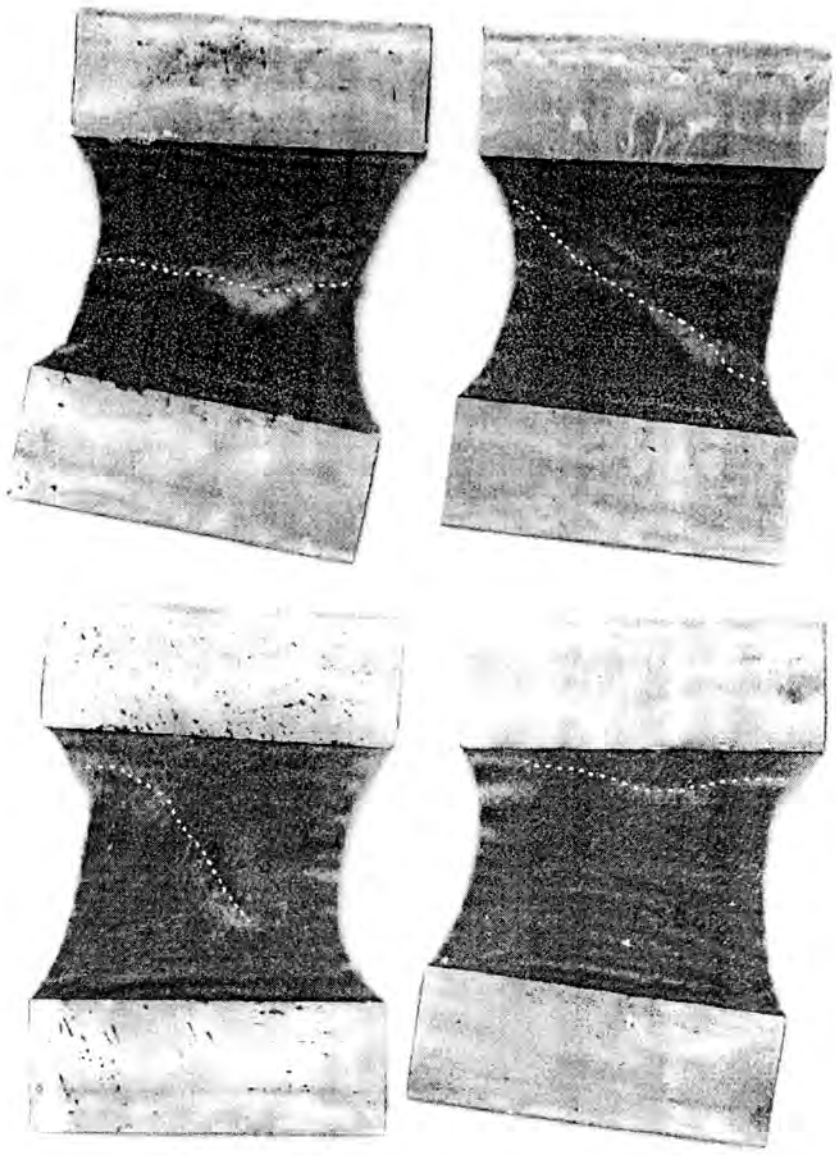

Figure 5-8: ***Test samples displaying typical rupture patterns and necking***

5.4.3 In-isolation tensile stress-strain relationship

From the load-elongation data, stress-strain relationships were computed assuming a constant thickness and width during testing. This assumption is not entirely correct, but due to limitations in electronic measuring equipment, it was not possible to measure the change in thickness and/or width during in-isolation tensile testing. The stresses were, therefore, simply calculated based on the measured thickness before testing (see Table 5-2). The stress versus strain responses of each test are presented in Figure 5-9.

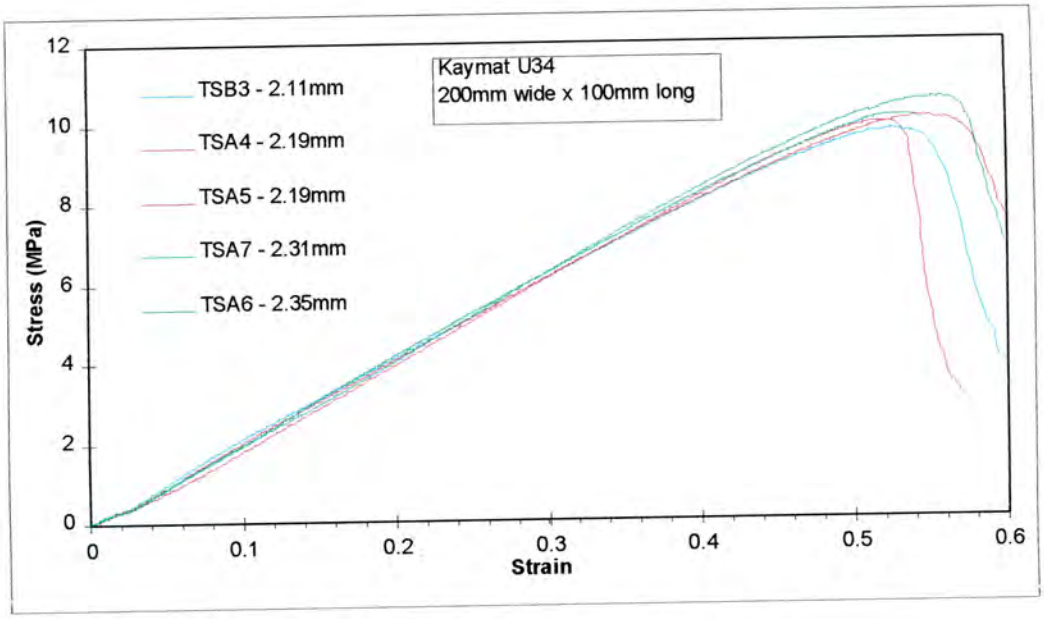

Figure 5-9: ***Stress - strain behaviour of non-woven geotextile***

As expected, the stress-strain curves are the normalised load-elongation responses of the in-isolation tensile tests for all specimen thickness'. The relationship between stress and strain appears to be a straight line, allowing a linear approximation to represent the typical in-isolation behaviour of the geotextile. The regression yielded a Young's Modulus of 20.95 MPa (the accuracy for the regression, i.e. r^2 value, was 0.9996). This indicates that the assumption of a linear stress-strain relationship is satisfactory for strains up to 0.45.

5.4.4 Summary

The geotextile material exhibits a linear load-elongation behaviour (i.e. constant load elongation modulus) prior to failure. The stress-strain relationship is linear and it was shown that a linear material model is adequate to describe the loading response of this geotextile product. A Young's modulus of 21 MPa can be employed with confidence for in-isolation conditions. Also, the tensile strength for a specific sample thickness can be determined.

It was also established that the thickness of the test samples affects both the load-elongation modulus as well as the tensile strength of this geotextile product. Since both of these parameters will influence the consistency of responses of pull-out tests (in terms of pull-out load versus clamp displacement relationship and confined tensile strength), it was therefore necessary to use only geotextile samples which fall within a defined thickness range.

Chapter 6
Laboratory Pull-out Tests of Geotextiles in Sand

Subsequent to investigating the in-isolation tensile behaviour of the geotextile, attention was placed on the interface between Cape Flats sand and the non-woven geotextile, which was subjected to tension. The first part of the experimental investigation of the sand/geotextile interface behaviour was done by means of pull-out tests. The test were performed in the Civil Engineering laboratory at the University of Cape Town using a specially manufactured test apparatus.

In this chapter, the test facilities will initially be described. A brief report on the geotechnical properties of the sand into which the geotextile is embedded is given. A procedure was developed to prepare each test sample and this will be briefly explained. A comprehensive test program was followed for the pull-out tests using a realistic range of confining pressures. This program will be introduced, and the results from the pull-out tests will be shown. The results include the pull-out resistance offered by the geotextile, the displacement and stretch of the sample and the maximum shear stress versus confining pressure responses.

6.1 Pull-out test arrangement

The test set-up consists of a universal tensile testing machine (i.e. Zwick, as described in Chapter 5.2), a pull-out apparatus connected to a compressed air supply, three extensometers, two pressure transducers and a HP Microlink data logger controlled by a HP 86 series PC for data capturing. A schematic of the arrangement of the various components is shown in Figure 6-1.

The pull-out test apparatus, into which the geotextile is confined in the sand, is placed vertically in the tensile testing. The geotextile is attached to the upper wide width clamp via a brass sheet which is in turn connected to a load cell. The pull-out load is applied in a displacement controlled manner. Pressure pads arranged on either side of the sand are supplied by a compressed air main (described in Section 6.1.1). The confining pressure measurements were taken by two pressure transducers which are placed in the soil before testing. Three linear variable displacement transducers (LVDT's) were employed to measure displacements along the geotextile sample. These measurements were monitored by a HP Microlink and stored on an HP 86 PC.

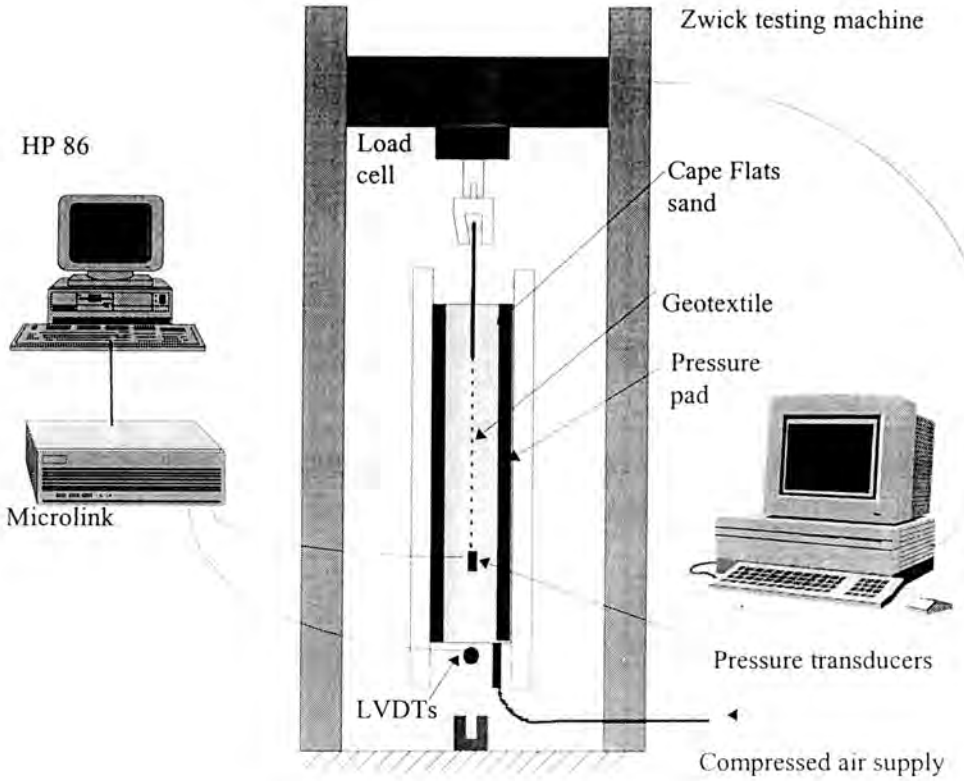

Figure 6-1: ***Schematic of pull-out test arrangement***

A pull-out test apparatus was manufactured specifically for this research project in the workshop of the Department of Civil Engineering. The apparatus consists of an aluminium frame into which the sand and the geotextile specimen are placed. A pressure pad is fitted on either side of the frame and is clamped together by means of a rigid clamping device. The pressure pads consist of parallel, flexible tubes which can be pressurised to confine the sand in a controlled manner. A bracket connects the apparatus to the fixed base crosshead of the tensile testing machine. The various parts of the pull-out apparatus are given in schematic form in Figure 6-2.

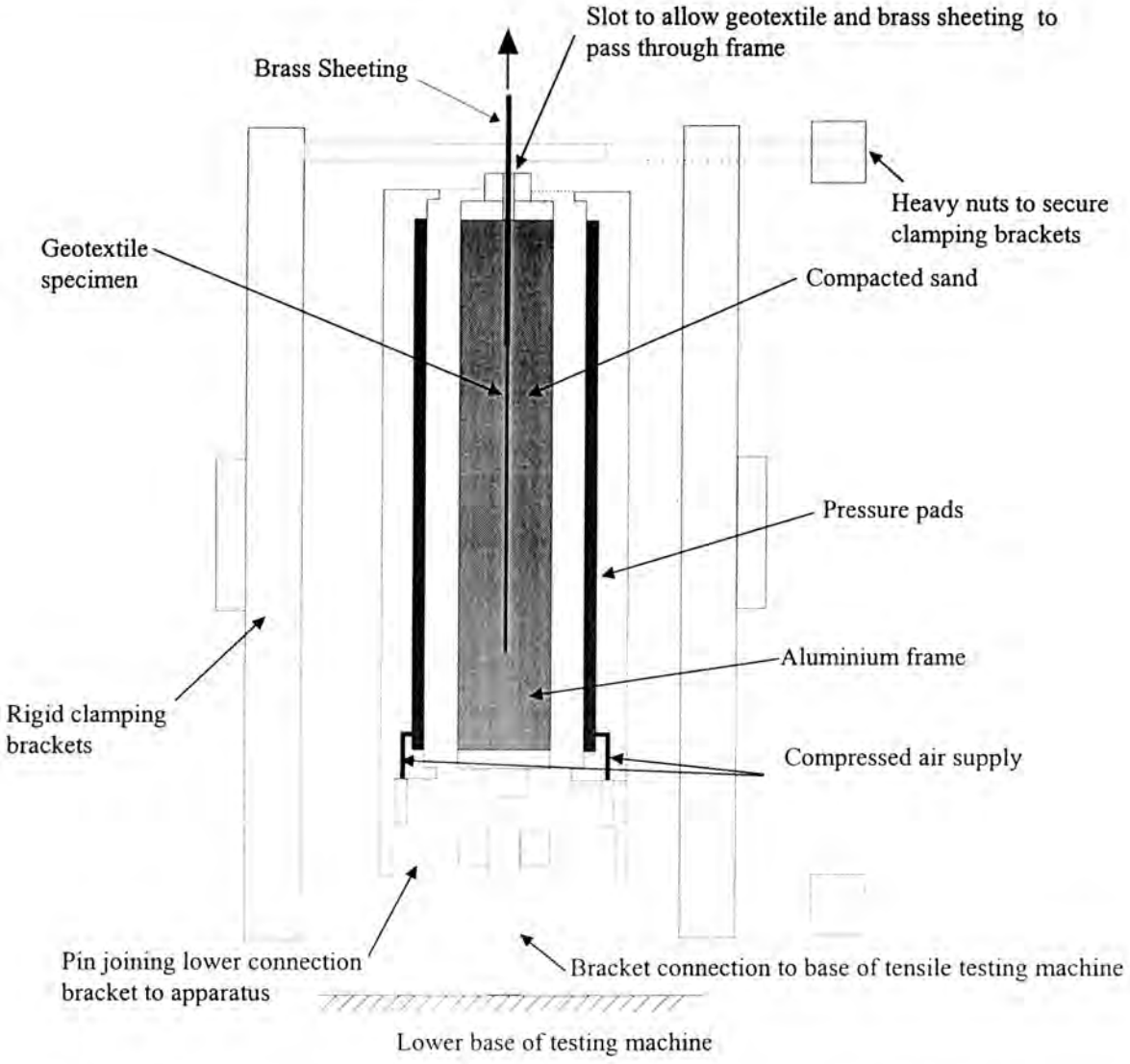

Figure 6-2: ***Laterally exploded cross-sectional view of the components of the pull-out apparatus***

The aluminium frame, which encloses the sand/geotextile test, is 50 mm thick by 288 mm long and 300 mm wide. A slot was provided in the upper sidewall of the frame to allow the 200mm wide geotextile sample, encased in brass sheeting, to pass through the frame. The geotextile is centrally located allowing a coverage of 25 mm of sand on either side of the sample (see Figure 6-3 (a)). In order to ensure that the geotextile sample remains in the soil throughout the entire test, the brass sheeting extends 50 mm into the soil mass (as is shown in Figure 6-3 (b)). A schematic of the cross-section of the frame and a plan view of the placement of the geotextile is shown in Figure 6.3(a).

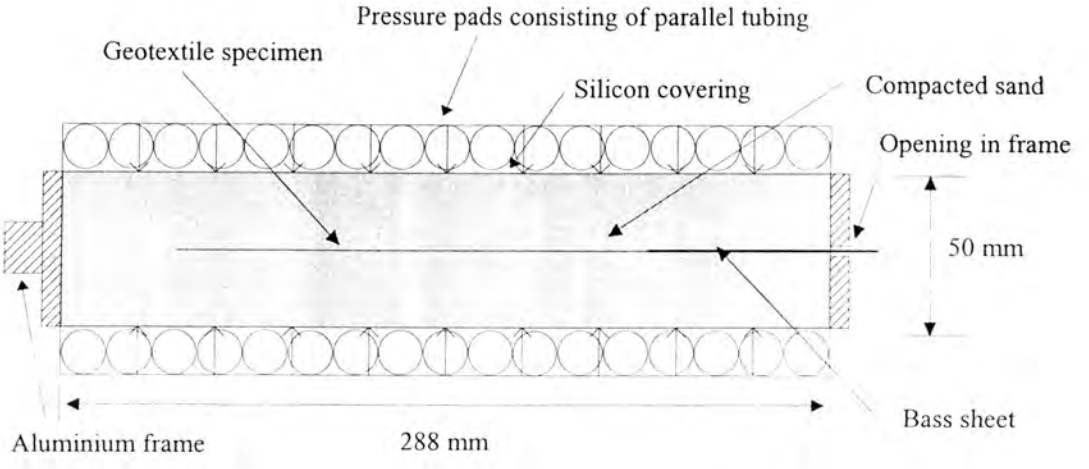

(a) Cross-section

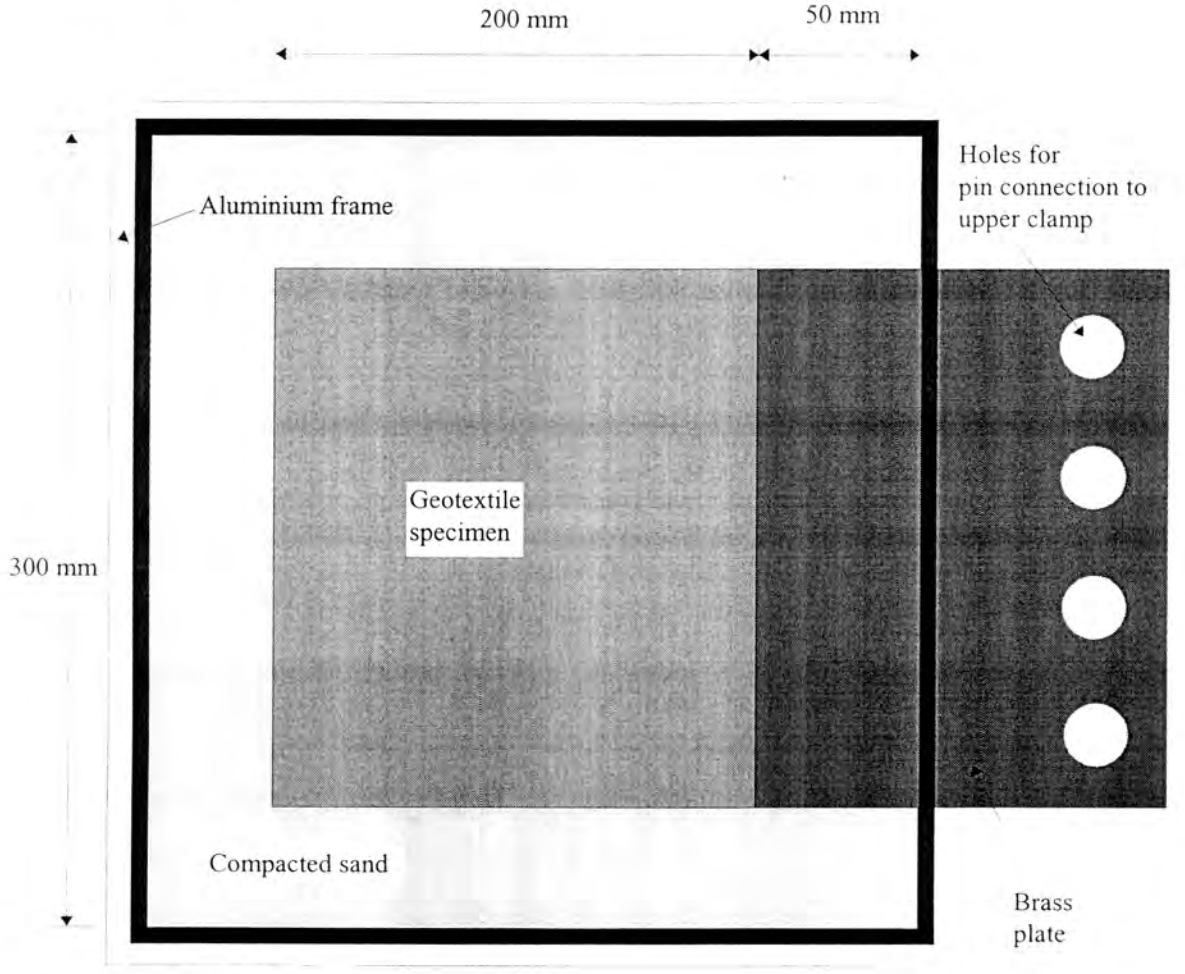

(b) Plan view

Figure 6-3: ***Cross-section and plan view of sand/geotextile arrangement in the pull-out apparatus.***

Normal pressures of up to 300 kPa may be applied to the soil by means of the pressure pads. The pressure pads comprise of rows of silicon tubing, encased in a silicon bed. Each tube is connected to an air supply manifold, which in turn is coupled to one of four input values. Compressed air is supplied to the pressure pads and is controlled with a pressure regulator. The pressure pads thus induce a uniformly distributed confining pressure at the interface between the sand and pads.

The pressure pads and frame are held together with a rigid clamping system, consisting of mild steel brackets clamped together at the four corners. The brackets and nuts are identified in Figure 6-2.

A connection bracket is coupled to the bottom of the apparatus with two steel pins. This bracket is slotted onto a mounting on the fixed end (bottom) of the Zwick testing machine and secured with a pin and two bolts.

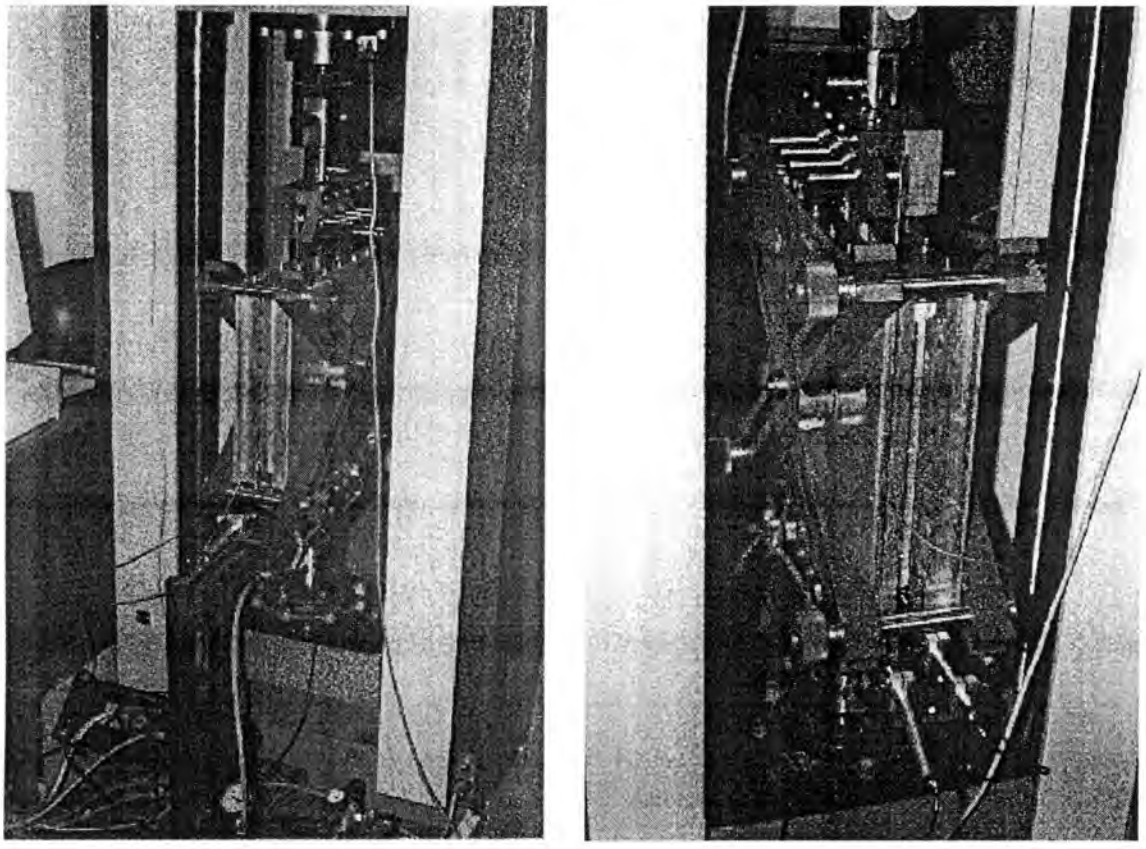

Figure 6-4: ***Pull-out apparatus mounted in the Zwick testing machine***

The brass sheet, which is bonded to the geotextile specimen, is clamped into the wide width clamp by means of four steel pins inserted through the clamp and brass. This arrangement completely eliminates slip between the brass and clamp (it was found that the clamping mechanism could be used for tensile loads of up to 8kN). The clamping arrangement is shown in Figure 6-5. The swivel connection between the clamp and load cell was employed to allow a uniform transfer of applied load to the test specimen.

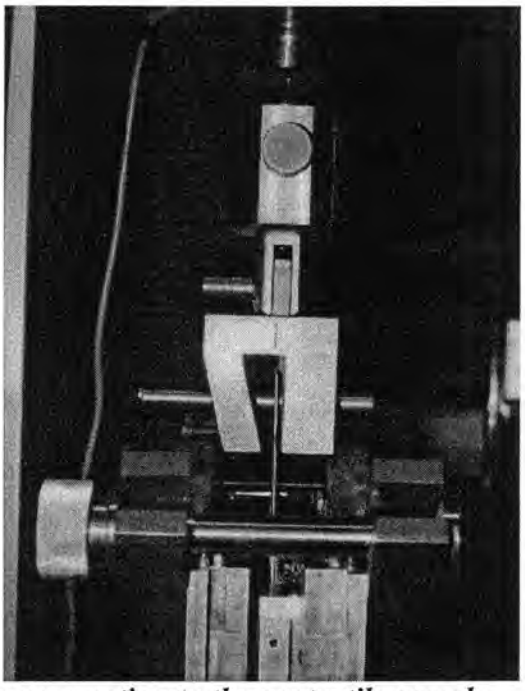

Figure 6-5: ***Upper clamp connection to the geotextile sample***

Two small pressure transducers were installed to measure the soil pressure close to the level of the soil-geotextile interface. The transducers have a diameter of 20mm, a thickness of 10mm and consist of two active faces.

In order to measure displacements at three localised points along the geotextile sample, three extensometers were specially assembled. Each extensometers consists of a thin cotton thread, attached at one end to the geotextile and at the other end to a Linear Variable Displacement Transducer (LVDT). Thus any movement that occurs along the geotextile will be measured by the respective LVDT.

Each thread was attached at one of three specific points on the geotextile sample and fed through stiff tubing to reduce the frictional force between the sand and the thread. The threads are guided through the frame and re-directed around pulleys to the horizontally aligned LVDT's which were mounted onto the lower connection bracket (as shown in Figure 6-6).

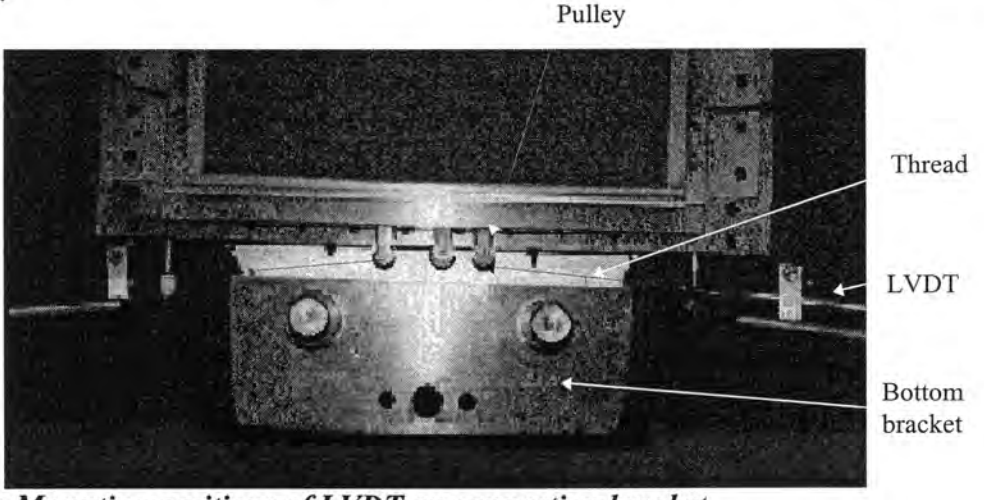

Figure 6-6: ***Mounting positions of LVDT on connection bracket***

The three LVDT's have a measurement range of -25 mm to + 25 mm, allowing a total displacement of 50 mm to be measured.

In order to read the signal voltages from the two pressure cells and the three LVDT's a data acquisition unit was set up. The system consisted of a Hewlett Packard Microlink which was controlled by a Hewlett Packard 86 series personal computer. Control and output information was transferred between the Microlink and PC through an Interface Bus (HP-IB). A photograph of the data acquisition equipment in shown in Figure 6-7. A simple BASIC computer program was coded for the PC to control and read the data supplied by the Microlink. The program instructed the Microlink to collect the voltage reading of a specific channel, store the data on a disk and address the next channel . Association of the voltage readings per channel with the pull-out load/displacements was undertaken by means of run time of the test.

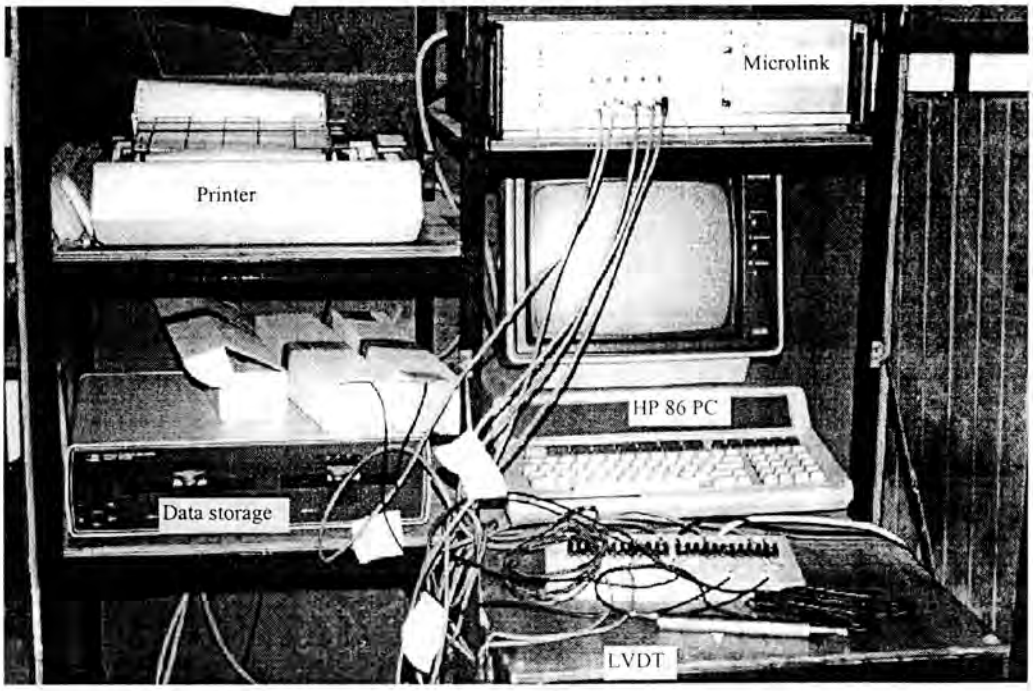

Figure 6-7: ***Data acquisition unit***

6.2 Properties of Cape Flats sand

In the pull-out test series one type of soil, namely Cape Flats sand, was used to embed the geotextile. It is a round grained, clean quartz sand that originates from the Cape Flats in the Cape area. It is a readily available and popular fill material within the local construction industry. The mechanical properties of the sand are summarised in Table 6-1.

Specific gravity, G_s [#]	2.65
Natural moisture content [*](after 1 year standing in laboratory)	3.1 %
Minimum dry density [*]	1487 kg/m^3
Maximum dry density [*]	1765 kg/m^3
Optimum moisture content [*]	7% and 13.4%
Effective grain size, D_{10} [#]	0.190 mm
D_{30} [#]	0.265 mm
D_{60} [#]	0.430 mm
Coefficient of uniformity, C_u [#]	2.26
Coefficient of gradation, C_g [#]	0.86
Angle of internal friction [*]	41°

[#] Lai Sang (1995); [*] Cowburn (1993)

Table 6-1: ***Soil mechanical properties of Cape Flats sand***

A grain size distribution of Cape Flats sand showing a uniformly graded medium sand is presented in Figure 6-8 (Lai Sang, 1995).

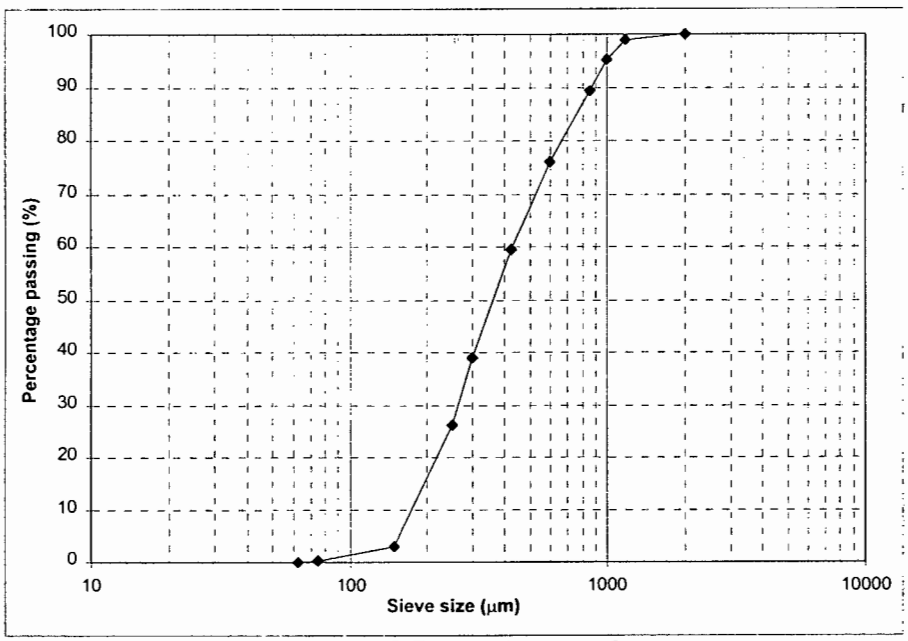

Figure 6-8: ***Particle size distribution of Cape Flats sand***

The dry density - moisture content relationship, obtained from modified Proctor tests, is shown in Figure 6-9 (after Cowburn, 1993). Two clear peaks are observed at optimum moisture contents of 7% and 13.4%. Based on this information is was decided to perform

all tests at the lower optimum moisture content of 7%. The target dry density of all tests for these investigations, pull-out tests and direct interface tests, was 1630 kg/m^3, which is approximately 2% lower than the optimum dry density. This slightly lower value was chosen because the relatively "flexibility" of the pull-out test frame did not allow a compaction of the same compaction energy as in the modified Proctor test.

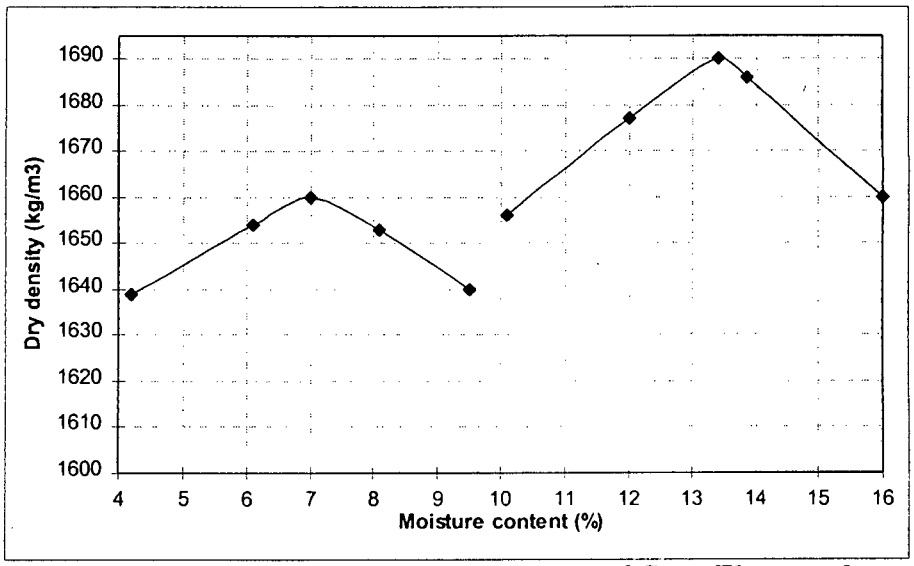

Figure 6-9: ***Dry density-moisture content relationship of Cape Flats sand***

Cowburn (1993) performed direct shear box tests on Cape Flats sand, at an average dry density of 1547 kg/m^3 and a moisture content of 3.8%. From those experiments, an angle of internal friction of 41° was determined. However, an independent investigation was performed to determine the internal angle of friction of Cape Flats sand, for the same density (1630 kg/m^3) and moisture content (7%) pertaining to the pull-out tests. These tests are described in Section 8.2.

6.3 Preparation of the geotextile sample

A special procedure was developed to prepare each geotextile sample for a pull-out test. In this way the:

- clamping of the geotextile sample to the Zwick testing machine was relatively simple and convenient, also
- any slippage at the clamp was completely prevented and
- a certain amount of consistency in the preparation and quality of the geotextile samples was achieved.

Pull-out tests samples were cut from the same roll of non-woven geotextile as those tested in the in-isolation tensile tests. The samples were trimmed to a size of 300mm by 200mm, such that the direction of pull-out load application was in line with the manufactured direction of the geotextile roll.

It was stated that the load-elongation modulus of Kaymat U34 was significantly influenced by a variation in thickness of the non-woven geotextile (Section 5.4.1). It would thus be expected that the relationship between pull-out load and elongation of the geotextile would also be influenced by sample thickness and would distort the results

obtained from the pull-out tests. Since the thickness of the geotextile was found to vary across the supplied batch, only geotextile specimens that fell within a specific thickness tolerance were used in the pull-out tests. The thickness tolerance was determined based on the in-isolation tensile test results described in Section 5.4.1. As was stated, the load-elongation modulus, for a 1m wide sample, increased by 0.0284 kN/mm for every 0.1 mm increase in thickness. The thickness tolerance was thus calculated to obtain a 98% confidence in this modulus. A value of 0.032 mm on either side of the average thickness of 2.209 mm was obtained, yielding a thickness tolerance from 2.18 mm to 2.24 mm.

In order to facilitate clamping of the non-woven geotextile to the tensile testing machine, one half of each geotextile specimen was initially soaked in polyester resin and wrapped in a brass sheet as is shown schematically in Figure 6-10. The resin was allowed to dry for at least 24 hours. The geotextile specimen now had the dimensions of 200 mm by 150 mm.

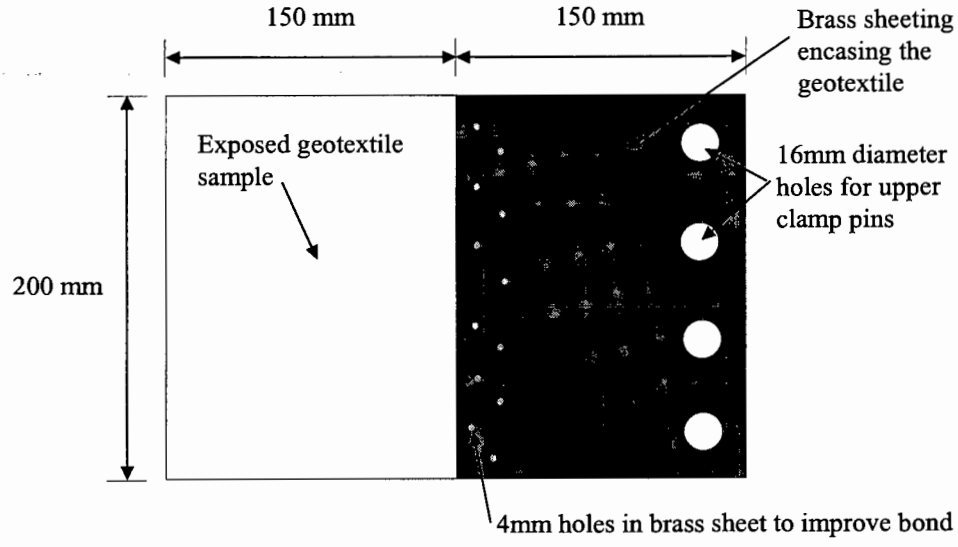

Figure 6-10: ***Schematic of a prepared pull-out test specimen***

Once the resin had hardened, the four 16 mm diameter holes were drilled through the brass sheet and geotextile to enable the specimen to be secured to the upper clamp with four steel pins (see also Figure 6-5).

The extensometer threads were then attached to the exposed geotextile surface either according to positions I or II as shown in Figure 6-11. By performing two identical pull-out tests, each with a different positioning of the extensometer, the displacement distribution along the geotextile, based on the three measuring points and clamp displacement, was evaluated (assuming that the behaviour of both specimens are identical).

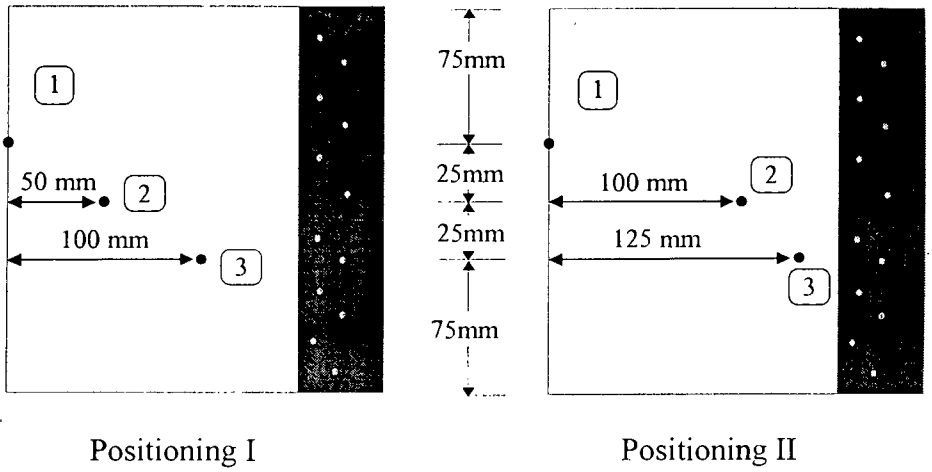

Figure 6-11: ***Displacement measuring points on the geotextile sample***

6.4 Pull-out test program

A total of 19 pull-out tests were undertaken with the geotextile embedded in Cape Flats sand. The variable in all the tests was the applied normal pressure which was varied between 25 and 225 kPa. The pull-out displacement of the geotextile in each test was applied at a rate of 10 mm/min. The dry density of the sand was targeted at 1630 kg/m^3 and a moisture content of 7% for all tests.

Every "standard" pull-out test was followed by a "control" test. The "control" test involved pulling only the brass plate (without the geotextile) out of the sand at the respective confining pressures, to determine the pull-out resistance offered by the brass only. By subtracting this force from the force measured in the standard test, the pull-out resistance offered by the geotextile itself could be determined. The "control" tests were also utilised to determine an adjustment required for the extensometer readings to account for friction forces between the threads and the sand as well as the pulleys. The extensometers were connected to the brass sheets and thus measured its displacement during the "control" test. These extensometer measurements were compared with the brass displacements measured by the Zwick testing machine and the difference between readings was applied accordingly to the geotextile displacement results. An assumption was also made that the brass was rigid and essentially did not deform during the tests. The full test program, which was carried out, is summarised in Table 6-2. "Control" tests are shaded for clarity.

Test Number	Type of Test	Normal Pressure (kPa)	Actual Dry Density (kg/m^3)	Extensometer Positions (distance from free end)
PO-01	Standard	25	1628	0 mm, 50 mm, 100 mm
PO-02	Standard	25	1628	0 mm, 100 mm, 125 mm
PO-03	Control (brass)	25	1636	
PO-04	Standard	65	1627	0 mm, 50 mm, 100 mm
PO-05	Standard	90	1625	0 mm, 100 mm, 125 mm
PO-06	Control (brass)	50	1636	
PO-07	Standard	125	1631	0 mm, 50 mm, 100 mm
PO-08	Standard	90	1627	0 mm, 50 mm, 100 mm
PO-09	Standard	95	1640	0 mm, 50 mm, 100 mm
PO-10	Control (brass)	95	1602	
PO-11	Control (brass)	95	1602	
PO-12	Standard	150	1626	0 mm, 100 mm, 125 mm
PO-15	Standard	225	1634	0 mm, 50 mm, 100 mm
PO-16	Control (brass)	225	1636	
PO-17	Standard	150	1627	0 mm, 100 mm, 125 mm
PO-18	Standard	105	1625	0 mm, 100 mm, 125 mm
PO-19	Control (brass)	150	1636	
PO-20	Standard	55	1638	0 mm, 100 mm, 125 mm

Table 6-2: ***Pull-out test program***

6.5 Pull-out test results

The data obtained in the pull-out tests was analysed and the results presented in the form of pull-out load versus clamp displacement diagrams. A detailed record of the movement of the free end of the geotextile is given and the distribution of the displacement along the geotextile in relation to the clamp displacement shown. A study of the influence of the confining pressure on the maximum shear stress and front end displacement is also presented.

6.5.1 Pull-out resistance versus clamped end displacement

The pull-out resistance was measured in a strain-controlled manner whereby the load cell readings were taken at displacement increments of 0.06 mm. From this data, three curves relating pull-out force with clamp displacement were obtained for each confinement. These are the pull-out load-clamp displacement relationships for the actual test (geotextile and brass), the control test (brass only) and geotextile only. A typical set of these curves is shown in Figure 6-12 for a test performed at a confining pressure (σ_n) of 90 kPa. The behavioural patterns shown in this figure are a typical representation of the results obtain from other tests. By subtracting the control test data (brass only) from the actual test data (geotextile and brass), the third curve is evaluated. This curve represents the relationship between the pull-out load response of the geotextile itself and the clamp displacement.

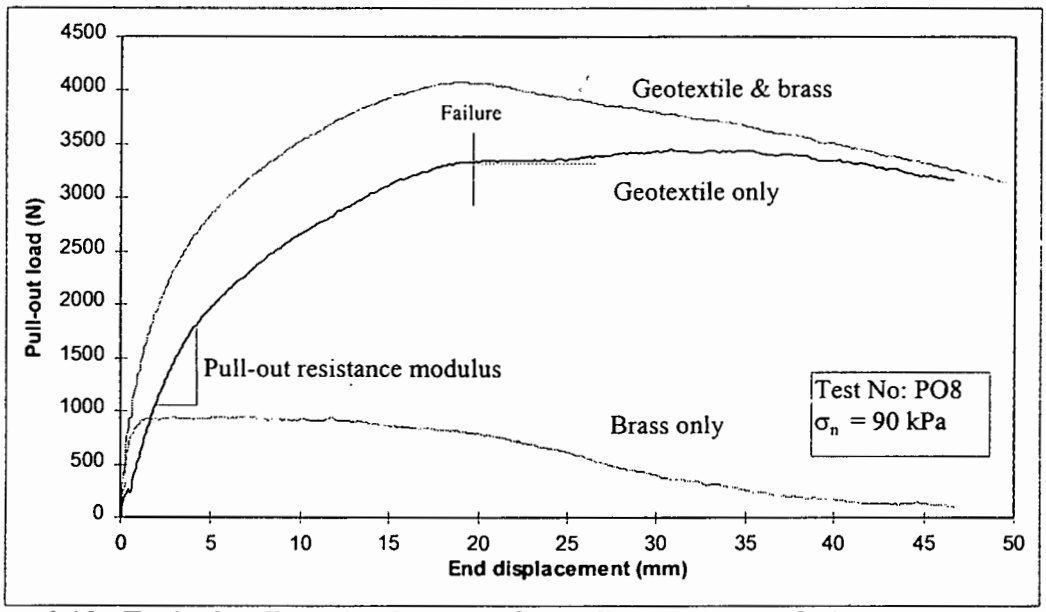

Figure 6-12: ***Typical pull-out load versus clamp displacement relationships (σ_n= 90 kPa)***

Clearly an approximately linear increase of the geotextile pull-out load with clamp displacement is the initial response. After about 4.5 mm displacement, the relationship becomes highly non-linear, which levels off to about 3.3 kN at about 20mm clamp displacement.

The rate of change of pull-out resistance with the clamp displacement is defined as the pull-out resistance modulus. At the beginning of the test, the pull-out resistance modulus is constant for all tests (i.e. the geotextile pull-out resistance increased in proportion to the clamp displacement). Thereafter, the pull-out resistance modulus decreases until a

constant pull-out resistance is attained. Failure is defined to take place when the pull-out load reaches a peak (i.e. the modulus becomes zero). For approximately 5mm after failure the sample holds the failure load, after which a slight increase in the pull-out load was observed.

This increase in the geotextile's pull-out resistance is only an apparent one and is a result of an occurrence which took place during the control tests. As soon as the clamp displacement was more than 25mm, sand particles around the brass sheet roll backwards into the void left behind by the displaced sheet. This caused pressure redistribution around the brass sheet and resulted in a reduced pull-out resistance offered by the brass. Thus, as the geotextile pull-out load is calculated, this decrease in the brass pull-out resistance causes an apparent increase in pull-out load offered by the geotextile itself. This phenomenon was observed in most tests.

The effect of confining pressure on the relationship between pull-out load of the geotextile and clamp displacement is shown in Figure 6-13. The graph shows the responses of 11 tests performed over a range of 8 different confining pressures. It would appear, from the spread of the results, that the adopted range of confining pressures covers the full spectrum of pull-out behaviour, with slippage failure at low confinements and rupture failure at high confinements.

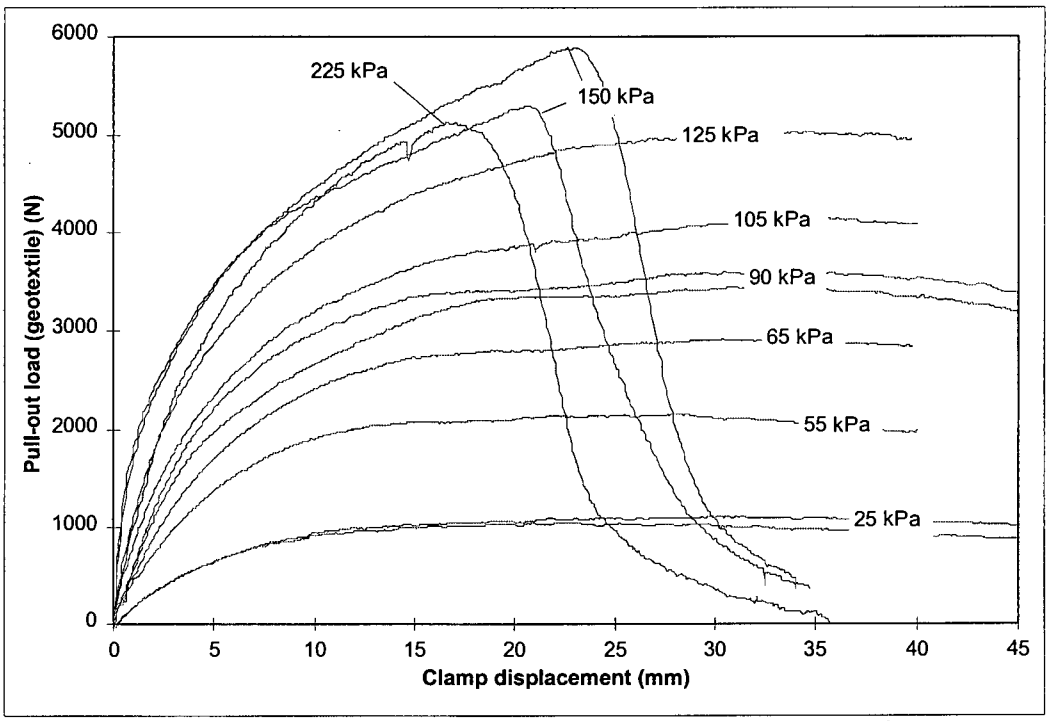

Figure 6-13: ***Effect of confining pressure on the pull-out load versus clamp displacement relationship***

From the chart it is immediately evident that the maximum pullout resistance of the geotextile increases as the confining pressure increases. Also, the pull-out resistance modulus before failure increases with an increase of the confinement.

The two, upper and lower limit failure modes, namely slippage and rupture failure, were observed during testing and it appears that the transitional stages in between have been well captured.

The samples for tests performed at confining pressures between 25 kPa and 125 kPa exhibited slippage failure. This type of failure is characterised by comparatively small changes in pull-out resistance after failure with relatively high clamp displacements. However, in tests where rupture of the geotextile occurred, the pull-out resistance decreased rapidly with clamp displacement. This can be seen in the results for the tests performed at confinements of 150 kPa and 225 kPa.

Comparing the rupture loads in confinement, one can notice that no significant increase in tensile strength of the geotextile was observed above a confinement of 150 kPa. It appears that at these high levels of confinement the ultimate "confined" tensile strength of the geotextile is reached at an average clamp displacement of 20mm. The average "confined" tensile rupture load from this geotextile in Cape Flats sand is 5.43 kN for a 200mm wide sample. This translates to an ultimate load of 27.15 kN per meter width of geotextile. The average in-isolation tensile rupture load of this non-woven geotextile, is approximately 22 kN per meter width of geotextile (see Section 5.4.2). Therefore, there is a 23% increase in rupture load of the geotextile material when it is highly confined in Cape Flats sand.

6.5.2 Necking of the geotextile specimen at various confinements

In Figure 6-14, the photographs of four geotextile samples after failure are shown for different confinements, namely for 25kPa, 90kPa, 125 kPa and 150 kPa. The lateral deformation of samples after failure, termed necking, are clearly visible for low, medium and high confinements. At a low confinements (25 kPa), the geotextile experiences a negligible amount of necking and as the confinement increases, necking also increases (90kPa, 125 kPa and 150 kPa). Unlike in-isolation conditions, the maximum amount of necking was concentrated near to the clamp. Very little lateral deformation was evident at the free end for any of the tests, indicating that the load carried at the free end of the geotextile was very low. No attempt was made to incorporate measurement of the necking into the analysis due to equipment limitations.

In rupture failure, the geotextile typically tears orthogonally near the front end of the geotextile samples. When rupture occurred, the free end of the geotextile did not move, and the entire clamp movement was due to the tearing of the material (see also PO17: 150 kPa).

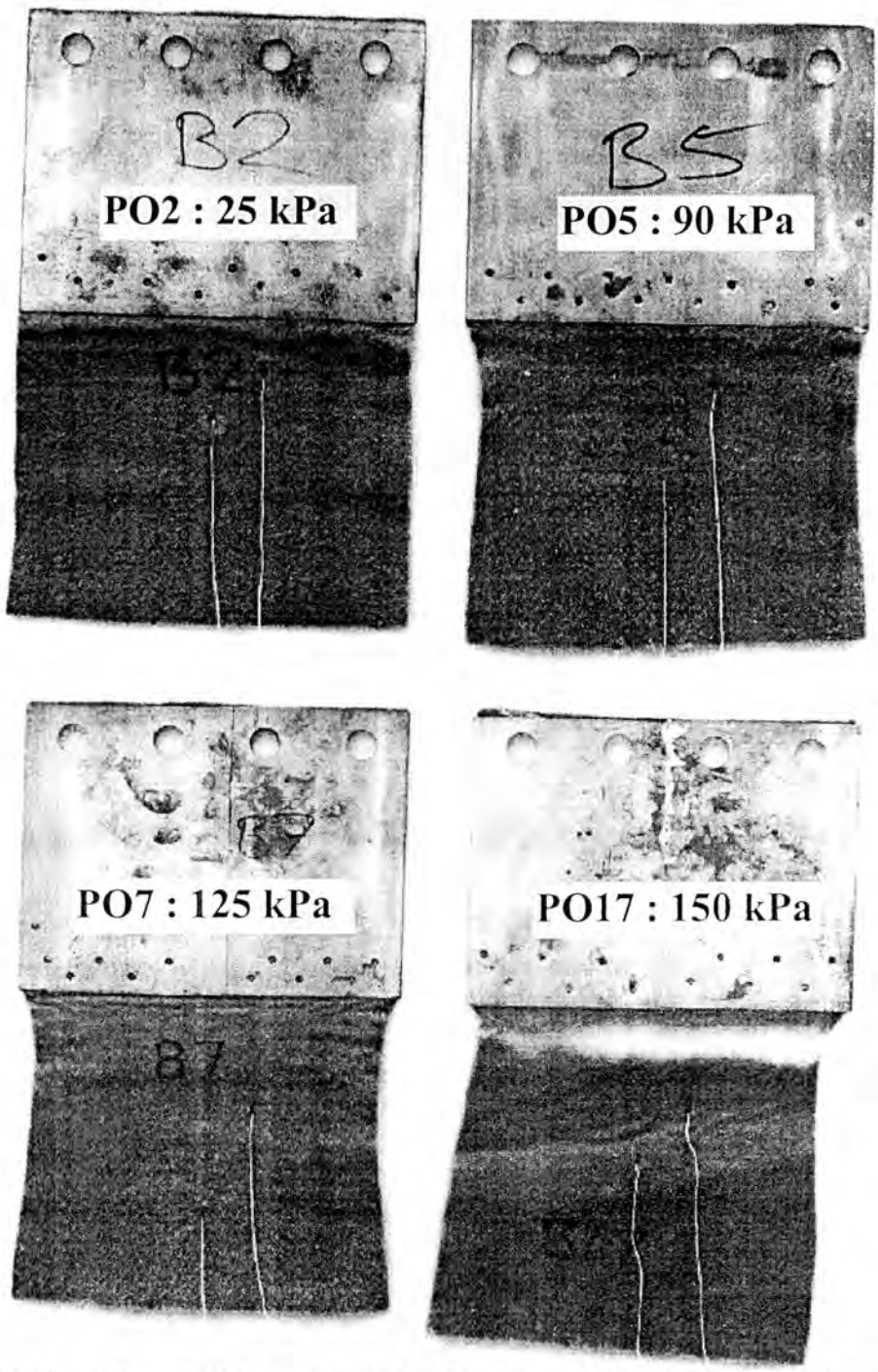

Figure 6-14: ***Failed geotextile samples after testing in the pull-out apparatus at various confinements***

6.5.3 Local displacement measurements along the geotextile sample

During the pull-out test, the displacement of specific points along each geotextile sample were monitored by means of the extensometers. The measurement technique and locations of the points are discussed in Section 6.3.

The displacements of the various points in the tests performed at medium confining pressures (55kPa and 90kPa), where slippage failure occurred, are plotted against the clamp displacement in Figures 6-15 and 6-16. These show the manner in which the geotextile displaced as the tests progresses. Because of the steel pins fixing the brass

sheets to the clamp, no slippage occurred at the clamp. Also the brass was assumed not to elongate and the clamp displacement was thus assumed to be equal to the displacement of the front end of the geotextile. The pull-out load versus clamp displacement in the respective test is plotted with the local displacements along the geotextile to show the association between the geotextile movement and the pull-out load.

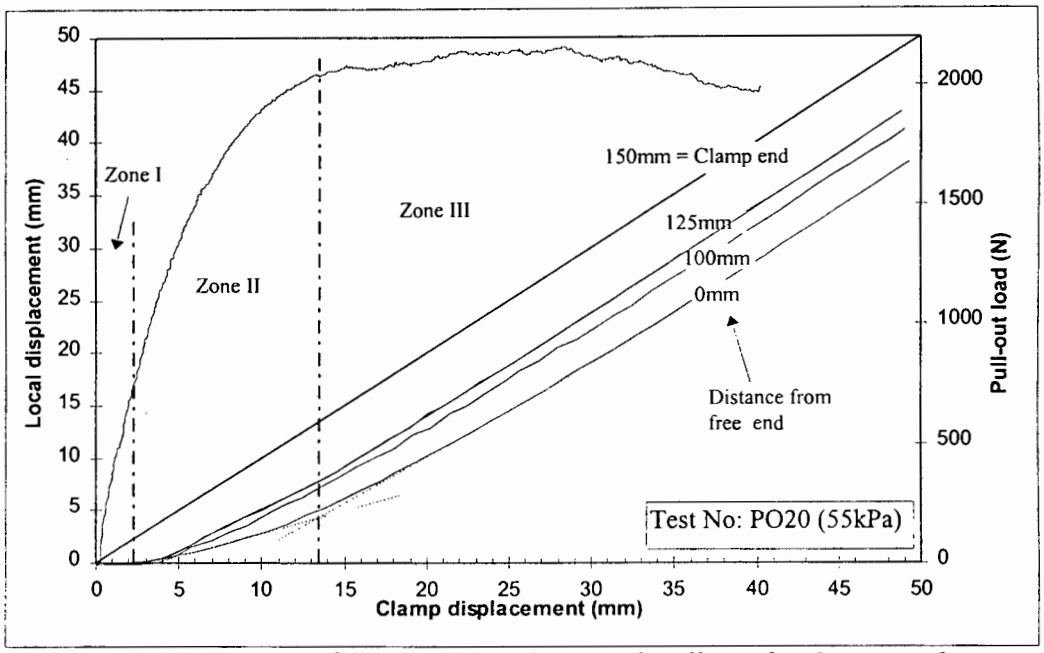

Figure 6-15: ***Displacement of geotextile sections and pull-out load versus clamp displacement (σ_n = 55kPa)***

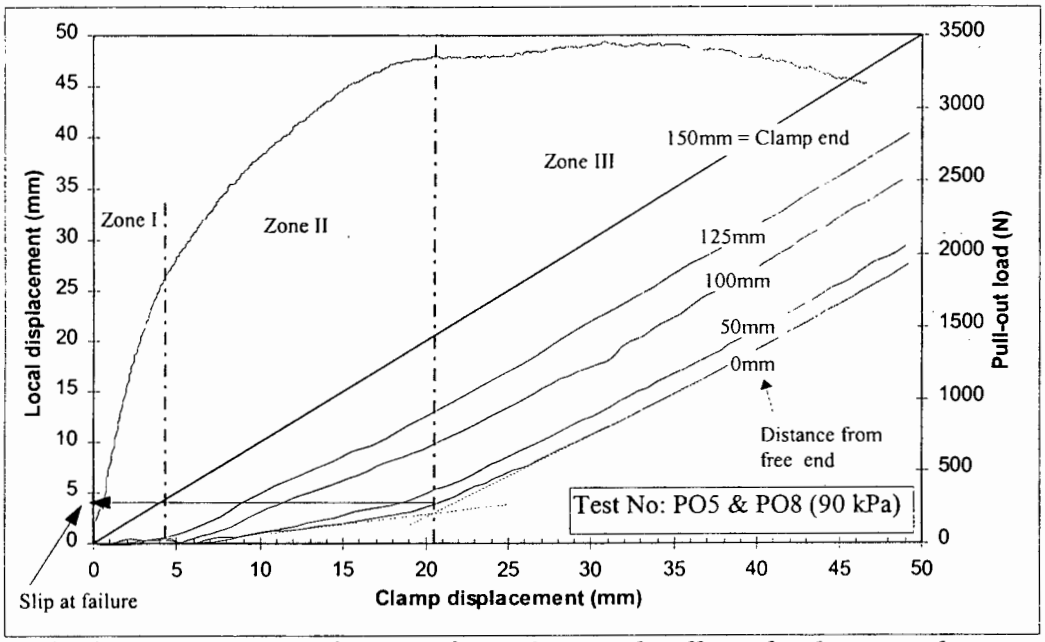

Figure 6-16: ***Displacement of geotextile sections and pull-out load versus clamp displacement (σ_n = 90kPa)***

Three characteristic behaviours in terms of the free end displacement of the geotextile during the pull-out tests can be identified. These behaviours are also reflected in the respective pull-out resistance modulus. In all tests it was observed that the free end of the geotextile did not move when the test started, although the clamp was displaced in a

controlled fashion. In fact, the load corresponding to a certain clamp displacement, in the order of 2mm to 9mm (depending on the confining pressure), was carried by the first 25mm of geotextile and the movement of the remaining geotextile was negligible.

In the tests at confining pressures of 55 kPa and 90 kPa, the free end started to move after a clamp displacement of 2.5mm and 5mm respectively. This period of zero displacement of the free end is defined as the Zone I.

Zone II marks out the region of steady movement at all sections of the geotextile up to a point where there is a clear and acute increase in the local displacement. The local displacement of the free end increases linearly in relation to the clamp displacement. As the failure load is approached, the displacement rate of the free end increases, until, after failure (indicated by the second vertical dashed line), the free end displaces in proportion to the clamp displacement.

Zone III is denoted as the region after failure and is characterised by a proportional increase of the free end displacement with the clamped end displacement. The ultimate pull-out load is essentially constant, as the geotextile is displaced as a whole.

In terms of the pull-out load, Zone I is characterised by a linear increase with clamp displacement. Once there is a free end displacement, the pull-out load drops off and the relationship becomes highly non-linear. In the test at 55 kPa confinement, the transition from Zone I to Zone II, in terms of the pull-out/clamp displacement relationship, is less pronounced.

The three zones were defined in a similar fashion in the tests at very high confining pressures, when rupture failure was experienced. In Figure 6-17 a typical example showing the local displacements as well as the pull-out load versus the clamp displacement is given. The test was performed at 150 kPa confinement.

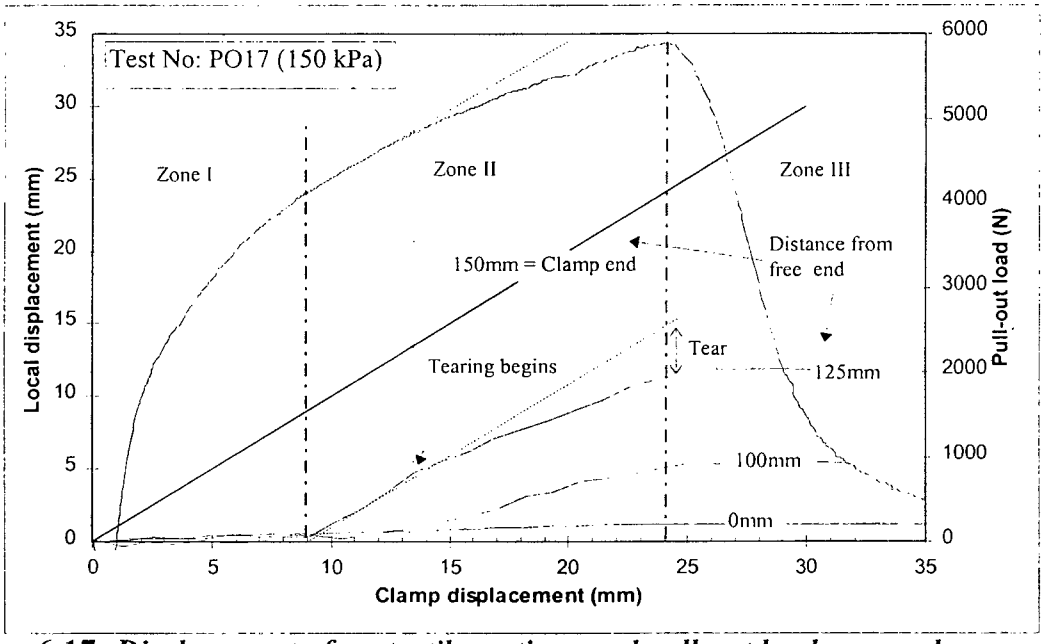

Figure 6-17: ***Displacement of geotextile sections and pull-out load versus clamp displacement (σ_n = 150kPa)***

Again, the first zone is defined by zero initial movement of the geotextile, i.e. the free end is practically not affected by the clamp displacement.

Zone II signifies the movement of the geotextile until rupture takes place. The movement of the clamp in this zone is characterised by the entire geotextile stretching, which can be seen by the increase on the movement of the geotextile at distances of 125mm and 100mm from the free end. The pull-out load versus clamp displacement relationship , in Zone II is bi-linear with a lower gradient occurring once tearing commences. Initially, the front 25mm of geotextile slides until the tensile load at this cross-section is too large to be carried by the geotextile. The increase in local displacement then drops off which indicates the start of the tearing of the geotextile.

Zone III occurs after the rupture of the geotextile, which takes place at the front of the sample, as is seen in the photograph in Figure 6-14. The rupture is represented by a zero increase of the local displacements. In terms of the pull-out load versus clamp displacement relationship, rupture is represented by the sharp drop-off after peak load. The termination in the movement of the geotextile due to tearing is gradual since the fibres of the material do not all tear instantly but progressively.

6.5.4 Distribution of displacement along the geotextile

In the Figures 6-15, 6-16 and 6-17 the kinematics at various cross-sections of the specimens are shown. However, the movement of the geotextile as a whole, at various stages during the pull-out test cannot be seen. Thus, in Figures 6-18 and 6-19, different graphs are given in which the displacement of the same four sections are plotted at five clamp displacements, namely at 5mm, 10 mm, 20 mm, 30 mm and 40mm. The pull-out loads related to these clamp displacements are also indicated. This plot was developed from the data in Figure 6-16 and 6-17 and thus shows the displacement distribution of the geotextile at confinements of 90 kPa and 150 kPa.

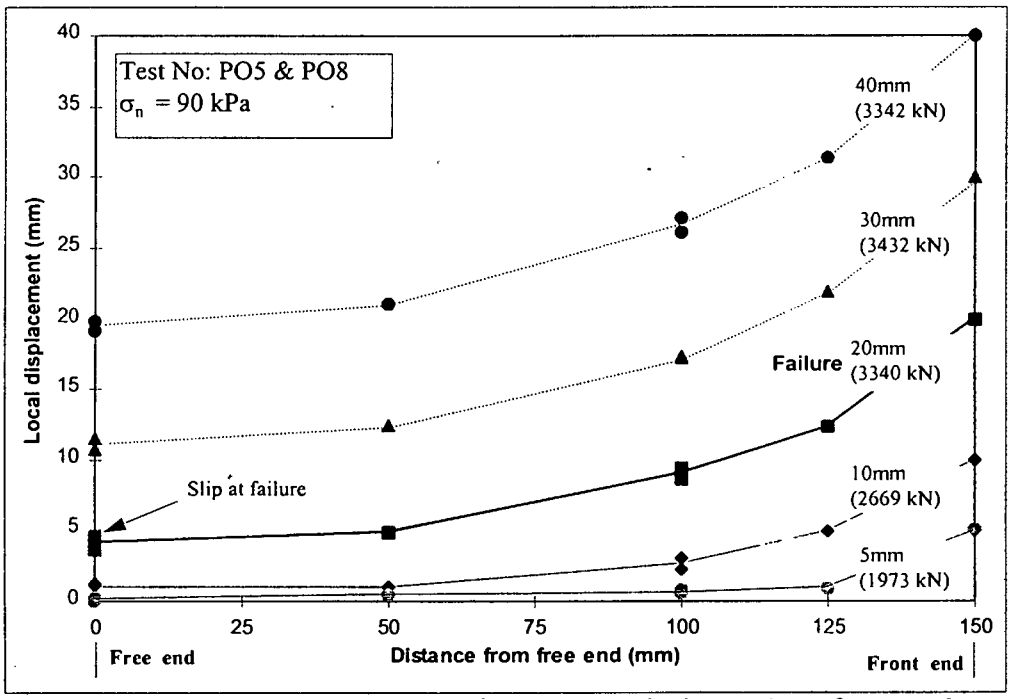

Figure 6-18: ***Displacement distribution of the geotextile for various front end displacements (σ_n= 90 kPa)***

The general displacement pattern for all stages of loading is a concave upward curved distribution with the lowest displacement occurring at the free end. The lowest line, depicting the displacement distribution at a clamp displacement of 5mm, clearly shows that the free end has not displaced yet while only the two front sections of the geotextile pick up the displacement. The remaining part of the sample undergoes minor straining. Since the geotextile has a linear stress versus strain relationship (see Section 5.4.3), the greatest stress is thus transferred to the sand at the front of the sample.

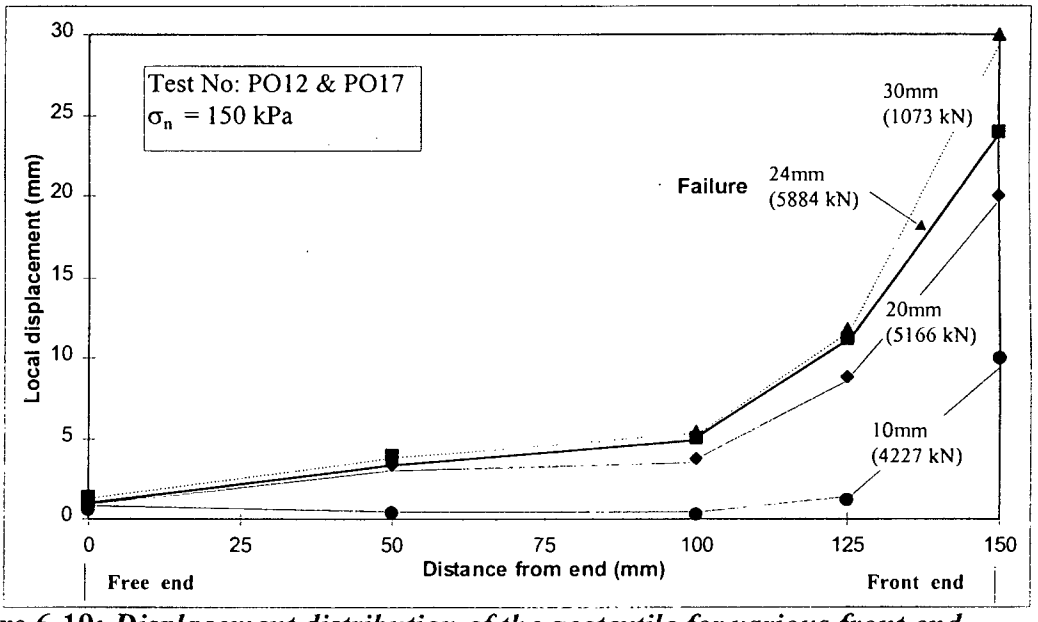

Figure 6-19: ***Displacement distribution of the geotextile for various front end displacements (σ_n= 150 kPa)***

It is seen here that at confinements where rupture failure occurs, the displacement of the geotextile is concentrated predominantly at the front of the sample, just behind the location where tearing takes place. The magnitude of displacement, experienced by the geotextile, drops off rapidly from this point as the free end is approached. After failure, which occurs at a front end displacement of 24mm, stretching of the geotextile was observed only along the front 25mm of the sample, indicating the tearing action at the front end. No movement of the free end occurred after failure.

6.5.5 Relationship between stretch and slip

The front end displacement of the geotextile sample comprises of two components. These are the slip and stretch of the geotextile. The slip is defined as the displacement of the free end and the stretch is the magnitude of elongation that the geotextile experiences during testing. The stretch of the geotextile was plotted against the slip in order to determine the relationship between the two displacement components. This relationship is shown in Figure 6-20 for a confining pressure of 90kPa.

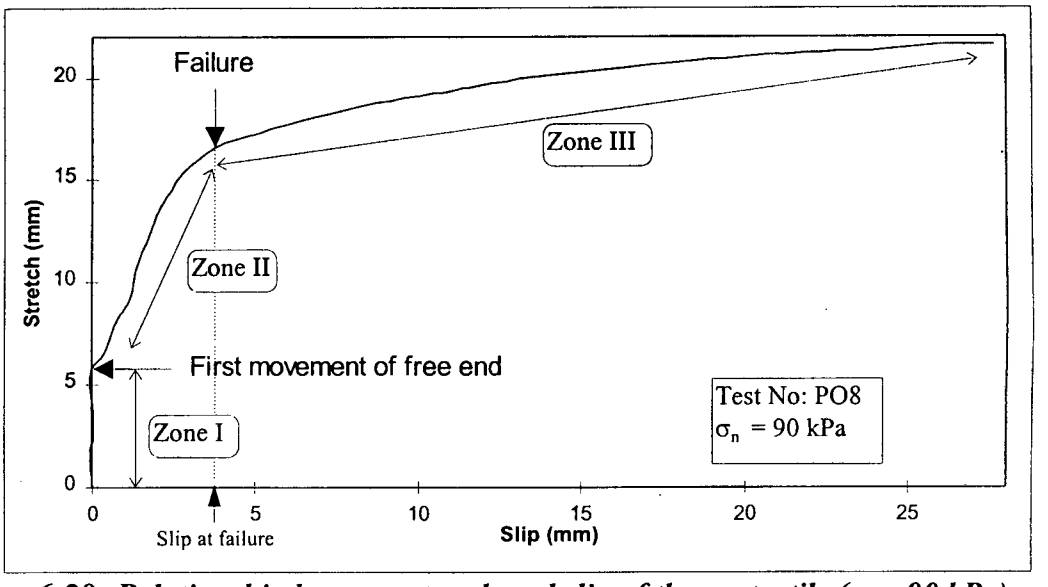

Figure 6-20: ***Relationship between stretch and slip of the geotextile (σ_n= 90 kPa)***

The typical pattern of slip and stretch is shown with the three characteristic zones as was previously identified. The geotextile initially stretches by approximately 5 mm upon loading before any movement of the free end (i.e. slip) takes place. Thereafter, a combined stretch and slip movement (at a ratio of about 2 : 1) is observed until failure takes place. Beyond the ultimate load the movement of the geotextile is due predominantly to rapidly increasing slip movement with comparatively very little stretching of the geotextile taking place.

The relationship between stretch and slip of the geotextile was found to be significantly influenced by the confining pressure. In Figure 6-21 the stretch and slip responses for the confining pressures employed in the various pull-out tests are shown.

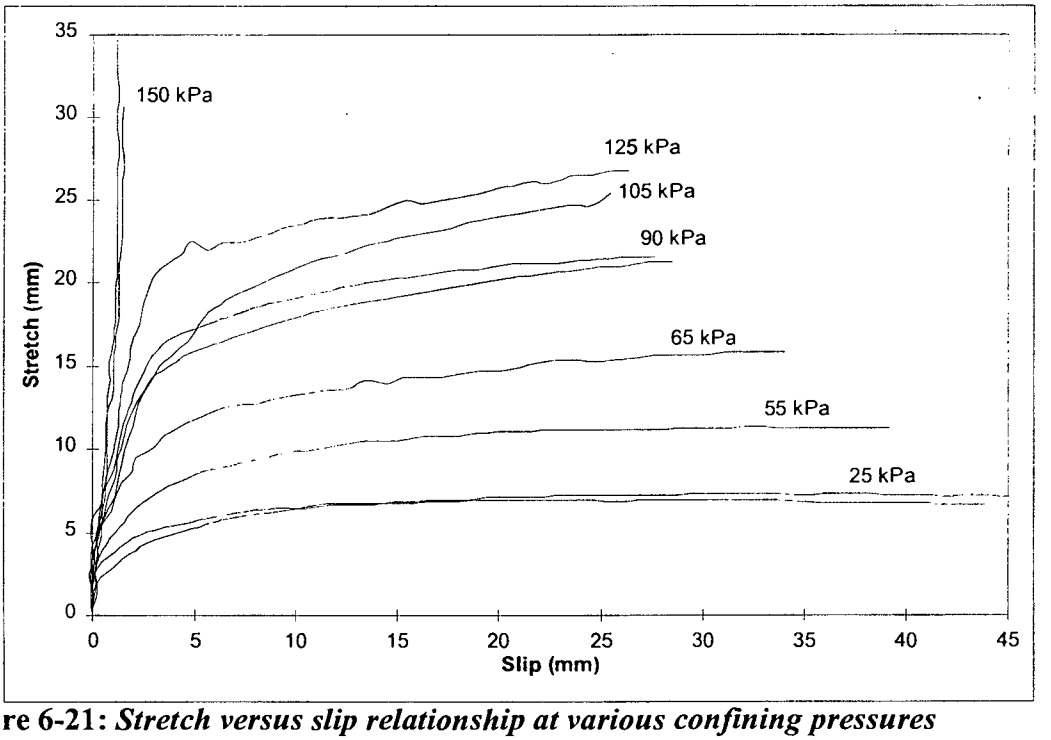

Figure 6-21: ***Stretch versus slip relationship at various confining pressures***

Two clearly different stretch/slip behaviour groupings can be identified, a curved interrelationship and a relatively linear one. At confinements of up to 125 kPa, slippage failure is observed, characterised by significant amounts of both stretch and slip during the test. On the other hand, a highly confined geotextile (at 150kPa) fails due to excessive stretching and tearing, with very little slippage occurring (rupture failure). The photographs in Figure 6-14 support this observation. Also, it was also noted that the total slippage of the geotextile during the test reduces as the confining pressure increases. The amount of stretch occurring after failure increases at higher confinements, but remains a fraction of the amount of slip occurring at this portion of the load history.

6.5.6 Influence of confining pressure on the maximum average interface shear stress

The maximum average interface shear stress is defined as the average shear stress across the sand/geotextile interface at failure. To determine this stress value, the average interface shear stress across the sand/geotextile interface was first calculated for each front end displacement to find the maximum average shear stress magnitude. The average shear stress was assumed to act over the entire surface of the interface and was thus calculated by dividing the geotextile pull-out load by the area of contact between sand and geotextile. i.e.:

$$\text{ave}\,\tau_i = \frac{P_g}{A_s} \qquad \text{..... (6-1)}$$

where

$\text{ave}\,\tau_i$ = Average interface shear stress across the entire sand/geotextile interface
P_g = Pull-out load of the geotextile
A_s = Area of contact between the sand and geotextile

The change in the area of contact between the sand and geotextile due the elongation of the sample was considered. Although necking of the geotextile sample did occur, it was experimentally not possible to determine the magnitude of this lateral deformation and the associated change in area. Thus, when calculating the area of contact, the reduction in area due to necking effects are ignored. The contact area was therefore calculated as follows :

$$A_s = W \cdot (L_o + \Delta l) = W \cdot (L_o + u_c - u_{fe}) \qquad \text{..... (6-2)}$$

where

A_s = Area of contact between sand and geotextile
W = Original width of the sample (200mm)
L_o = Original length of the sample (150 mm)
Δl = Elongation ($= u_c - u_{fe}$)
u_c = Clamp displacement (displacement of the front end of the sample)
u_{fe} = Displacement of the free end (or slippage)

A limitation to this method does exist, in that the interface shear stress is assumed to be distributed uniformly across the entire area of the geotextile. It was, however, suggested by Solomone et al. (1980) that, at failure, the interface shear stress is acting across the entire sand/geotextile interface. Assuming the maximum average interface shear stress occurs at failure, this conservative approach (Equation 6.2) can be used to determine this maximum shear stress value.

The maximum shear stress for each test was plotted against the respective confining pressure of the test, shown in Figure 6-22. The specific failure modes (slippage and rupture failure) experienced in the test are represented by different symbols.

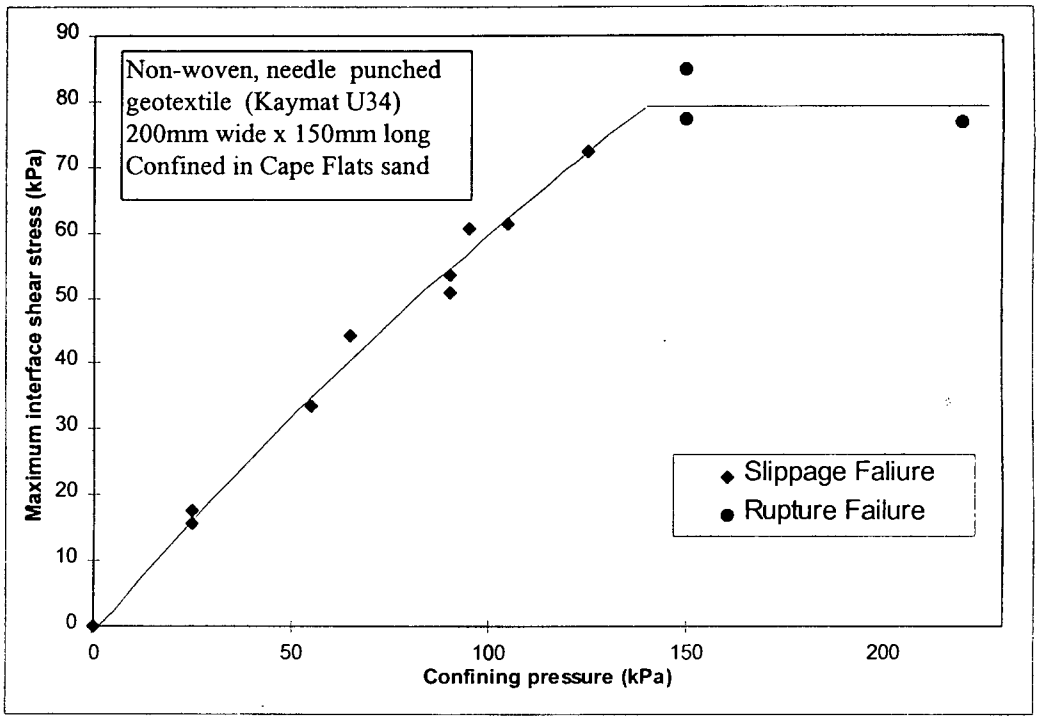

Figure 6-22: ***Influence of confining pressure on the maximum average shear stress at the sand/geotextile interface.***

The relationship between the maximum interface shear stress and confining pressure can be described as initially being linear up to approximately 50 kPa above which the gradient decreases. A limiting stress of about 80kPa is reached at a confinement of 140 kPa where the actual maximum interface shear stress between the sand and geotextile equals the tensile stress required to tear the fabric when confinement in sand. At higher confinements, the geotextile therefore ruptures before slippage can occur.

When rupture failure occurs, the maximum average interface shear stress is not a measure of the frictional force between the sand and geotextile at failure, but is actually the maximum tensile stress that the geotextile can withstand under confinement. The rupture failure data points consequently depict the tensile rupture load of the geotextile when confined in sand.

6.5.7 Influence of confining pressure on the front end displacement at failure

An important parameter in the design of geotextile reinforced structures is the magnitude of the front end displacement at failure. The maximum average shear stresses at the sand/geotextile interface is fully mobilised only once the front end of the geotextile sheet has undergone this specific displacement. This measure can be established from pull-out test results with ease. This particular front end displacement is plotted in Figure 6-23, at the various confining pressures employed in the pull-out tests. The displacement of the free end at failure is also plotted on the chart.

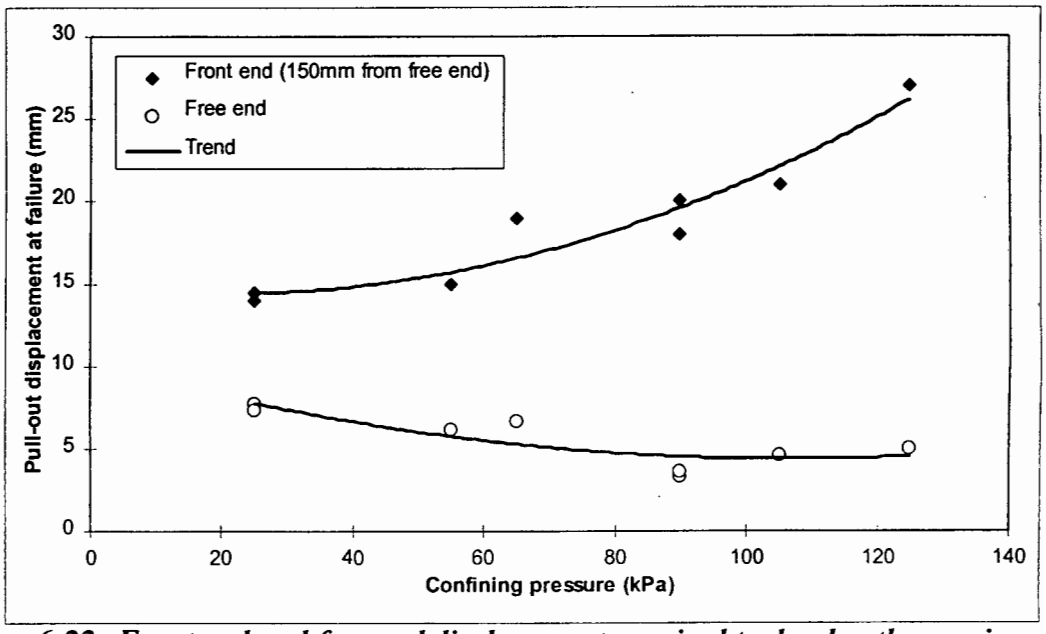

Figure 6-23: ***Front end and free end displacement required to develop the maximum average shear stress for various confining pressures***

From the chart it is seen that, the front end displacement required to mobilise the maximum average shear stress increases non-linearly with confining pressure. The trends of this data are represented by the solid black lines, which were obtained from least square regression analyses.

The data points at a confinement of 65 kPa do not fit into the pattern. It was found that in this specific test the dry density of the sand was unusually high (i.e. 1640 kg/m^3) compared with the target dry density of 1630kg/m^3. It therefore appears that, for an increase in the sand density, the sand/geotextile interface requires an increased front end displacement to fully develop the average shear stress across the interface. Also, in that specific test, the free end displacement at failure was affected in a similar manner.

6.5.8 Influence of confining pressure on the combined stiffness of the geotextile and sand at failure

The stretch at failure was determined for each test based on the front end and free end displacement (Figure 6-23). Since the geotextile has a linear stress-strain relationship (see Section 5.4.3), the stretch of the geotextile is proportional to the stiffness. The combined "stiffness" of the geotextile and sand for various confinements could thus be estimated at failure in the following manner. By extrapolating the measured stretch of the geotextile at failure, a stretch of 4.96 mm at zero confinement was calculated. The stretch measurements at each confinement were then increased proportionally such that the stretch at zero confinement was equal to the unconfined geotextile stiffness value (21 MPa), determined in the unconfined tensile tests (see also Section 5.4.3). The estimated combined "stiffness" of the geotextile and sand, at failure, for the various confinements is plotted in Figure 6-24.

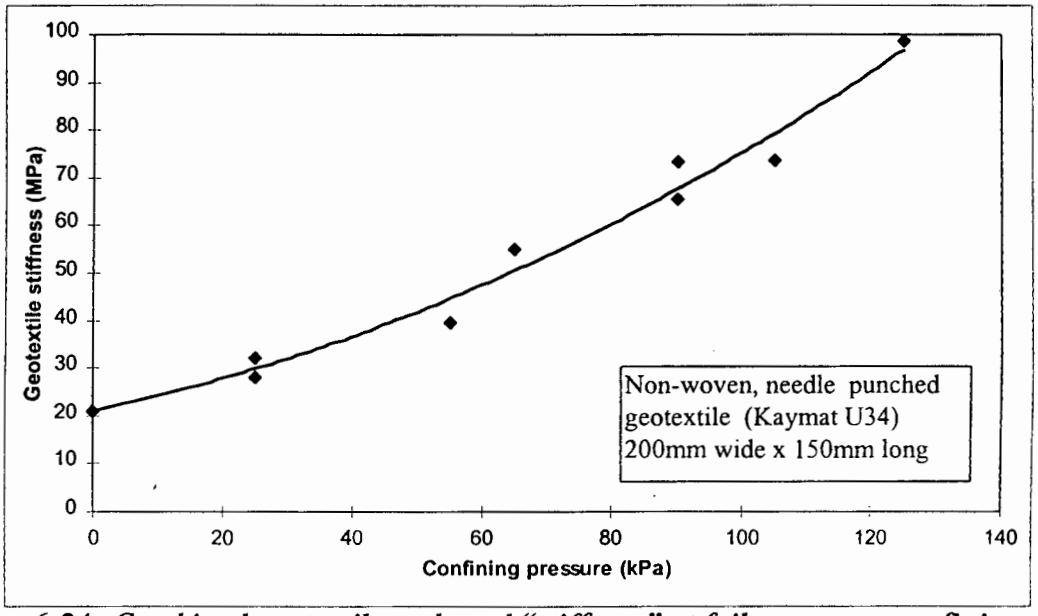

Figure 6-24: ***Combined geotextile and sand "stiffness" at failure versus confining pressure***

It was found that the "stiffness" of the sand/geotextile combined increased non-linearly with confining pressure. This result was verified in the finite element analysis which is described in Chapter 9. The relationship is very useful in determining geotextile stiffness values for serviceability design calculations (see Section 2.3), if the assumption is made that the stiffness behaviour of geotextile sheets is the same on a field scale.

Chapter 7
Laboratory Direct Shear Tests on the Sand/Geotextile Interface

In the previous chapter the pull-out responses and thus the friction parameters for a sand/geotextile interface were determined. It is expected that the loading results realistically predict the full-scale behaviour, since a geotextile experiences pull-out in actual reinforcement applications . However, the British code of practice for geosynthetic reinforced soil structures, BS 8006 (1994), specifies that direct shear tests are undertaken to determine the sand/geotextile friction parameters for design. It was thus desirable to compare the frictional parameters obtained from the pull-out tests, with those from direct shear tests in terms of the friction coefficient and the interface shear stress development as a whole. There has also been some doubt expressed as to whether the direct shear test is a realistic simulation of the reinforced soil mechanism and whether it yields valid quantities for the friction parameters (Kharchafi and Dysli, 1993). This doubt is expressed because the geotextile remains unstressed during direct shear testing, while, in the field, the geotextile is highly stressed.

By comparing the friction parameters obtained from direct shear tests with those from the pull-out tests, some clarification about the adequacy of the test method for investigating the soil-geotextile interface is expected.

7.1 Direct shear test equipment

The direct shear tests on the sand/geotextile interface were performed in the Wykeham Farrance SB1 constant rate of strain shear box, as is shown in Figure 7-1. Although this equipment is usually associated with the testing of soil materials, it has been used in this study to determine the soil-geotextile shear parameters in direct shear conditions.

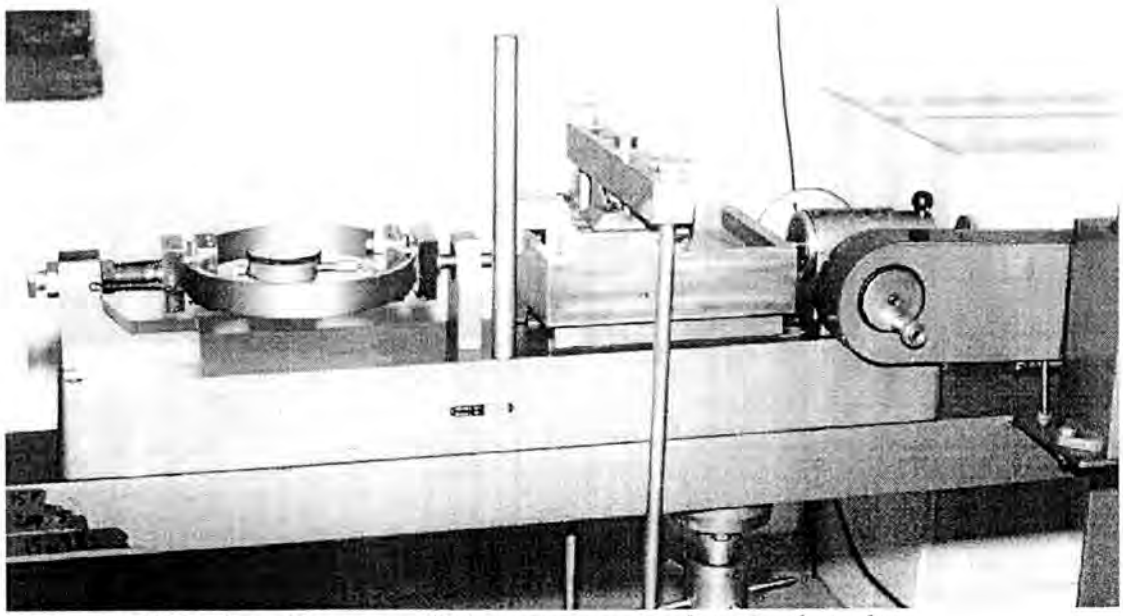

Figure 7-1: ***Wykeham Farrance SB1 constant rate of strain shear box***

The test involved displacing a sand sample, subject to uniform vertical pressure along the surface of a geotextile sheet. The horizontal load developed between sand and geotextile was measured and the interface shear stress acting between the two surfaces determined. A vertical load was applied to the soil mass via a loading cap and a hanger to induce a normal pressure on the geotextile. Tests were performed at different normal pressures to investigate the effect on the interface shear behaviour.

The box is split horizontally in two as is schematically shown in Figure 7-2. The geotextile was placed in the lower half of the box at the level of the shear face while the sand was compacted in the upper half of the shear box. Shear forces generated due to the relative displacement of the two surfaces were measured with the proving ring.

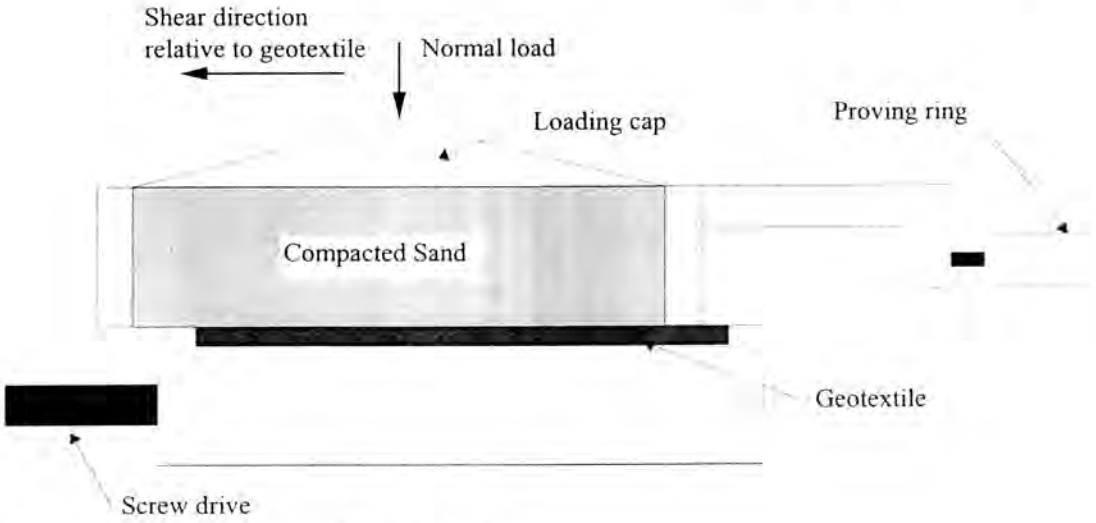

Figure 7-2: ***Schematic of the shear box***

Two test arrangements were employed to determine direct shear friction parameters for the sand/geotextile interface. The first involved compacting sand into the top half of the 100 mm x 100 mm shear box and shearing it over a 100 mm x 100 mm geotextile sample. However, boundary effects, caused by interaction between the edges of the geotextile and the frame, influenced the test results. The set-up is shown in Figure 7-3. Due to the compressible nature of the geotextile, it was found to be difficult to keep the geotextile aligned with the shear face. In the second test arrangement, the soil was compacted into the upper half of a 60 mm x 60 mm shear frame. This smaller upper shear frame was placed inside a 100mm x 100mm upper shear frame and sheared over a 100 mm x 100 mm geotextile sample, shown in Figure 7-3. This eliminated the boundary effects and facilitated a constant area of contact between sand and geotextile throughout the test.

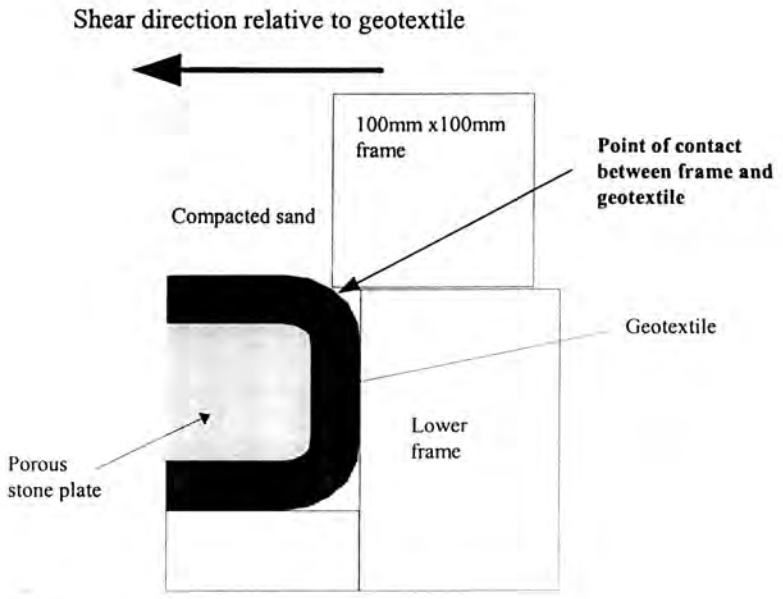

(a) Test arrangement with 100mm x 100mm shear box

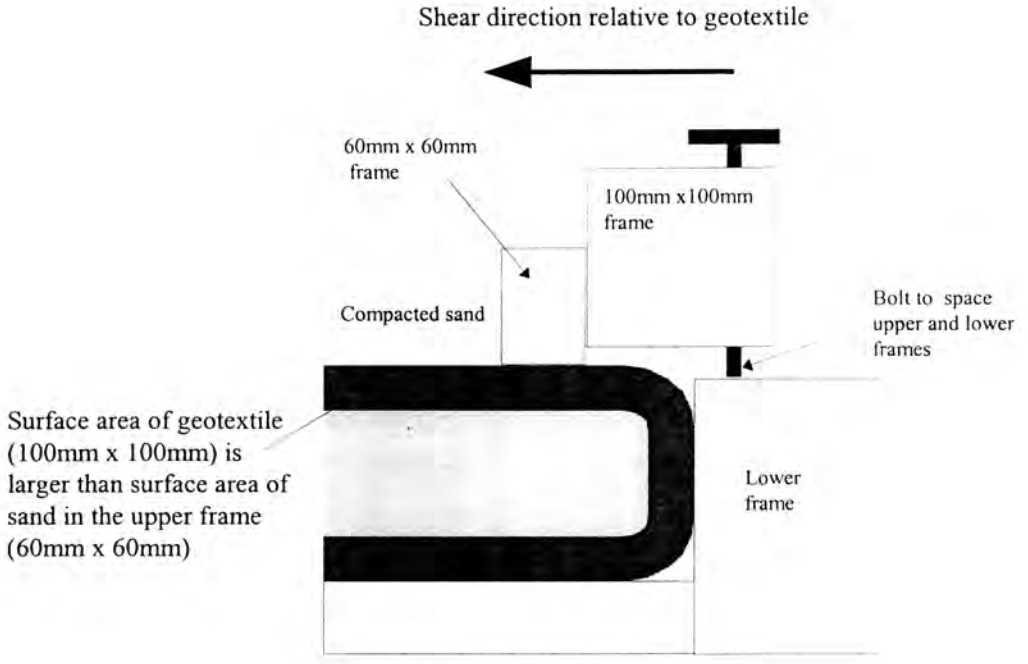

(b) Test arrangement with the 60mm x 60mm upper shear frame on a 100mm x 100mm geotextile

Figure 7-3: ***Comparison of the two test arrangements***

7.2 Direct shear test procedure

The procedure for performing the 14 direct shear tests is briefly outlined.

The Cape Flats sand was mixed with water to a moisture content of 7% and with the geotextile sample already in place, compacted into the upper shear frame. Compaction was achieved with a small hand compactor and was aimed at a dry density of approximately 1630 kg/m^3. The shear box was then placed into the carrier and the respective normal pressure was applied. Shearing was performed at a rate of 0.61 mm/min (0.024 inches / min).

Three corrections to the results obtained from the shear tests were required. Two adjustments involving the displacement measurements while the third one was applied to eliminate the frictional force of the steel frame itself.

In terms of direct shear testing, the shear displacement is defined as the relative displacement of the geotextile surface to the sand surface. The use of the displacement of the screw drive is not an accurate measure of the shear displacement, because the proving ring experiences a certain horizontal compression to indicate the horizontal load. In Figure 7-4, these shear displacements are schematically indicted. A correction of the shear displacement calculated based on the displacement rate of the screw drive was thus applied.

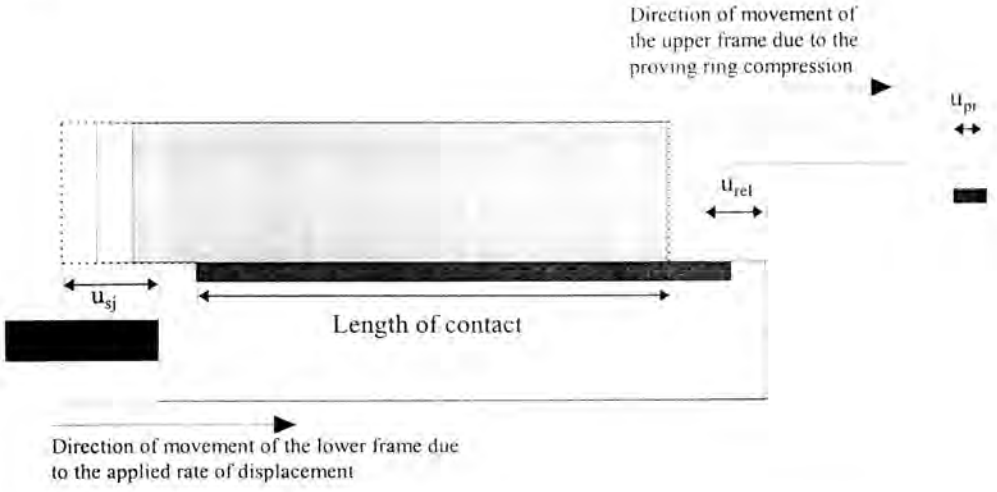

Figure 7-4: ***Schematic of the various shear displacement measures***

The actual shear displacement, u_{rel}, was determined by subtracting the proving ring compression measurement, u_{pr}, from the displacement of the lower frame, u_{sj}, as follows:

$$u_{rel} = u_{sj} - u_{pr} \qquad \text{..... (7-1)}$$

where

u_{rel} = relative (or corrected) shear displacement
u_{sj} = displacement of the screw jack (i.e. of the lower half of the box)
u_{pr} = displacement of the proving ring

$$A_{corr} = W \cdot (L - u_{rel}) = W \cdot (L - u_{sj} + u_{pr}) \qquad \text{.....(7-2)}$$

where

A_{corr}= corrected shear area
W = width of the shear box
L = length of the shear contact

The third correction, which was applied in both test arrangements, involved the friction force introduced by the upper frame sliding on the geotextile. A portion of the applied vertical load on the sand was transferred to the sand/geotextile interface through the upper frame due to side friction of the sand contained in the frame. An additional friction force therefore developed between the geotextile and frame. This additional force, which is included in the force measured by the proving ring is not indicative of the sand/geotextile interface. The vertical force transferred though the frame was calculated as being approximately 10% of the applied vertical load (based on elastic half space considerations). The vertical force transmitted to the frame, for a total normal pressure of 250kPa, was placed on an "empty" frame. The frame was then moved over the geotextile sample and the force recorded at the same displacement rate as was applied during the direct shear tests.

The friction force between the "empty" frame and geotextile was found to be consistent for the full range of shear displacements encountered. Values of 42 N and 33 N were measured for the 100mm x 100mm and 60mm x 60mm shear boxes respectively (at 250kPa). This friction force was proportioned according to the confining pressure applied in each test (assuming a linear relationship) and subtracted from the frictional force indicated by the proving ring. Consequently, the interface shear stress was calculated as:

$$\tau_i = \frac{P_{corr}}{A_{corr}} \quad \text{for the 100mm x 100mm test arrangement}$$

or

$$\tau_i = \frac{P_{corr}}{A} \quad \text{for the 60mm x 60mm test arrangement} \qquad \text{.....(7-3)}$$

where

τ_i = interface shear stress
P_{corr} = corrected shear force between the sand and geotextile
A_{corr} = corrected shear area (contact area between sand and geotextile)

7.3 Direct shear test program

A total of 14 direct shear tests were undertaken at normal pressures ranging from 50 kPa to 350 kPa. There were 8 tests performed in the 100mm x 100mm shear box (Figure 7-3a) and 6 in the 60mm x 60mm shear box (Figure 7-3b) as listed in Table 7-1. Although tests SH-A1 to SH-A8 exhibited boundary effects, it is believed that these effects did not significantly influence the peak interface shear stress. These test results are also included when the maximum interface shear stresses were considered (see Section 7.4.2).

significantly influence the peak interface shear stress. These test results are also included when the maximum interface shear stresses were considered (see Section 7.4.2).

Test Number	Test Arrangement	Normal Pressure (kPa)	Remarks
SH-A1	100 mm upper frame	50	↑ Boundary Effects ↓
SH-A2	100 mm upper frame	100	
SH-A3	100 mm upper frame	100	
SH-A4	100 mm upper frame	150	
SH-A5	100 mm upper frame	150	
SH-A6	100 mm upper frame	250	
SH-A7	100 mm upper frame	250	
SH-A8	100 mm upper frame	250	
SH-B1	60 mm upper frame	50	↑ No Boundary Effects ↓
SH-B2	60 mm upper frame	50	
SH-B3	60 mm upper frame	100	
SH-B4	60 mm upper frame	100	
SH-B5	60 mm upper frame	250	
SH-B6	60 mm upper frame	350	

Table 7-1: ***Direct shear test program***

7.4 Direct shear test results

The results obtained from the direct shear tests of the sand/geotextile interfaces are presented. The development of the interface shear stress with shear displacement is described for tests performed with the 60mm x 60mm box arrangement. Also, a relationship between the maximum interface shear stress and normal pressure was established which is presented for both the 60mm x 60mm and 100mm x 100mm shear box tests.

7.4.1 Development of interface shear stress with shear displacement

In Figure 7-5 the interface shear stresses, calculated using Equation 7-3, were plotted against the shear displacement for four different normal pressures. These results were derived from the 60mm x 60mm shear box test data.

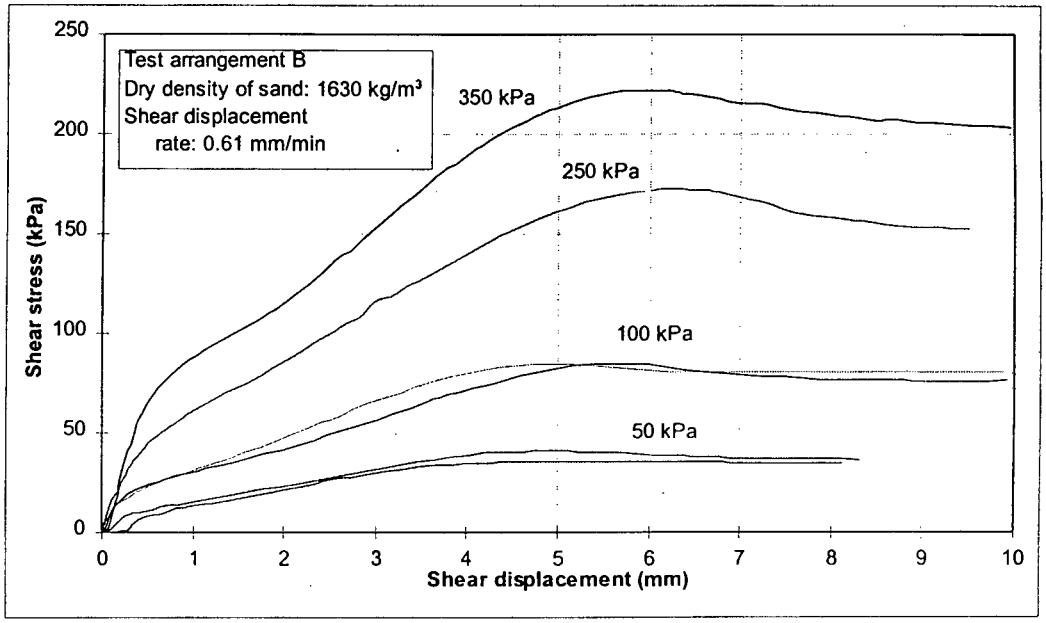

Figure 7-5: ***Interface shear stress development at various normal pressures***

It was observed that the interface shear stress developed in 3 distinct zones, bounded by specific shear displacements. Initially the interface shear stress increased linearly with shear displacement and at a similar rate for all normal pressures (except for 50 kPa normal pressures). In this zone it is postulated that the individual fibres on the geotextile surface are being re-oriented in the direction of shear. When a shear displacement of approximately 5mm is reached, the surface fibres are thought to be lying parallel to one another. The shear resistance offered by the random orientation is then reduced and the rate of increase of interface shear stress drops slightly. At this point the second zone is entered. The interface shear stress in this zone increases generally in a fairly constant manner because there is very little change in the nature of the interface. The interface shear stress increases until it eventually reaches the limiting interface shear stress (τ_{max}) that can be sustained by the sand/geotextile interface. At this shear displacement, failure has occurred. This defines the start of the third zone where the interface shear stress decreased to a residual value which was between 88% and 95 % of the maximum interface shear stress.

From Figure 7-5, it can also be seen that the rate of development of interface shear stress with shear displacement increases as the normal pressure increases.

7.4.2 Influence of confining pressure on the maximum interface shear stress

The maximum interface shear stress calculated for each test was compared with the normal pressure applied (σ_n) in the respective test and the results shown in Figure 7-6. Test results obtained using the 60mm x 60mm shear box as well as the 100mm x 100mm shear box are shown.

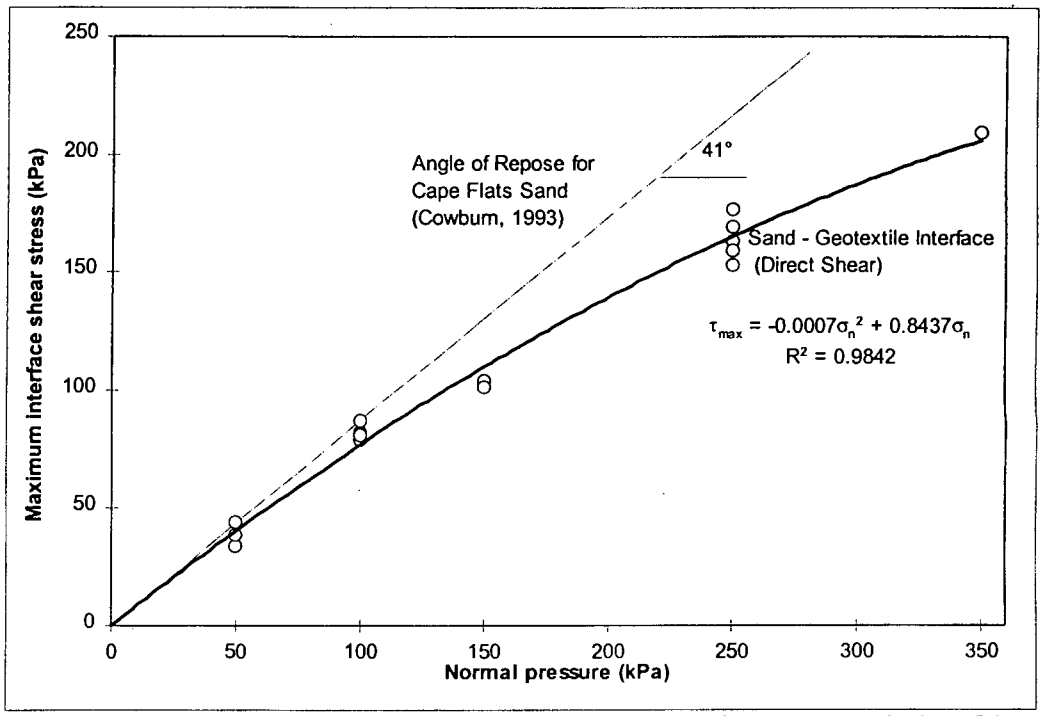

Figure 7-6: ***Maximum interface shear stress versus normal pressure relationship***

A curve drawn connecting the various test results and passing through the origin presents the τ_{max} - σ_n relationship which appears to be non-linear. The trend curve, shown in the figure, is a 2nd order polynomial which was fitted to the data using a least squares regression. The index of determination (r^2) from the regression is 0,98. Assuming a non-linear τ_{max} - σ_n relationship, the friction coefficient is thus not constant for various confining pressures for this specific sand/geotextile combination in direct shear conditions.

However, some researchers have obtained a constant friction coefficient from direct shear testing (Myles, 1982) with sands and geotextiles different to that employed in this study. This therefore indicates, that the linearity of τ_{max} - σ_n relationship, obtain from direct shear tests, is influenced greatly by the combination of soil and geotextile in consideration.

The direct shear strength of Cape Flats sand, obtain by Cowburn (1993), is plotted in the Figure 7-6 for comparison. To relate these results to the sand/geotextile interface behaviour, it can be assumed that at normal pressures below 100 kPa, the sand/geotextile friction angle is approximately equal to the friction angle of the sand of 41°. However, at normal pressures above 100 kPa, the sand/geotextile friction angle is somewhat less. In general, it can be said that, the shear strength of the sand/geotextile interface is less than the shear strength of the sand .

7.4.3 Displacement required to mobilise the maximum interface shear stress

The shear displacement measured at failure is the displacement required to completely mobilise the interface shear stress. In Figure 7-7, these shear displacements are plotted against the various normal pressures. The triangles represent results from tests using the 100mm x 100mm shear box and the circles represent results obtained from the 60mm x

60mm shear box arrangement. In all the tests, the shear displacement at failure was between 4.8 mm and 6.9 mm (See also Figure 7-5).

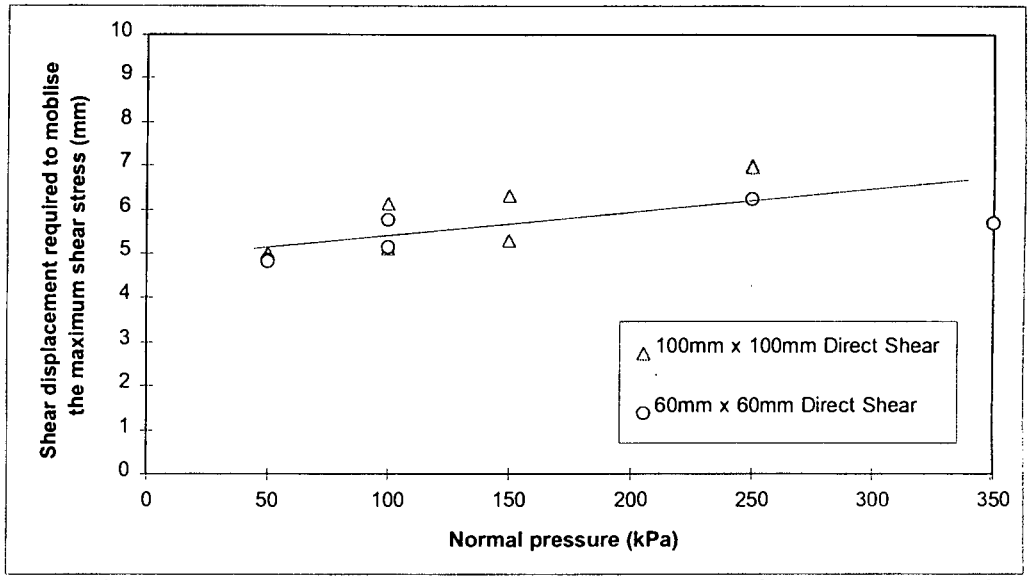

Figure 7-7: ***Shear displacement required to mobilise the interface shear stress for various confining pressures***

There is an experimental scatter, but the data points fall within a relatively narrow range of 3mm. There appears to be a clear trend in that the shear displacement required to mobilise the maximum interface shear stress increases slightly with confining pressure. These shear displacements were however not influenced by the size of the two shear areas investigated. Also the boundary problems had no effect on the test results, since they occurred only at initial shear displacements.

Chapter 8
Finite Element Analysis of Pull-out Tests

Finite element modelling is a numerical technique which has been implemented very successfully in the past to model various geotechnical interaction problems (Desai and Christian, 1977). It is useful as is provides detailed analyses of stress and strain distributions within complex systems where measurement of these values is difficult. Laboratory tests may be simulated with finite element techniques which greatly aid in the understanding of the processes experienced in these tests. Various material and interaction analysis models can be employed and results compared with actual experimental data.

A finite element model was developed to simulate the laboratory pull-out test (PO8, σ_n =90kPa), as described in Chapter 6. The analysis was performed using ABAQUS, a multi-purpose commercial finite element package. An input deck, containing the model description, is read by the analysis program. The response of the sand, geotextile and interface to loading is then obtained from an incremental solution procedure. Results can be viewed with relative ease by means of post-processing software.

The finite element analysis of the pull-out test was used as a comparative analysis and verification tool for this research. Also, the applicability of friction models to simulate the soil/geotextile interaction could be determined. Information pertaining to the stress distribution in the soil could not be measured during the laboratory pull-out tests and the finite element simulation was also employed to obtain this data.

The finite element model developed to simulate the pull-out test consisted of three components: the soil, geotextile and interface. Each is idealised with a different material model and element type. This chapter will describe the details of each of these components. It begins with a description of the mesh discretisation, boundary conditions and loading of the system. Here the element types will also be discussed. The three sections following this outline describe the constitutive models of soil, geotextile and interface. Finally, the results obtained from this analysis are presented. These will be compared with the experimental data.

8.1 Mesh discretisation, boundary conditions and loading

The pull-out problem was modelled under plane strain conditions employing the same dimensions as the laboratory pull-out box. The model is shown schematically in Figure 8-1. The elements used to simulate the sand were 4-noded linear plane strain elements. These were laid in 14 rows of 72 elements to simulate the two sand layers above and below the geotextile. The elements for the lower and upper half of the sand were generated separately and joined behind the free end of the geotextile. Two noded linear beam elements model the geotextile and brass sheet. Interface elements were generated between the geotextile and sand by the contact pair interface formulation available in ABAQUS. The details of this formulation is discussed in Section 8.4. Although the pull-out tests were performed vertically in the laboratory, the figures of the finite element

model in this chapter are presented horizontally for convenience. The respective loads, including the gravity loads, were applied in the appropriate directions.

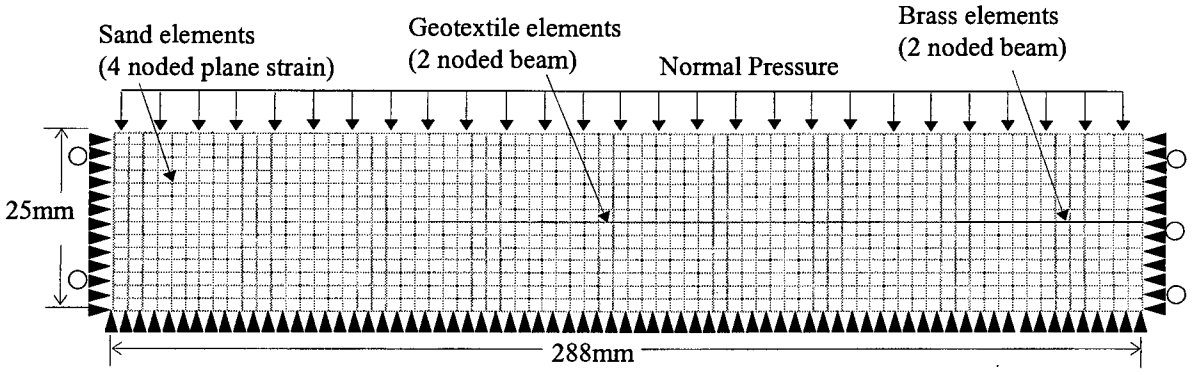

Figure 8-1: ***Mesh discretisation, boundary conditions and loading of the pull-out test***

The boundary conditions and loading are also shown in Figure 8-1. The analysis was performed in three steps. The first step was the application of the self weight of the sand, which is applied, in the context of Figure 8-1, from right to left. An average sand bulk density of 1750 kg/m^3 was employed in this step. This translates to a dry density of 1630 kg/m^3 at 7% moisture. In the second step, a uniformly distributed load (normal pressure) was applied to the surface of the sand. This resulted in a uniformly distributed lateral pressure throughout the soil elements. For simplicity, the normal pressure was not applied on both sides of the sand embedment. A horizontal boundary condition was applied to the clamped end of the brass during these two steps to prevent rigid body motion. Rigid body motion is a condition which exists when certain degrees of freedom are un-restained which allows the structure to translate at constant velocity under a given loading. Finally, the tensile loading was applied to the clamped end of the brass sheet by means of a specified displacement and the horizontal boundary restriction on the end node of the brass element was removed.

8.2 Constitutive modelling and advanced testing of sand

In this section the constitutive model selected to simulate the sand in the finite element analysis is described. The modified Drucker-Prager Cap model was selected since it is generally accepted to be the most suitable for granular materials. This model was successful in the simulation of Cape Flats sand in an analysis of a pile/sand interaction problem (Heath, 1994). Certain parameters, characterising the model were required and stress path tests were thus performed to determine these parameters. These tests and the results thereof will thus also be presented.

8.2.1 Description of the modified Drucker-Prager Cap model

The modified Drucker-Prager Cap model was chosen to describe the sand material behaviour. It is a model described as "intended for geological material which exhibit pressure dependent behaviour" (Hibbitt, Karlson & Sorensen, ABAQUS Theory manual, 1995). Symbols denoted here are specific for the Hibbitt, Karlson & Sorensen modified Drucker-Prager cap model. The constitutive model is an extension of the Drucker-Prager model consisting of three components. These are a shear failure surface (equivalent to the

one in the Drucker-Prager model), a cap and a transition surface which links the cap to the shear failure surface. In the principal stress space the shear failure surface is a cone centred around the hydrostatic stress axis (J_1 or p axis). The cone is closed with an elliptically shaped cap, which perpendicularly intersects the hydrostatic axis. This cap moves along the hydrostatic stress axis as a function of the volumetric plastic strain. A transition surface is a modification to the original Drucker-Prager Cap model specific for the model available in ABAQUS. This transition curve is tangential to the shear failure surface and the cap is to ensure a smooth transformation between the two surfaces.

The model is shown in 2-dimensional graphical form in Figure 8-2 in the p-t stress space. The symbol p corresponds to $J_1/3$, the first invariant of the stress tensor and t is $\sqrt{3\,J_{2D}}$, the second stress invariant of the deviatoric stress tensor.

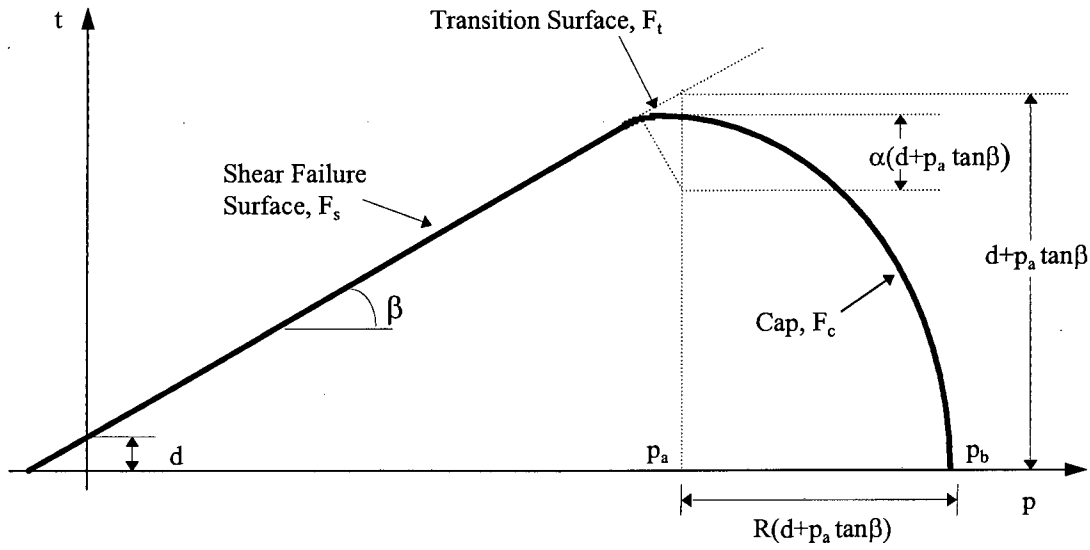

Figure 8-2: ***Modified Drucker-Prager cap model in the p-t stress space (after Hibbitt, Karlson & Sorensen)***

The shear failure surface, F_s, is represented by the following linear equation:

$$F_s = \sqrt{3 \cdot J_{2D}} - J_1 \cdot \tan\beta - d = 0 \qquad \text{.....(8.1)}$$

where

J_1 = first invariant of the stress tensor
J_{2D} = second invariant of the deviatoric stress tensor
β = slope of the shear failure surface in the J_1 - $\sqrt{3\,J_{2D}}$ stress space
d = intercept of the shear failure surface with the $\sqrt{3\,J_{2D}}$ axis

The cap is an ellipse, described by:

$$F_c = \sqrt{(J_1 - J_1^a)^2 + \left[\frac{R \cdot \sqrt{3 \cdot J_{2D}}}{(1 + \alpha - \alpha / \cos\beta)}\right]^2} - R\left((d + J_1^a \cdot \tan\beta\right) = 0 \qquad \text{.....(8.2)}$$

where

R = cap shape factor, the ratio of the major to the minor axis of the ellipse
α = non-dimensional parameter defining the transition surface (see Equation 8.5)
J_1^a = value of J_1 at the intersection of the cap with the transition curve (or p_a)

The J_1^a parameter is an evolution parameter driven by the volumetric plastic strain and is a function of J_1^b. This is the J_1 - value at the point where the cap intersects with the J_1 axis (or p_b) and is also a function of the volumetric plastic strain. The expression for J_1^a is given as:

$$J_1^a = \frac{J_1^b - R \cdot d}{(1 + R \cdot \tan\beta)} \qquad \text{..... (8.3)}$$

The relationship between J_1^b and ε_{vol}^{pl} is termed the hardening behaviour. It is represented by the following function (Zaman et al., 1982):

$$J_1^b = -\frac{1}{D} \cdot \ln\left(1 - \frac{\varepsilon_{vol}^{pl}}{W}\right) + Z \qquad \text{.....(8.4)}$$

where

D = hardening parameter
W = hardening parameter
Z = initial cap stress (i.e. the J_1 - value from where the cap starts to move)

Finally, the transition failure surface (F_t) is represented by:

$$F_t = \sqrt{(J_1 - J_1^a)^2 + \left[\sqrt{3 \cdot J_{2D}} - (1 - \frac{\alpha}{\cos\beta})(d + J_1^a \cdot \tan\beta)\right]^2} - \alpha(d + J_1^a \cdot \tan\beta) = 0 \qquad \text{....(8.5)}$$

where

α = non-dimensional transition surface parameter

The parameters required to characterise the entire model are d, β, α, R, D, W, ε_{vol}^{pl} and Z. Procedures followed to derive these parameters are published in Zaman et al.(1982). These procedures involved performing stress path tests on the soil material at the appropriate density and moisture content. These tests were therefore performed on Cape Flats sand and are described in the following section.

8.2.2 Laboratory stress path tests on Cape Flats sand

The stress path tests were performed on a conventional triaxial compression machine at the Ninham Shand geotechnical laboratory in Cape Town. The Cape Flats sand samples were compacted in a cylindrical mould to a target dry density of 1630 kg/m^3 at a moisture content of 7%, which are the same properties as used in the pull-out tests. Samples were 100mm long and 25mm in diameter. Each sample was fully saturated under a confinement of 20kPa. In total, thirteen tests were undertaken. Three stress paths were followed: a conventional triaxial compression (CTC), a hydrostatic compression (HC) and a triaxial compression (TC) stress path. These stress paths are shown in Figure 8-3 in the principal stress space and were attained by controlling the confinement, σ_3, and the

axial stress, σ_1. The conventional triaxial compression (CTC) path involved keeping the confinement constant while increasing the axial stress until failure. In the hydrostatic compression (HC) test, the confinement was simply increased while measuring the volumetric strain. The triaxial compression (TC) stress path was attained by decreasing the confinement at a third of the rate of increase of the deviatoric stress (σ_1- σ_3). This results in a vertical stress path in the p-t stress space (see also Figure 8-6).

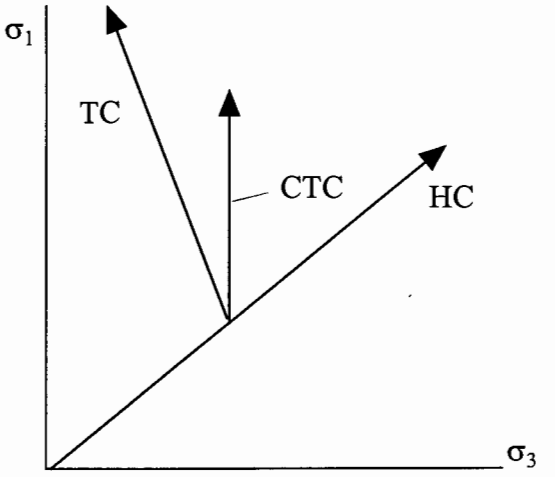

Figure 8-3: ***Stress paths in the principal stress space***

The stress path test program in given in Table 8-1.

Test Number	Saturation Time (hrs)	Stress Path	Cell Pressure (kPa)	Back Pressure (kPa)	Confinement	Axial strain rate (mm/min)
CTC1	0	CTC	700	200	500	0.0462
CTC2	18	CTC	700	200	500	0.1016
CTC3	3	CTC	400	200	200	0.1016
CTC4	15	CTC	400	200	200	0.1016
CTC5	3	CTC	300	200	100	0.1016
CTC6	5	CTC	300	200	100	0.1016
CTC7	15	CTC	400	200	200	0.1016
CTC8	4	CTC	550	200	350	0.1016
HC1	4	HC	220-1000	200	20-800	N/A
HC2	5	HC	220-1000	200	20-800	N/A
HC3	15	HC	20-1000	20	0-980	N/A
HC4	16	HC	220-1000	200	20-800	N/A
TC1	4	TC	700-400	200	500-200	N/A

Table 8.1: ***Stress path test program***

The actual dry densities and moisture contents of each test sample are plotted in the Proctor diagram of the Cape Flats sand in Figure 8-4. All the tests, except for CTC1 and CTC2, were performed at moisture contents very close to the lower optimum value of 7%.

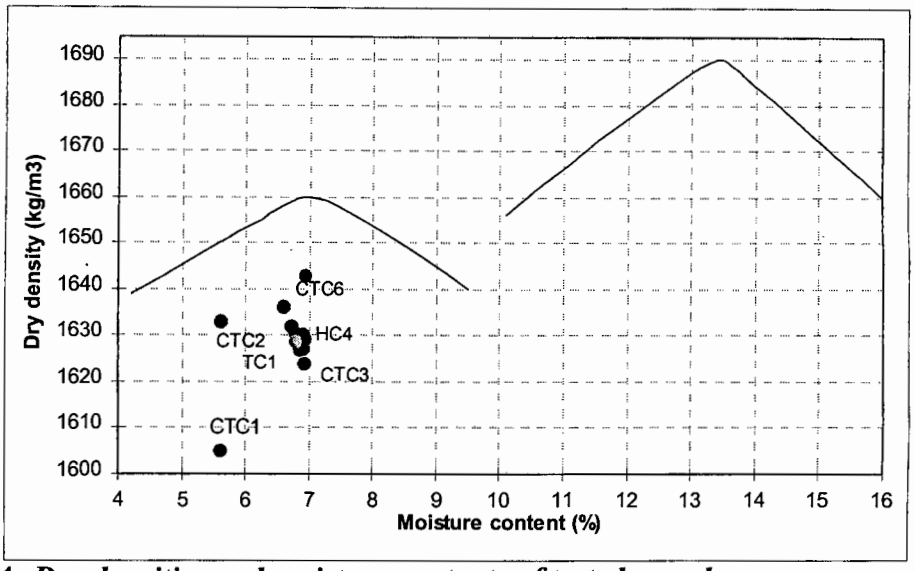

Figure 8-4: ***Dry densities and moisture contents of tested samples***

In Figure 8-5, the deviator stress versus axial strain results for each CTC test are shown. The deviator stress is the difference between the hydrostatic stress and the applied axial load. The deviator stress approached the failure stress gradually and the samples held the maximum stress long after failure. There is a clear distinction in the maximum deviatoric stress for each confining pressure. However, there is a certain degree of variation for a given confinement, which is presumably due to differences in dry densities of each sample. Generally, it was observed that a higher initial dry density results in a higher deviator stress at failure if subjected to the same confinement.

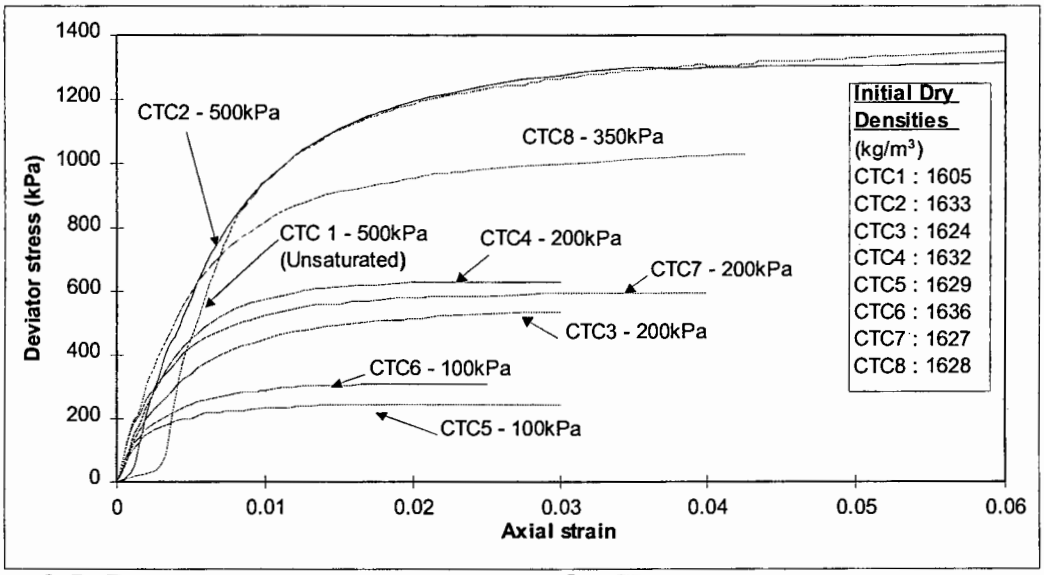

Figure 8-5: ***Deviator stress versus axial strain for CTC tests***

From these relationships, the initial Young's modulus for the elastic range of Cape Flats sand was determined. By fitting a tangent line through the initial linear portion of the curves in Figure 8-6, a Young's Modulus of 120 MPa was estimated. Inconsistencies occurred in the volumetric measurements (not shown here) and the Poisson's ratio was thus approximated as 0.24. The failure points for the CTC and TC tests were plotted in the p-t stress space to evaluate the shear failure surface for the Drucker-Prager Cap

model. By fitting a straight line to the failure points using a least squares regression, the shear failure surface was determined. This data along with the stress paths are presented in Figure 8-6.

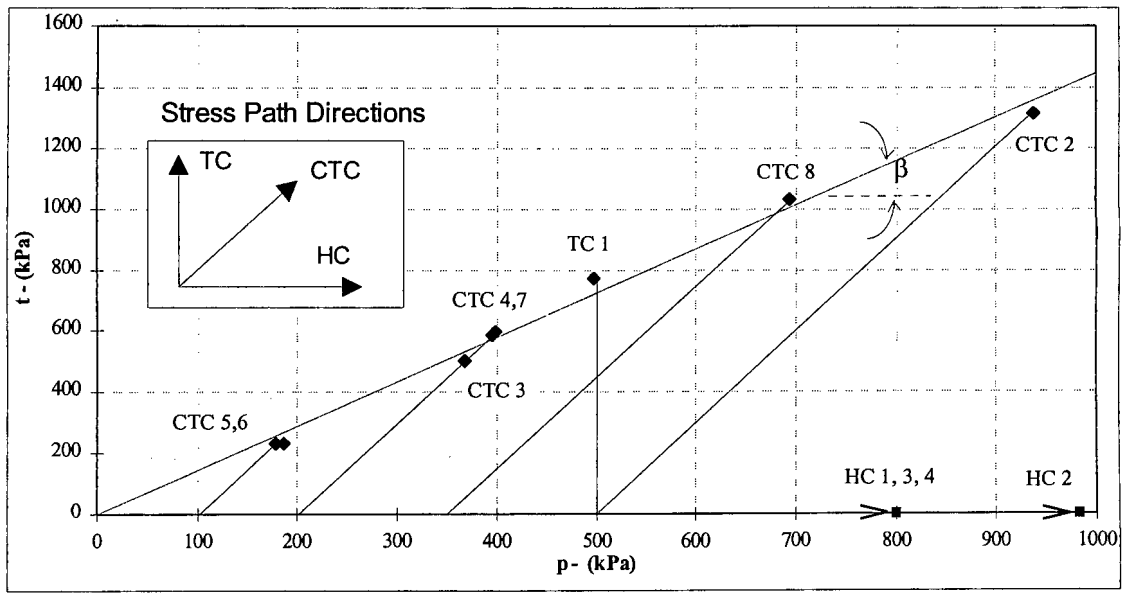

Figure 8-6: ***Failure points and stress paths of Cape Flats sand plotted in the p-t stress space***

The regression yielded an intercept of approximately zero and a slope (i.e. β – value) of 55.3°. This corresponds to an internal angle of friction of 36°.

Following this, an attempt was made to determine the value of the cap shape factor, R. This however became practically very difficult due to the inconsistency in the volume readings. Thus, a value of 0.5 was assumed for R which is the same value employed successfully by Heath (1994) using the same material.

The hardening behaviour of the Cape Flats sand was determined with the aid of the hydrostatic compression (HC) test results. The mean stress was plotted against the volumetric strain for test number HC4. This test was chosen as it best represented the hydrostatic behaviour when compared with the other three tests. Equation 8.4 was then fitted to this curve by adjusting W, D and Z in a trial and error procedure. It was found, for the volumetric strains encountered in the finite element simulation, that the values evaluated for W, D and Z resulted in a good fit between laboratory and estimated hydrostatic test data. In Figure 8-7, the hydrostatic behaviour of Cape Flats sand is presented.

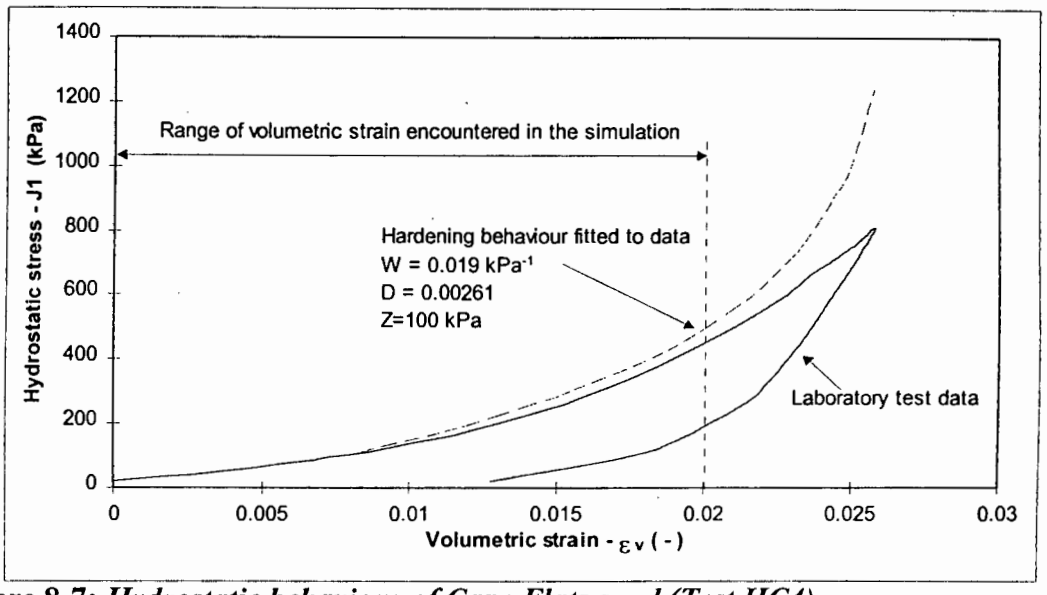

Figure 8-7: ***Hydrostatic behaviour of Cape Flats sand (Test HC4)***

The value selected for α, the transition surface parameter, was 0.01. A summary of the Drucker-Prager cap model parameters is given in Table 8-2.

Failure angle	β	55.3°
Cohesion	d	0 kPa
Transition surface parameter	α	0.01
Cap eccentricity parameter	R	0.5
Hardening parameter	D	0.00261
Hardening parameter	W	0.019 kPa^{-1}
Initial cap stress	Z	100 kPa

Table 8-2: ***Drucker-Prager Cap plasticity parameters for Cape Flats sand***

The modified Drucker-Prager Cap model implemented in the finite element model is presented in Figure 8-8, the actual failure points from the laboratory tests with the approximated failure surface is also shown.

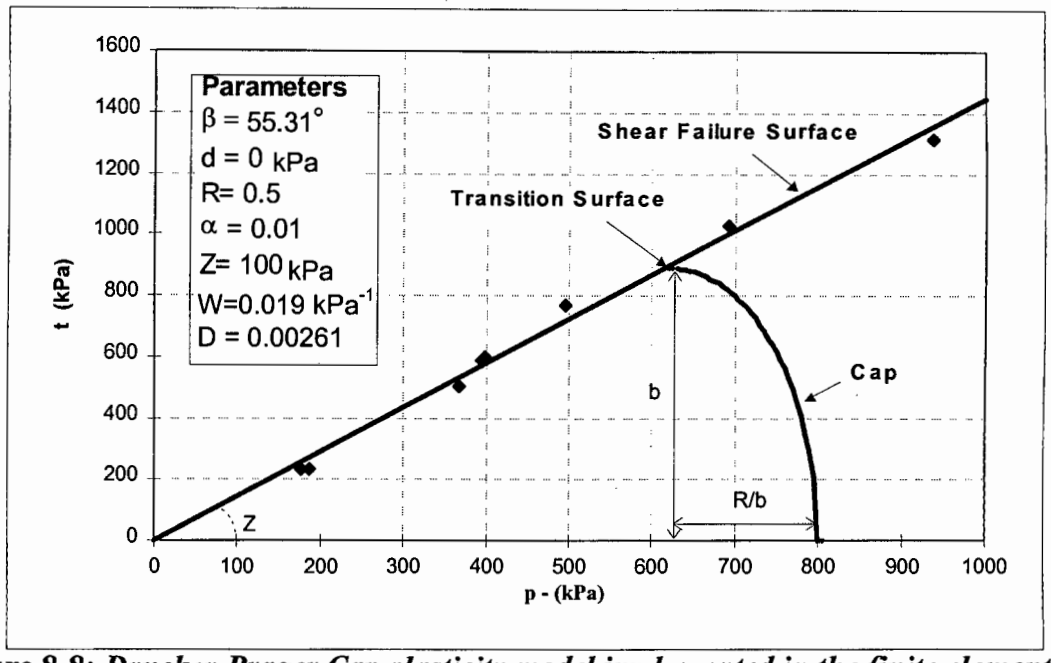

Figure 8-8: ***Drucker-Prager Cap plasticity model implemented in the finite element program to model Cape Flats sand***

8.3 Constitutive modelling of the geotextile

In Chapter 5, a linear assumption for the stress-strain relationship of non-woven geotextile was shown to be adequate. Therefore, the geotextile behaviour in the finite element analysis was simulated with a linear elastic material model, which did not include fabric rupture. This model is defined by a Young's Modulus and Poison's ratio. In addition, to model the beam elements appropriately, the geotextile thickness was also required.

The in-isolation tensile testing yielded a Young's modulus of approximately 21 MPa (see Chapter 5). However, it was shown in Chapter 6 that the Young's modulus of non-woven geotextiles increases with confinement (see Figure 6-24). The Young's modulus of 75 MPa implemented in the finite element analysis (see Table 8-3) was thus determined from Figure 6-24 for the confinement in consideration (90kPa).

The Poisson's ratio was not determined experimentally, as thickness measurements were not taken during in-isolation tensile testing. However, no significant change in the thickness of geotextile samples was evident during the in-isolation tests (although a significant necking of the sample was observed). Thus, a low Poisson's ratio of 0,05 was assumed in the plane of analysis.

Once the finite element model was fully developed, two simulations were run to determine the sensitivity of the finite element stress-strain results to the geotextile Poisson's ratio. The two simulations were run with Poisson's ratios of 0.05 and 0.25 and no significant difference in the resultant stresses or strains were observed. This verified that the magnitude of the selected Poisson's ratio is not of significance to the stress and strain patterns.

In Figure 8-9, the relationship between the thickness of the geotextile and the confinement applied to the fabric is shown. The observed thickness was found to be 16% greater than the manufacturers specification at 2 kPa. The manufactures specified thickness at greater confinements of 20 kPa and 200 kPa was therefore increased by this 16%. Thus, the thickness of the geotextile in the simulated pull-out test, at the confinement of 90kPa, was interpolated using these adjusted thicknesses.

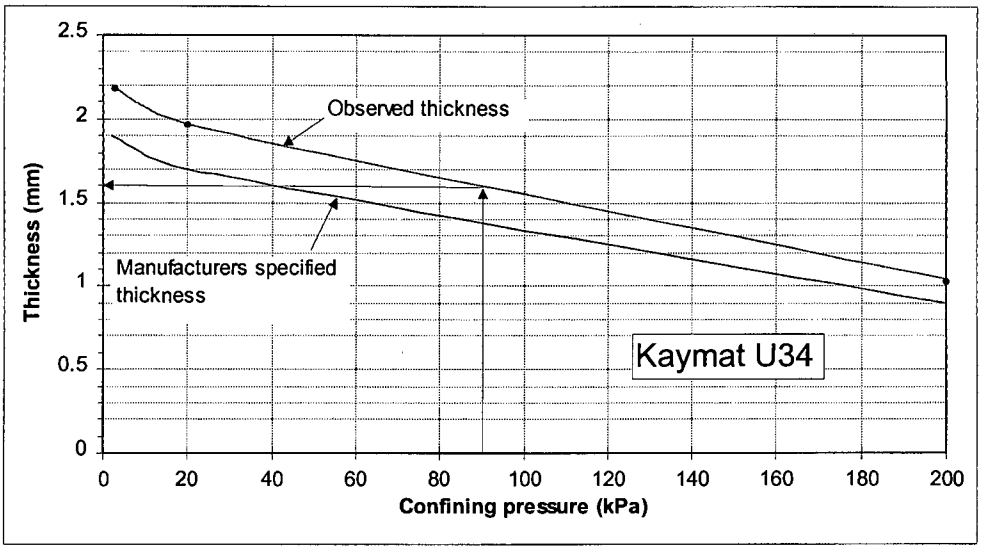

Figure 8-9: ***Variation of geotextile thickness with normal pressure***

8.4 Interface modelling

The interface between the soil and geotextile is modelled by means of interface elements. These interface elements control the magnitude of the normal and shear forces which are transmitted between the soil and geotextile. They also define the amount of relative movement between the surfaces. The interface elements implemented in this simulation are zero thickness interface elements. These are placed on either side of the geotextile, between the soil and the geotextile elements. It was not within the scope of this research work to develop a suitable interface model for the sand/geotextile interface. However, based on the findings of the research, an approach towards developing a model is suggested in a later chapter.

8.4.1 Interaction formulation

Two types of interaction formulation are available in ABAQUS, a contact pair and a slide line formulation. Both interaction formulations employ a finite-sliding contact approach. This allows for separation as well as sliding between the two bodies with a finite magnitude. In a preliminary simulation of the pull-out mechanism, both formulations were employed and it was observed that the contact pair approach produced more sensible results in terms of the symmetry of shear stress distribution about the geotextile layer. It was therefore decided to use the contact pair approach for this finite element analysis. In order to accommodate the finite sliding, non-linear geometry was accounted for in the analysis.

The contact pair approach requires the definition of two surfaces which are in contact, here, the soil and the geotextile. A master-slave concept is used, whereby one of the

surfaces is defined as the master surface (geotextile), while the other is defined as the slave surface (soil). This is shown schematically in Figure 8-10. The nodes of the slave surface (i.e. soil nodes) are not allowed to penetrate the master surface (i.e. the geotextile nodes), however, a master node can penetrate the slave surface. Contact therefore occurs between the nodes of the slave surface and master surface. The finite sliding approach allows a node of the slave surface to come in contact anywhere along the master surface. However, while it is in contact, it may only move along the path defined by the master surface. ABAQUS tracks the movement of each slave node relative to the master surface. The direction of the normal forces transmitted between the surfaces is always perpendicular to the master surface and shear forces are transmitted parallel with the master surface at the point of contact. Since the nodes move along the master surface, it is necessary that the surface be smooth to prevent slave nodes from sticking at the asperity of the master surface. This was warranted as the master surface (i.e. the geotextile) remains flat throughout the simulation.

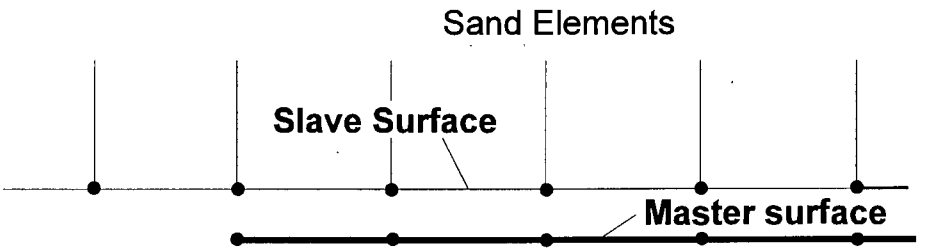

Figure 8-10: ***Slave and master surface definitions***

8.4.2 Surface contact interaction

The surface contact interaction defines the contact behaviour normal to the surfaces when contact is established. It is concerned with conditions of contact and separation as well as the transmission of normal pressure between the surfaces under these conditions.

For this analysis a "hard" contact was adopted. The surfaces are defined as being in contact when the clearance between the surfaces is zero or less than zero millimetres. Then, there is no limit to the magnitude of contact (normal) pressure that can be transmitted. If the contact pressure reduces to zero, separation can occur. A schematic of the two conditions is shown in Figure 8-11.

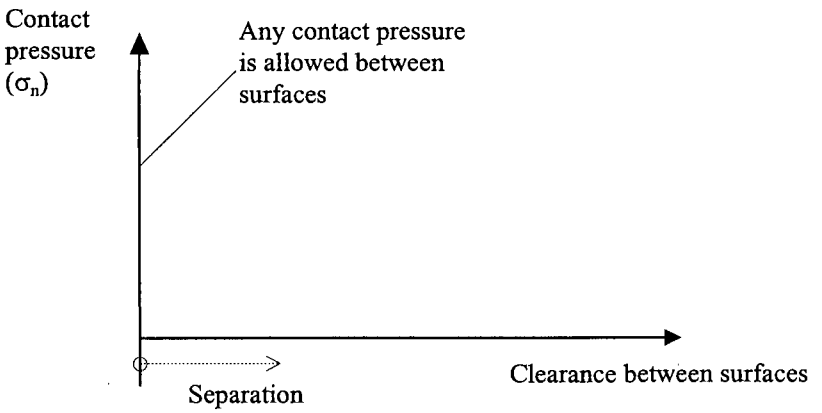

Figure 8-11: ***The "hard" contact pressure-clearance assumption***

8.4.3 Frictional interaction between surfaces

The friction model in the numerical simulation defines the behaviour parallel to the surfaces, once contact has been achieved. Two aspects of the contact model are important, namely: i) the shear stresses between the surfaces and the
ii) relative displacement between the two surfaces.

The primary aspect of the model is concerned with the transmission of shear forces. The magnitude of shear stress transmitted is a function of the normal pressure between the two surfaces. The relationship between the transmitted shear stress and normal pressure was assumed to be a Coulomb friction model. The model, supplied by ABAQUS, makes use of an equivalent shear stress, τ_{eq} , for a two dimensional interface, which is defined by:

$$\tau_{eq} = \sqrt{\tau_1^{\,2} + \tau_2^{\,2}} \qquad \text{.....(8.5)}$$

where

τ_1 and τ_2 are the two shear stresses in the interface stress tensor in both directions on the contact surface

The Coulomb friction model states that no relative motion of the two bodies occurs if the equivalent shear stress (τ_{eq}) is less than the critical shear stress. The critical shear stress is defined as:

$$\tau_{crit} = \mu \cdot \sigma_n \qquad \text{.....(8.6)}$$

where

μ = friction coefficient

σ_n = normal pressure transmitted at the interface

This therefore represents a linear relationship between the critical shear stress and normal pressure as is shown in Figure 8-12.

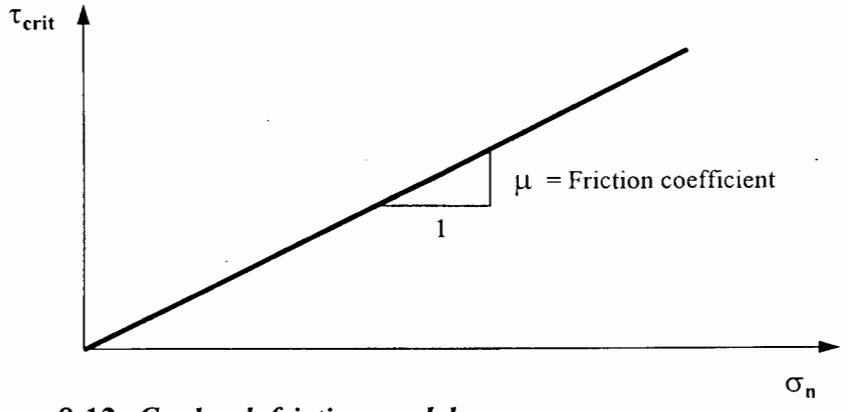

Figure 8-12: ***Coulomb friction model***

The results from the laboratory pull-out tests indicated a non-linear relationship between the critical shear stress, τ_{crit} , and normal pressure, σ_n (see Section 6.5.6). This laboratory relationship was employed to find an appropriate friction coefficient to be used in the finite element simulation. The calculation was performed by defining the friction coefficient for a specific confinement as the secant modulus of the laboratory τ_{crit} - σ_n curve (Figure 6-22), calculated at the pertinent normal pressure. This is shown diagramatically in Figure 8-13 for the confining pressure in consideration. A friction coefficient of 0.566 was determined for the confinement of 90 kPa.

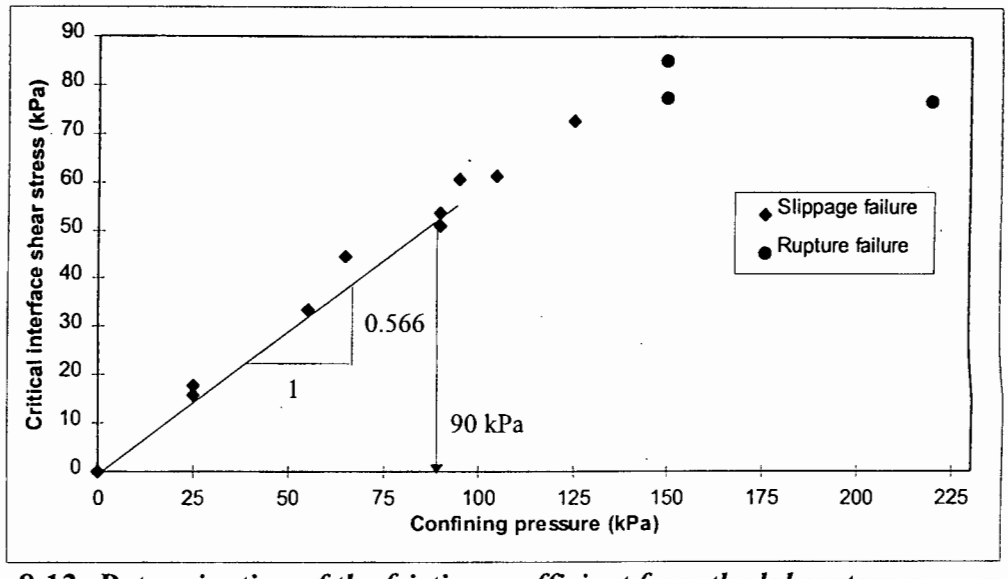

Figure 8-13: ***Determination of the friction coefficient from the laboratory*** τ_{crit} - σ_n ***relationship***

The second aspect of the friction model is associated with the relative displacement between the surfaces. Although no relative motion of the two bodies is possible at shear stresses below the critical shear stress in the friction model, a certain amount of elastic slip is allowed at these stresses. Elastic slip is defined as an apparent relative movement of the surfaces due to deformation of one or both of the surfaces at the interface. This deformation is in the same direction as the relative displacement between the surfaces. Thus, in shearing problems, the total interface displacement is made up of two components:

1. Relative shear displacement as a result of the attainment of the critical shear stress, termed real slip (γ^{rl}).
2. Deformation of the surfaces at the interface in the direction of shearing, termed elastic (or virtual) slip (γ^{el}).

Once the critical shear stress is reached, the elastic slip component is negligible compared with the increase in the real slip component.

ABAQUS assumes that the magnitude of the elastic slip is governed by the interface shear stress in a linear manner. This is given as:

$$\tau = k_s \cdot \gamma^{el} \qquad \text{.....(8.8)}$$

where

k_s = stiffness constant which is defined as:

$$k_s = \frac{\tau_{crit}}{\gamma_{crit}} \qquad \text{.....(8.9)}$$

The parameter γ_{crit} is the elastic slip tolerance and defines the "stiffness" of the interface. This parameter was employed to calibrate the finite element model with the experimental results. The finite element model relationship between relative shear displacement (slip) and shear stress at the interface is shown schematically in Figure 8-14.

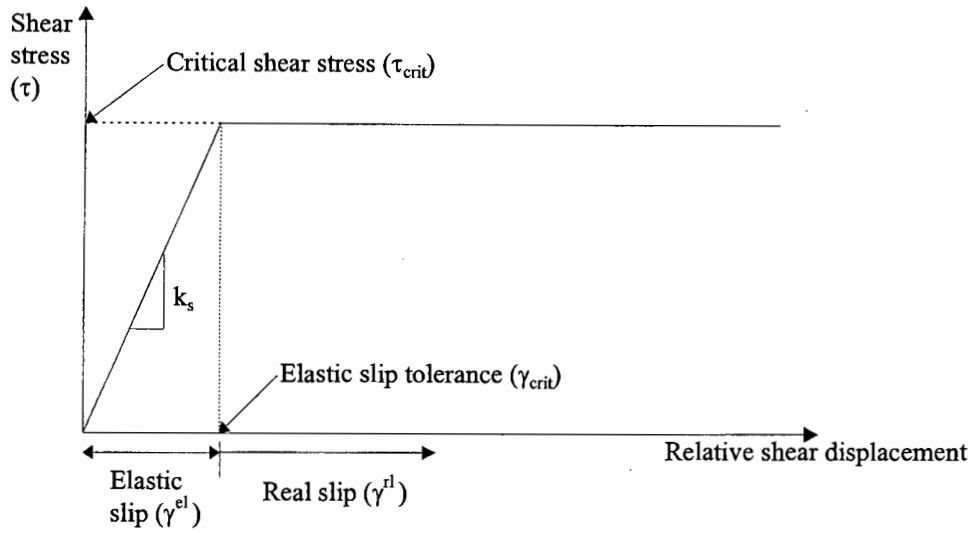

Figure 8-14: ***Finite element model relationship between shear displacement and shear stress***

The simulation of frictional behaviour between the sand and geotextile is thus controlled by two parameters; the friction coefficient, μ, and the elastic slip tolerance, γ_{crit}.

It was decided to perform the simulations with the assumption that the brass sheet exhibited no frictional resistance with the sand (i.e. μ=0), since no convergence of the finite element solution could be achieved when friction between the brass and sand was considered. Therefore, the pull-out loads from the finite element model are comparable with the laboratory pull-out loads calculated for the geotextile only (i.e. control pull-out test loads subtracted from the actual pull-out test loads).

8.5 Comparison of numerical and experimental results

Results for the finite element simulation of the pull-out test at a confinement of 90kPa are presented and compared with the results from the laboratory test at the same confinement. The finite element model was calibrated with the laboratory pull-out test results by varying the elastic slip tolerance until the best agreement between the experimental and finite element analysis was achieved. Both, the pull-out load of the geotextile and the displacement of the free end were employed as the basis for the calibration. The respective parameters which were eventually used in the simulation are summarised in Table 8-3. The material model parameters for Cape Flats sand can be found in Table 8-2.

Parameter	Symbol	Value
Normal pressure	σ_n	90 kPa
Geotextile Young's Modulus	E	75 MPa
Geotextile Poisson's ratio	ν	0.05
Geotextile thickness (at 90 kPa)	t	1.6 mm
Friction coefficient (at 90 kPa)	μ	0.566
Elastic slip tolerance	γ_{crit}	0.5mm

Table 8-3: ***Interface and geotextile material model parameters used in the finite element analysis***

The calibration of results enabled the verification of the friction parameters obtained from the experimental data and helped to ascertain the validity of the Coulomb model. The stiffness of the geotextile under confinement could be also verified with the aid of this comparison. Most importantly, a better understanding of the shear stress development and movement of the geotextile could be achieved.

As is typical of finite element analyses, a wide variety of results are available from the simulation. In this section, however, only the more relevant data is presented. Various results are then compared. These include the pull-out force versus clamped end displacement relationship, the displacement of the free end, and the displacement along the geotextile sample. The development of the shear stress and relative displacement across the sand/geotextile interface, is presented to describe the load transfer and displacement mechanism involved in the pull-out test.

8.5.1 Comparison of the pull-out force versus clamp displacement

The pull-out load versus clamp displacement relationship obtained in the simulation is shown in Figure 8-15. Note that the force presented is the resistance offered by the geotextile only, since the friction between the brass and soil is assumed to be non-existent. The pull-out resistance of the geotextile versus clamp displacement response of the equivalent laboratory test is plotted for comparison (see also Figure 6-19).

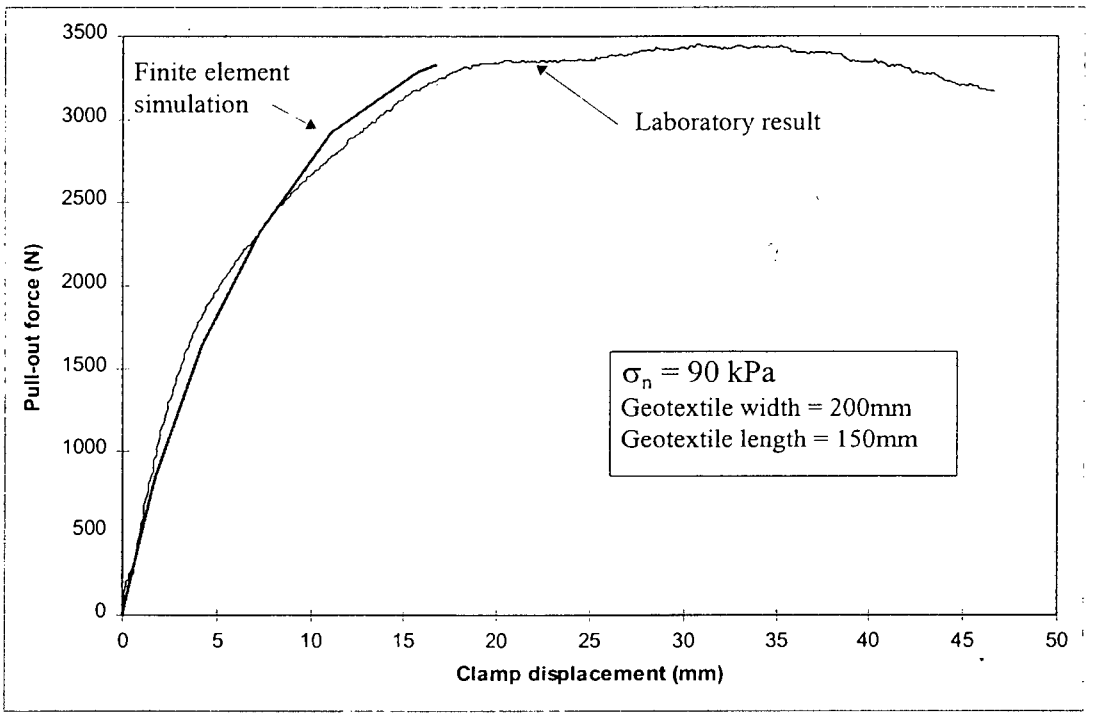

Figure 8-15: ***Pull-out load versus clamp displacement relationship for geotextile only, finite element simulation and laboratory test***

The results from the finite element simulation is a multi-linear response curve because the pull-out loads were generated at specific displacement increments. The actual pull-out behaviour is continuous, a good correlation was however achieved between the finite element and laboratory results in terms of the pull-out force versus clamp displacement

curve. This suggests that the friction model in the finite element analysis adequately simulates the overall load transfer at the sand/geotextile interface.

Implementing the friction coefficient calculated from laboratory pull-out tests (see Section 8.4.3) resulted in the finite element model predicting a very similar maximum pull-out force, compared to the actual experiment. This therefore verifies that the use of the secant modulus of the τ_{crit} - σ_n relationship is a suitable method to determine an acceptable friction coefficient for a specific confining pressure. It also appears that the assumption of a linear elastic material model for the geotextile material behaviour is sufficient for this study.

8.5.2 Comparison of the free end displacement

Figure 8-16 shows the simulated displacement of the free end of the geotextile compared with the actual laboratory result for the test performed at 90kPa. Here it is seen that the finite element simulation predicts that the free end displaces immediately upon loading. However in the laboratory test the free end begins to move only after the clamp had displaced by 5.6mm (see Figure 6-15). The finite element simulation thus fails to predict the lag in the movement of the free end, because of a limitation in the friction model. This is seen in Figure 8-14, where the initial relative displacement of the interface (i.e. elastic slip) is assumed to occur immediately upon the application of shear loading. However, from experiment, is appears that elastic slip (i.e. the initial movement if the free end) occurs only once a limiting shear stress (less than the critical shear stress) is attained at the interface. Despite this limitation however, the pattern of the movement of the free end agrees very well with the laboratory observations if shifted by 5.6mm.

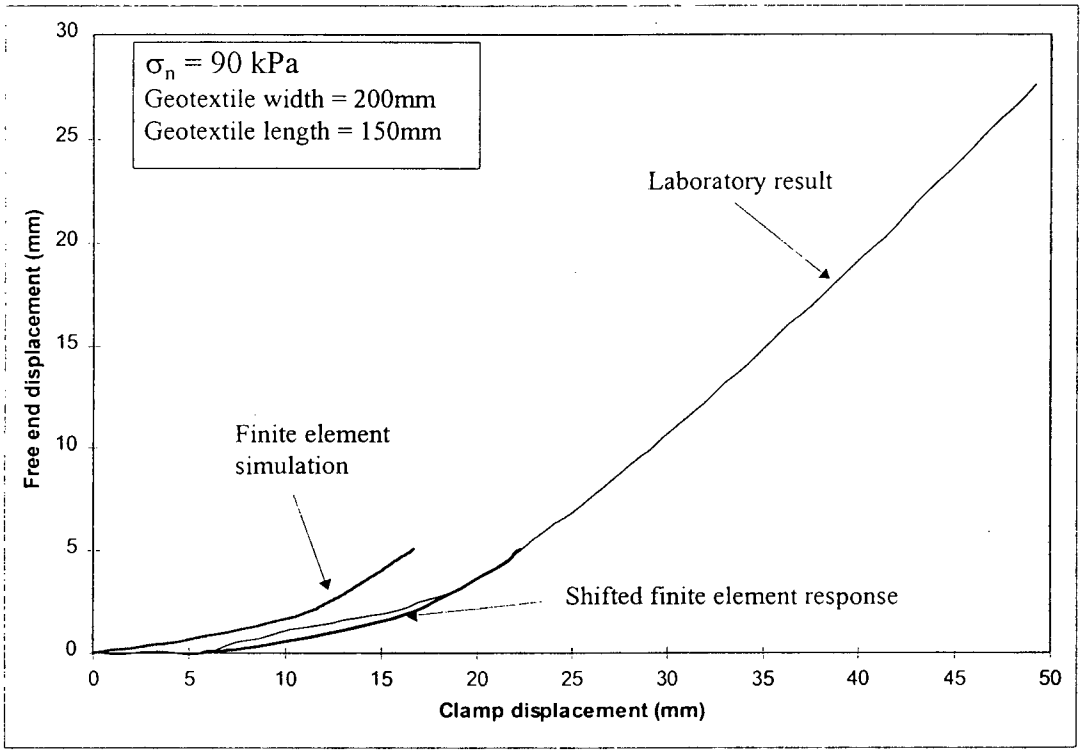

Figure 8-16: ***Simulated and actual displacement of the free end during pull-out testing***

Since detailed results were available from the finite element simulation, a more comprehensive analysis of the shear stresses associated with the displacement of the geotextile was possible. It was found, by studying the predicted stresses obtained from finite elements, that the initial movement of the free end (up to 10mm) was due to elastic slip. In this region, the interface shear stress and shear displacement are less than their respective critical values and are located on the inclined portion of the friction model (in Figure 8-14). Here, the movement is due only to deformation of the surfaces (elastic slip) and no real slippage takes place. The shear stress and shear displacement increase until the critical shear stress (and elastic slip tolerance) is reached. The movement then abruptly changes to real slip and the free end displaces at a constant rate (see Figure 8-14). Another limitation in the friction model is thus apparent in that the transition from elastic slip to real slip is not gradual as is observed in the experimental results. It must be noted here that the development of a more suitable friction model for the sand/geotextile interface behaviour was not in the scope of this thesis, however an suggested approach is discussed in Chapter 9.

8.5.3 Comparison of the displacement distribution along the geotextile

The distribution of the displacement along the geotextile in the pull-out direction is shown for selected front end displacements corresponding to various loadings in Figure 8-17. Results from the laboratory tests are included for comparison for clamped end displacements of 5mm and 12.6mm.

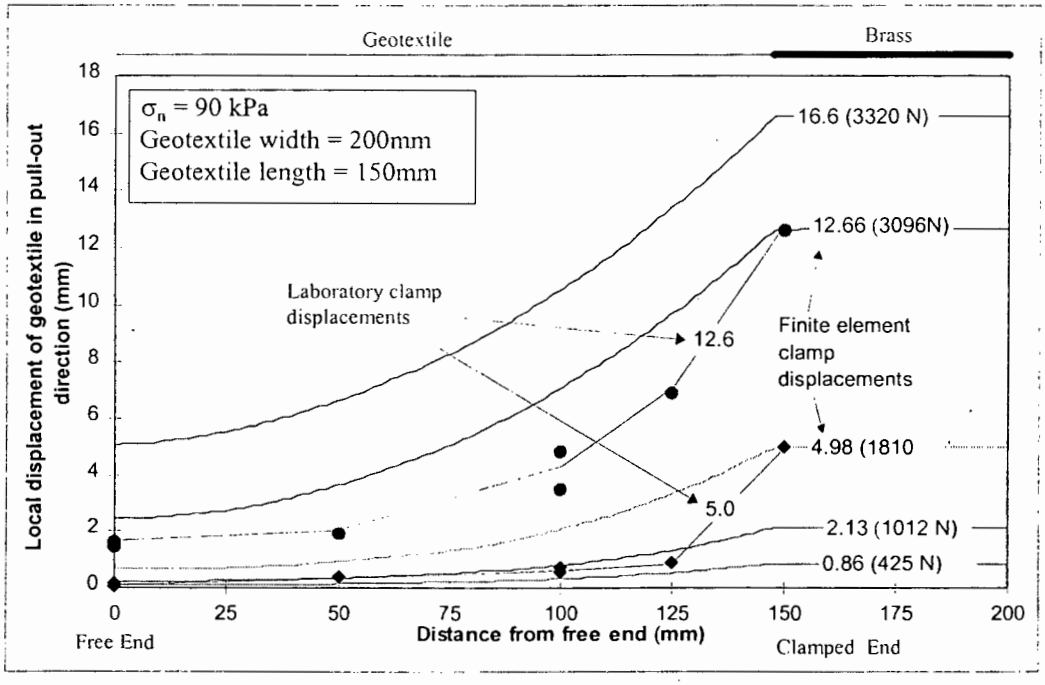

Figure 8-17: ***Displacement distribution at various points along the geotextile***

The displacement along the geotextile decreases non-linearly from the clamped towards the free end. Also, the strain in the brass plate is negligible throughout the loading.

When comparing the finite element with the laboratory results for the same clamp displacements, it is shown that the finite element simulation generally over-predicts the displacement of the geotextile. At a clamp displacement of 5mm, the free end of the geotextile has not displaced in the laboratory test. However, the finite element simulation predicts that the free end displaces by 0.6mm at a clamp displacement of 4.98mm.

The measured displacements from the laboratory tests drop off more rapidly than the finite element results as the free end is approached. This indicates that the adopted friction model does not adequately simulate the displacements associated with the load transfer mechanism at the sand/geotextile interface as was discussed earlier. A similar displacement pattern is observed at a clamp displacement of 12.6mm. The loads given in brackets are the finite element results which correlate well with the loads obtained from experiment (see Figure 8-15).

8.5.4 Development of shear stress along the geotextile

Figure 8-18 shows the development of the shear stress along the interface between Cape Flats sand and the geotextile, which is derived from the finite element simulation.

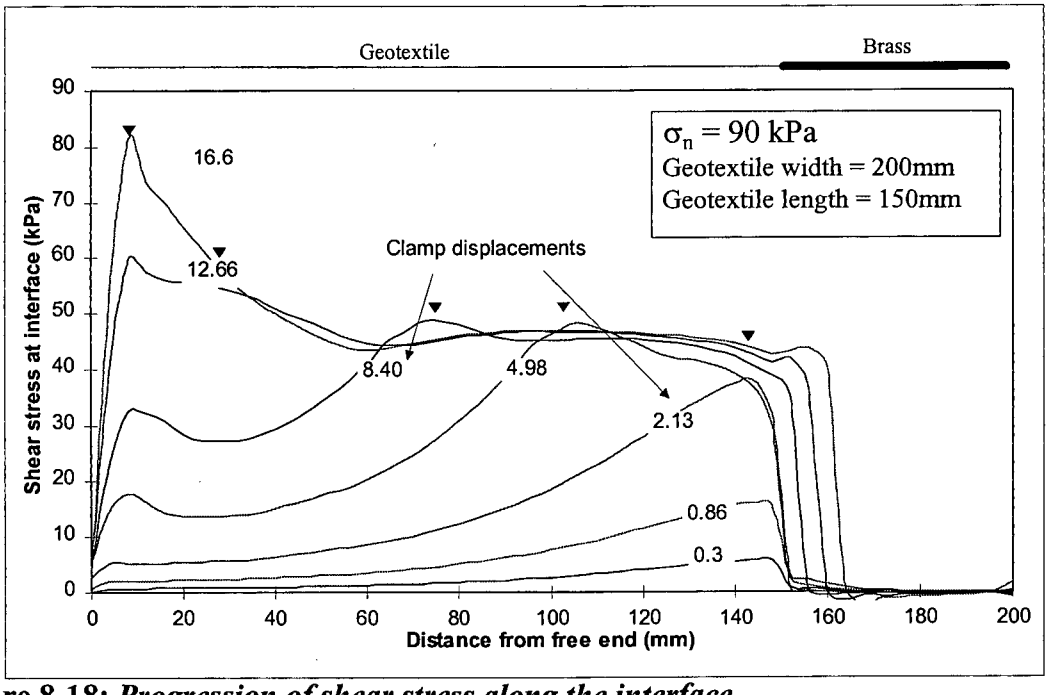

Figure 8-18: ***Progression of shear stress along the interface***

Initially, the shear stress at the interface is greatest near the clamped end and decreases gradually towards the free end. As the clamp displacement (i.e. loading) increases, the magnitude of the peak stress increases. The position where this peak shear stress occurs along the geotextile remains at about 5mm from the front end, up to a front end displacement of 2mm when the peak shear stress attains the critical shear stress value. The peak shear stress then progressively migrates along the geotextile until the critical shear stress is developed along the entire interface.

The distance from the front of the geotextile sample to the point where the peak shear stress has attained the critical shear stress, is defined as the activated length. Within this

length of geotextile real slip is occurring. The activated length increases as the clamp displacement increases until the entire interface has attained the critical shear stress. The end of the activated length of geotextile is indicated by the arrow in Figure 8-18 for each clamp displacement. At any position beyond this point along the geotextile, the shear stress is less than the critical shear stress and any displacement of the geotextile occurring, outside the activated length, is entirely due to elastic slip.

It was also observed that at clamp displacements of 2mm or greater, the lowest shear stress no longer occurred at the free end of the geotextile, but at approximately 25mm from the free end. A localised peak in the shear stress is noticeable near the free end and was found to increases as failure is approached. Similar stress concentrations were observed by Hohberg and Schweiger (1992) who vaguely attributed these to the selection of the value defining the "stiffness" of the sand geotextile interface. Based on this, it is believed that the stress concentrations are actually caused by the difference in the "stiffness" of the sand/geotextile interface and the sand/sand interface just behind the free end. The sand-sand interface behind the geotextile had zero slip tolerance, while the sand/geotextile interface had a slip tolerance of 0.5 (see Section 8.4.3). This abrupt change in the interface stiffness thus causes stress concentration near to the free end which is schematically shown in Figure 8-19.

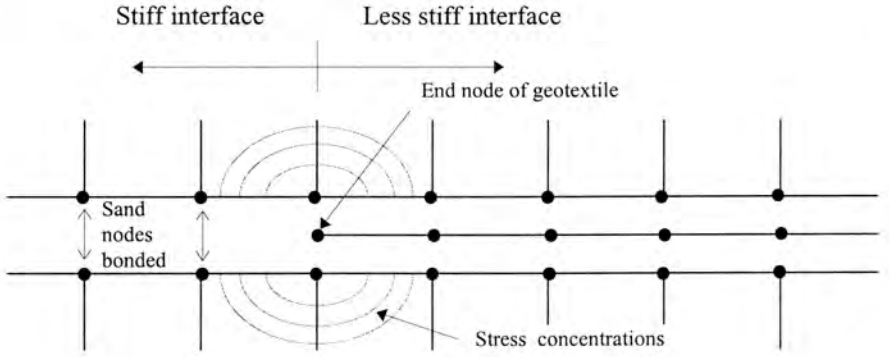

Figure 8-19: ***Mesh arrangement at the free end of the geotextile***

The shear stress development and progressive activation of the geotextile is also seen in the shear stress distribution in the sand. In Figure 8-20 contour plots of the change in the sand shear stress distribution as the front end is displaced, again for a confinement of 90 kPa, are presented. The characteristic development of the shear stresses in the soil, as shown here, is typical for all normal pressures simulated.

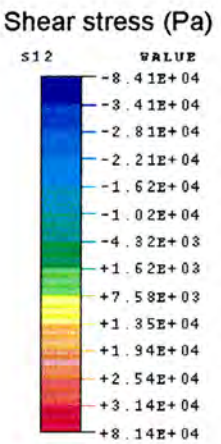

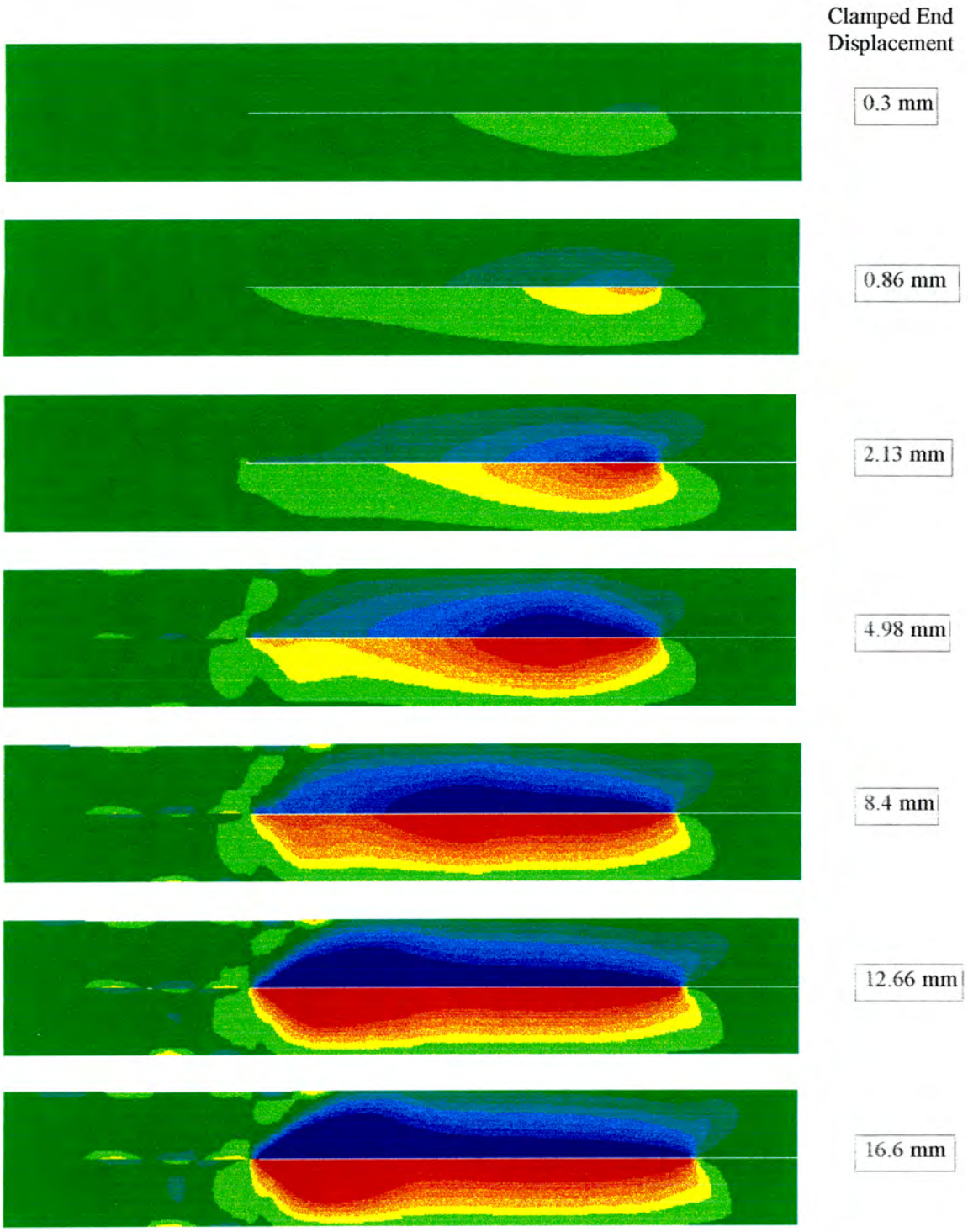

Figure 8-20: ***Shear stress distribution in Cape Flats sand at various clamp displacements***

In these plots the shear stress at the interface is initially distributed along a small portion of the geotextile sample. The shear force is also not very large at this point. An increase in pull-out load is then balanced by an increase in the area of interface over which the shear stress is distributed , i.e. the dark red and blue zones extend along the geotextile. As the pull-out displacement increases, the shear stresses in the sand progressively increase and translate towards the free end of the geotextile (dark red and blue zones).

8.5.5 Slip required to develop the critical shear stress

The displacement at the interface (i.e. slip) which is required for the critical shear stress to fully develop is illustrated in Figure 8-21. Here the development of the shear stress at specific points along the geotextile/sand interface are shown in relation to the slip between the geotextile and soil at that point. This was determined by subtracting the displacement of a geotextile node from the displacement of the adjoining soil node and plotting this against the shear stress at the interface at that location. Thus, the relative shear displacement shown is the sum of real slip and elastic slip. For clarity, the relationships are plotted such that the origins of the curves are located at a displacement equal to 10% of the distance of the node from the free end.

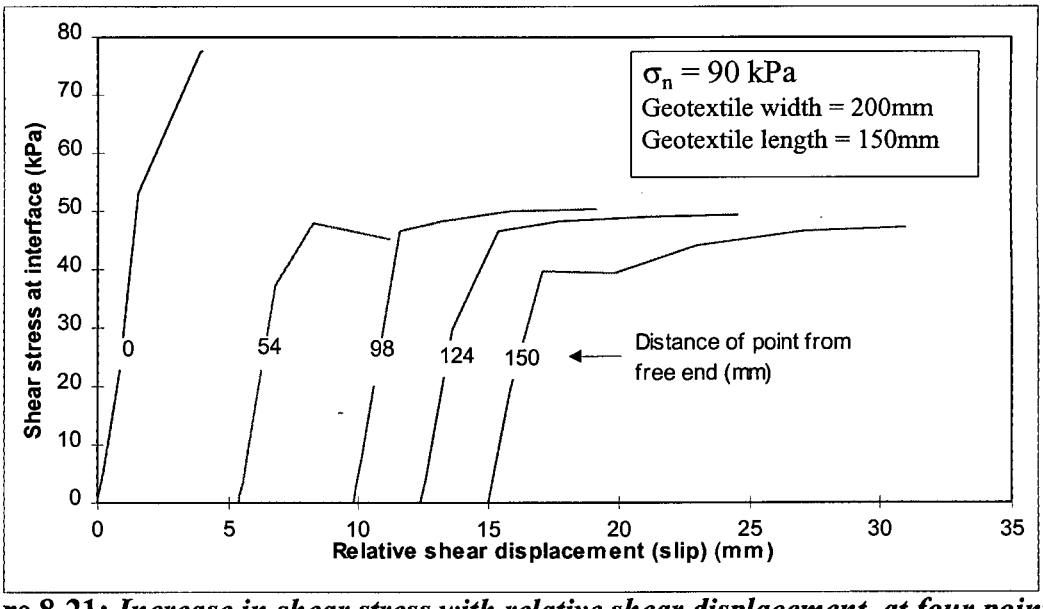

Figure 8-21: ***Increase in shear stress with relative shear displacement at four points along the geotextile***

The figure shows that the shear stress develops in a very similar manner along most of the geotextile sample. It is only at the free end that the development is different. This is due to the locally developed stress concentrations as mentioned in Section 8.5.4. It is also observed that a greater magnitude of relative movement between the sand and geotextile occurs near the front of the geotextile, since the stretch of the sample increases towards the front end. The actual relative displacement at the specific points along the interface, required to develop the critical shear stress at 90kPa, are given in Table 8-4. The development of the shear stress at the free end is not truly representative because of the influence of the stress concentrations mentioned earlier and thus the slip at the free end was not included in Table 8-4. The average slip at failure, measured in the laboratory experiment at 90kPa is also shown.

Distance from free end (mm)	Slip required to develop critical shear stress - Finite element analysis (mm)	Slip required to develop critical shear stress across the entire geotextile - Experiment (mm)
54	2.9	
98	3.4	
124	2.9	
150	3.2	
Average:	3.1	3.5

Table 8-4: ***Comparison of slip required to develop interface shear stress for finite element simulation and laboratory experiment***

A good correlation between the finite element simulation and laboratory experimental results is evident. The development of the shear stress thus appears to occur in the same rate of displacement at any point along the entire length of the geotextile. The critical shear stress is developed at the interface once the geotextile has slipped by approximately 3.1 mm to 3.5mm relative to the sand.

Chapter 9
Summary, Comparison and Evaluation of Results

A combined summary of the findings from the pull-out tests, the direct shear tests and the finite element analyses are presented in this chapter. The results from these tests are evaluated and also compared with published research. Moreover, some consequences of the findings of this research for the design approach of geotextile reinforced soil walls and embankments are indicated.

The displacement and shear mechanisms associated with the geotextile in pull-out are initially addressed. This is followed by the description of the confining pressure conditions associated with slippage and rupture failure. The maximum interface shear stress in relationship with the confining pressure, obtained from the pull-out tests, is briefly summarised. Finally, results from the pull-out tests and direct shear tests are compared in terms of maximum shear stresses and displacement required to mobilise those stresses.

9.1 Displacement and shear stress development along the geotextile

9.1.1 Geotextile displacement responses

The displacement responses which are a reflection of the shear stress behaviour, associated with the pull-out of a geotextile sheets is shown in Figure 9-1 for confining pressures of 55 kPa, 90 kPa and 150 kPa. The relevant pull-out responses for the same tests are superimposed.

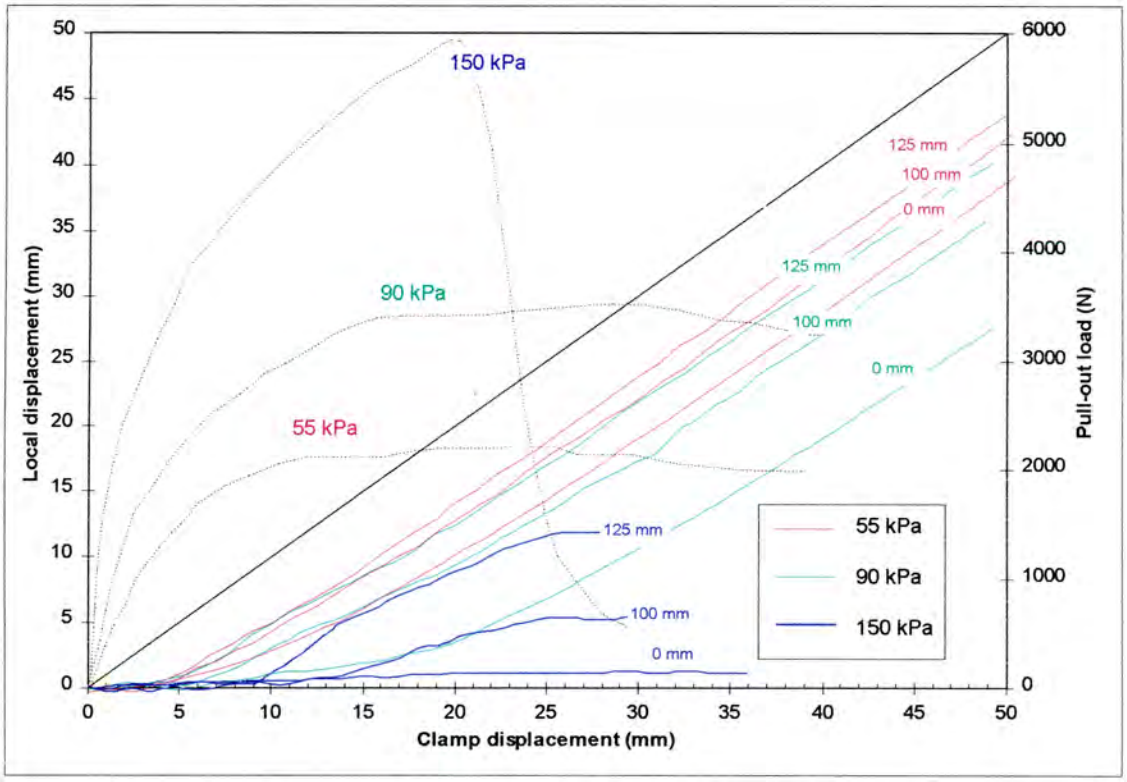

Figure 9-1: ***Displacement of geotextile sections and pull-out load versus clamp displacement for various confining pressures (σ_n = 55kPa, 90kPa, 150 kPa)***

The displacement responses of the specific points (125mm, 100mm and 0mm) along the geotextile at low (55 kPa) and medium (90 kPa) confinements, subjected to pull-out loading, are characterised by two distinct and constant gradients in the local displacement versus clamp displacement diagram. These two phases are separated by a transition phase. Initially there is a zero gradient indicating no movement of the measured points. However, since the clamp (150mm) displaces, the section from the clamped end to the observed point along the geotextile stretches. Once the stretch along the geotextile has extended to the specific point of measurement, movement is observed reflected in a steady increase of the gradient. This transition phase continues until the gradient becomes constant again and is equal to the gradient of the straight (black) line indicating the control rate of displacement (clamped end). The specific point along the geotextile displaces then in the same rate as the clamp. The section of geotextile in front of this location does not stretch any more and the movement is due entirely to slippage.

The local displacement responses in the case of the highly confined geotextile (150 kPa) is clearly different. The transitional phase appears not to exist i.e. zero movement at the 125mm observation point is followed directly by slippage (gradient at the rate of clamp displacement). Stretching in the subsequent 25mm section of the geotextile is observed, however to a lesser extent since tearing starts immediately thereafter indicated by the gradient dropping back to zero.

The overall stretch of the geotextile is, in the case of the low confinement, only one half of the stretch experienced in the medium confinement test. It is noted that in both confinements, the measure of stretch in the front 25mm of the specimen is approximately the same.

The overall stretch in the high confinement test has no meaning since the geotextile tears with the free end of the geotextile undergoing zero displacement.

9.1.2 Displacement distribution along the geotextile sample

By plotting the displacements of the various sections along the geotextile for various pull-out loads (at a confinement of 90 kPa), the distribution of the displacement across the sample could be highlighted in a different manner (see Figure 6-18). It was found that the displacement is distributed non-linearly along the geotextile sample. The displacement pattern shown is typical for all pull-out test for the various confinements, although a concentration of local displacements close to the front of the geotextile is observed as the load and confinement increases. This in turn results in a steeper drop-off towards the free end. Very similar patterns in the displacement distribution were shown by Khachafi and Dysli (1993) at low confinements (33 kPa). After failure, the relative displacement distribution along the sample remains in principal the same since the geotextile is slipping.

9.1.3 Pull-out load in relation to stretch of the geotextile

The relationship between the pull-out load and stretch of the geotextile is shown in Figure 9-2 for confining pressures of 55 kPa, 90 kPa and 150 kPa. For the purpose of comparison, the load versus stretch behaviour of the geotextile in an in-isolation test is also shown.

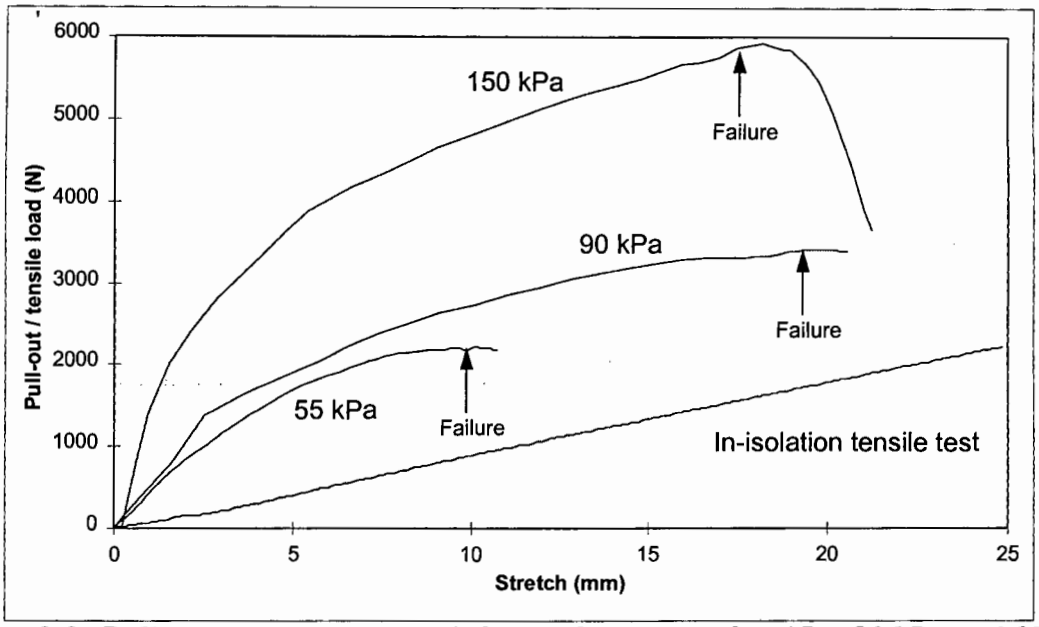

Figure 9-2: ***Pull-out load versus stretch for confinements of 55 kPa, 90 kPa and 150 kPa***

It is clearly demonstrated that the geotextile is able to carry a significantly higher tensile load for a given stretch when it is confined in sand due to the shear interaction between sand and geotextile. The in-isolation tensile strength versus elongation relationship provided by the geotextile manufacturers are therefore not applicable for design purposes.

The initial increase of pull-out load with stretch is approximately the same for the low and medium confinement tests. This is an indication that the front 25mm of the geotextile responds similarly to the load applied for both confinements. However, there is significant difference in the pull-out load versus stretch at the high confinement where a steep initial increase in pull-out load, followed by a drop off to a more steady increase up to failure, is observed.

There is a distinct difference in the respective patterns after slippage and rupture failure. For rupture failure the pull-out load drops rapidly after failure as the torn geotextile cannot sustain the load, while only negligible changes of the pull-out load are observed after slippage failure.

The "snap-back" behaviour described by Abramento et al. (1995) is not detected in these pull-out test results. The most likely reason is a difference in the Young's modulus of the "extensible" nylon geotextile used by Abramento et al. (1995) and the geotextile product used in this research.

9.1.4 Development of shear stress along the geotextile sample

The development of the shear stress along the geotextile was determined based on the finite element simulation since the experimental results do not allow an analysis in terms of shear stresses without appropriate shear stress-strain relationships for the respective sand material. The stresses along the geotextile for various stages of loading are shown in Figure 8-18 for a test performed at a confinement of 90 kPa.

The critical shear stress of approximately 50 kPa for the confinement of 90 kPa is first developed at the front of the sample. Clearly, a migration of this limiting shear stress towards the free end stress is noted as the clamp displacement (and thus the pull-out load) increases.

From the finite element results it was also observed that at a clamp displacement of approximately 5mm, the free end of the geotextile begins to move and this is reflected in an increase of the interface shear stress at the free end. After a clamp displacement of about 16mm, the whole geotextile is activated (i.e. the critical shear stress has been attained across the entire sand/geotextile interface). Stress concentrations were identified at the free and are attributed to the transition between interfaces with differing "stiffness" at the end of the geotextile.

An activated length, the distance from the front of the geotextile to the point where the critical shear stress has developed, could be identified. This characterises the length of geotextile undergoing real slip (i.e. this length of geotextile is as a whole moving relative to the sand). This development of shear stress along the geotextile is very similar to that obtained by Handel et al. (1990) also with the aid of the finite element technique (see also Figure 3-17). Shear stress concentrations at the free end of the geotextile were also identified by Handel et al. (1990) and Hohberg and Schweiger (1992).

9.1.5 Performance of the finite element friction model

Good correlation between the finite element and experimental results was achieved in terms of the pull-out load versus clamp displacement. This indicates that the interaction model adequately simulates the load transfer mechanism. Also the linear elastic material model appears to be a satisfactory model for the geotextile material behaviour in tension.

However, the finite element model fails to predict the lag in the initial movement of the free end with clamp displacement which was observed in the experimental results. The pattern of movement is, however, very similar. The distribution of displacement along the geotextile also does not agree too well with the experimental results. This deficiency in the finite element model to predict the geotextile displacements occurs because:

- there are limitations that exist in the friction model and
- the Young's Modulus of the geotextile appears to be too high.

The limitation in the friction model are pointed out with the aid of Figure 9-3, in which the numerical and experimental results are compared in terms of pull-out load versus free end displacement (i.e. slip).

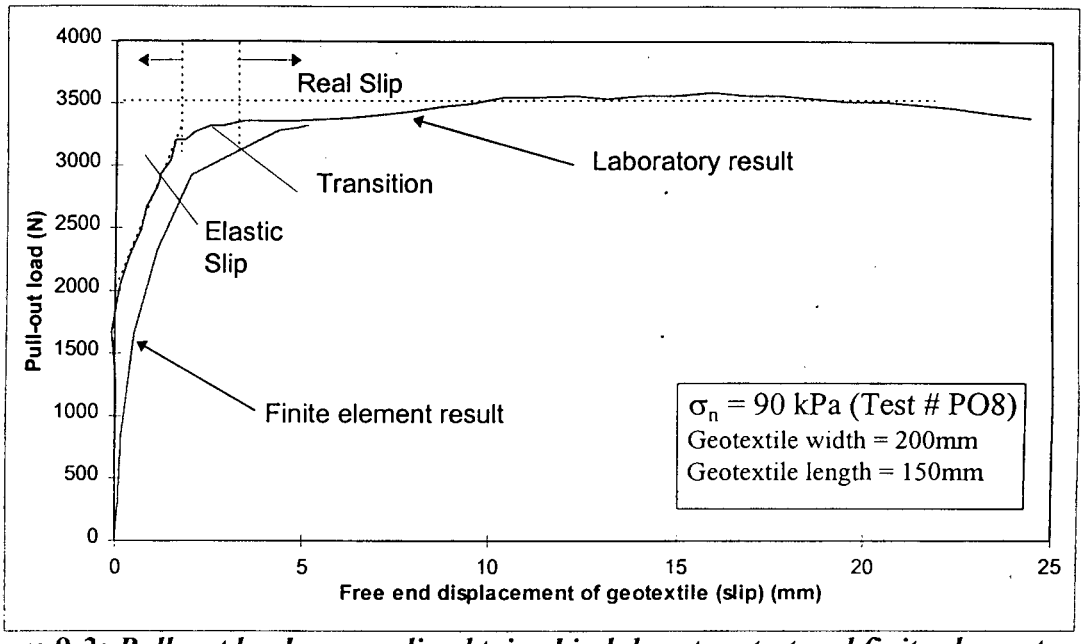

Figure 9-3: ***Pull-out load versus slip obtained in laboratory test and finite element analysis***

The primary inconsistency between the finite element simulation and actual behaviour, is that in the laboratory tests, slip (displacement of the free end) occurs only after a specific pull-out load has been applied, while in the finite element simulation, slip occurs immediately upon loading. It can also be seen that a gradual transition occurs between elastic slip and real slip conditions.

Based on this, the following changes are suggested to improve the friction model so that it will more accurately predict the movement of the geotextile. This is shown schematically in Figure 9-4. A limiting shear stress needs to be incorporated below which no slip occurs. Above this limiting shear stress, elastic slip, which is defined as usual by the elastic slip tolerance, is permitted. This will have the effect of allowing the friction model to simulate Zone I of the geotextile displacement by preventing initial movement of the free end before a specific pull-out load has been applied. Also, by preventing this initial slip, the displacements calculated along the geotextile during the finite element analysis will be lower for a given front end displacement, and a better correlation of the displacement distribution results will be achieved.

A smoother transition from elastic slip to real slip conditions is also suggested as this is evident in the actual behaviour. This could be implemented with the addition of a linear piece-wise shear stress versus slip relationship. The three zones of displacement of the geotextile can be identified in the suggested model as shown in Figure 9-4.

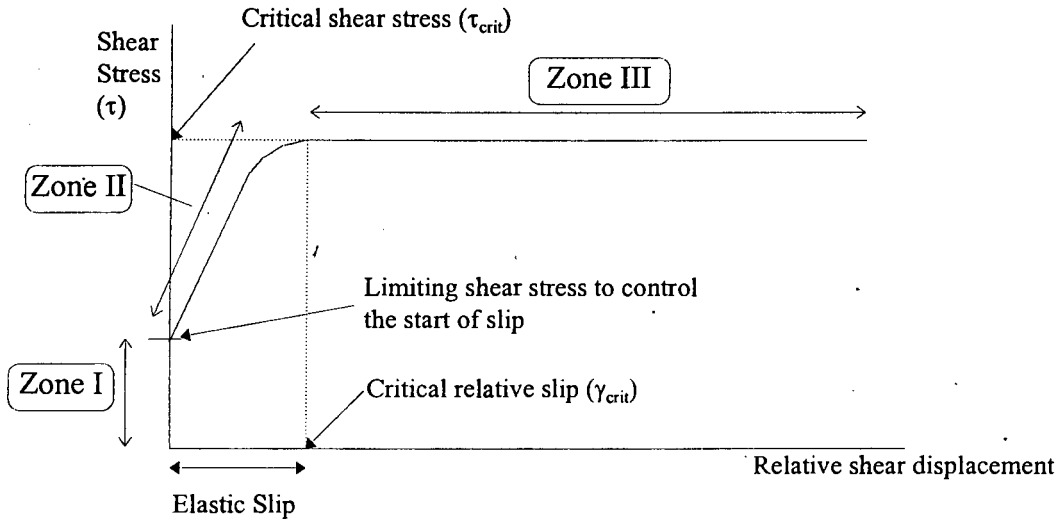

Figure 9-4: ***Suggestions to an improved shear stress versus shear displacement model***

9.2 Failure in pull-out

Two failure modes in the pull-out tests were noted, namely slippage and rupture failure. There was no evidence of a transitional failure mode between slippage and rupture, as was initially questioned (see Section 3.3.2) . However, there appears to be a specific confining pressure above which the geotextile will fail in rupture mode. Based on the maximum average interface shear stress versus confining pressure relationship (Figure 6-22), this confining pressure is in the order of 140 kPa for the test conditions in this study.

At confinements above 140 kPa, it appears that the resisting response of the geotextile, when confined in the sand, does not increase any further as the confinement increases. Thus, the rupture of a confined geotextile sheet will occur at the same pull-out load for a given sample size, irrespective of the magnitude of confinement above 140 kPa. This so called confined tensile strength of the geotextile in Cape Flats sand is 27 kN per meter width of geotextile, which is 23% greater than the in-isolation tensile strength of 22 kN/m.

These findings are contrary to those of Leshchinsky and Field (1987) who indicated that the confined tensile strength increases with confinement (see Figure 3-5) . However, that conclusion was drawn based on a test performed in a modified shear apparatus (Figure 3-4) which does not adequately simulate the pull-out process since slippage of the geotextile was prevented in the experimental set-up.

The pull-out test results indicated that failure (both rupture and slippage) is approached gradually (see Figure 6-13), which is consistent with other research (Palmeira and Milligan, 1990; Forsman and Slunga, 1994; Tzong and Cheng-Kuang,1987; Bonczkiewicz et al., 1988; Kharchafi and Dysli, 1993 ; El Mogahzy et al., 1994, Juran and Chen, 1988). Also, regarding the post failure behaviour, no decrease in the pull-out load to a residual value was observed in tests where slippage failure occurred, which is again consistent with the findings of Palmeira and Milligan (1990) (see also Figure 3-9).

Necking in the pull-out test samples was found to be concentrated close to the clamped end. This is where the tearing of the fabric ultimately took place, just behind the brass sheets (see Figure 6-14).

Three characteristic zones in the displacement behaviour of the geotextile during the pull-out tests were identified. These zones are defined in terms of the free end displacement (slip). The relationship between the stretch and slip of the geotextile as well as the interface shear stress development along the geotextile characterise each zone.

The three zones are shown in Figure 9-5 in terms of a generic relationship between the stretch and slip of the geotextile sample during a pull-out test where slippage failure occurs.

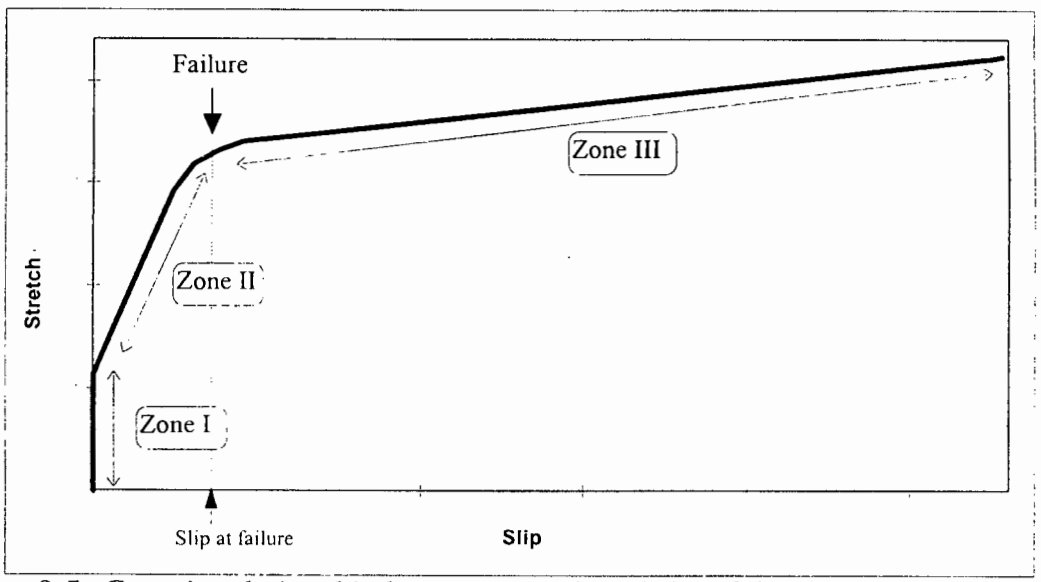

Figure 9-5: ***Generic relationship between stretch and slip of the geotextile for each zone of movement***

In the first zone of displacement response, the free end of the geotextile does not displace (i.e. no slip) and the clamp displacement induces stretching of the geotextile in the section up to the first displacement measurement point at 125mm. This is also reflected in the distribution of the shear stresses along the interface, analysed with the finite element method, which showed that the shear stresses were developed only along the front section of the sample (See Figure 8-18). The measure of stretch (in Zone I) in these tests is in the order of 2mm to 9 mm, depending on the confinement.

In Zone II combined stretching and slippage of the geotextile takes place. As failure is approached, stretching reduces significantly (see Figures 6-15 and 6-16). The movement of the free end (slip) corresponds to the elastic slip in the finite element analysis and is, in fact, an apparent slippage of the geotextile due to deformation of the sand and geotextile surfaces in contact.

The region after failure is defined as Zone III. At failure, according to the finite element analysis, the interface shear stress across the entire geotextile has attained the critical shear stress which allows the whole geotextile to slip relative to the sand surface. Thus,

this zone is characterised by the entire geotextile slipping with the occurrence of a negligible amount of stretching of the sample. This is contrary to the proposal by El-Fermaoui and Nowatzki (1982) who suggested that the free end moves only once the peak shear stress was reached (i.e. at failure).

It was shown that as the confinement increases, the magnitude of the stretch of the geotextile in Zone I increases. Also, the total amount of stretch of the sample during the test increases while the amount of slip decreases. Once the confinement is large enough to cause rupture of the geotextile, slipping is negligible and tearing of the geotextile controls the response (see also Figure 9-1).

9.3 Maximum average interface shear stress versus confining pressure

The maximum average shear stress acting along the geotextile was calculated making use of a method which takes the geotextile slippage into consideration, but ignores necking of the specimen. This method is an improvement on the method suggested by Leshchinsky and Field (1987). The maximum average interface shear stress at various confining pressures is shown in Figure 6-22.

In pull-out, the maximum average interface shear stress increases bi-linearly with the confining pressure. The inflection point of this relationship is at about 50kPa. The highest calculated maximum average interface shear stresses were in the order of 80 kPa at confinements of 140kPa and above. This is the level of confinement at which the geotextile fails in rupture.

Other research (Bonczkiewicz et al., 1988; El Mogahzy et al., 1994; Khachafi and Dysli, 1992) did not indicate the nature of the maximum shear stress versus confining pressure relationship at confinements above 100 kPa. The results of this research thus expands on the understanding of this relationship.

The diagram (Figure 6-22) can be used in the internal stability design of a geotextile reinforced embankment or wall to determine the maximum load that can be applied to a single sheet given an embedment length and the overburden stress.

It was shown that a certain front end displacement of the geotextile is required before the maximum shear stress is fully developed. Based on the pull-out tests, the measure of this required front end displacement of the geotextile could be established as a function of the confinement (see Figure 6-23). At low confinements this is in the order of 15mm and it increases non-linearly to a measure of about 30mm for these tests.

9.4 Comparison of pull-out and direct shear results

The development of the shear stress with clamped end displacement / shear displacement differs greatly between pull-out and direct shear tests. This can be seen in Figure 9-6 which is a plot of the interface shear stress versus the clamp or shear displacement for the pull-out and direct shear tests respectively, at two levels of confining pressure of similar magnitude.

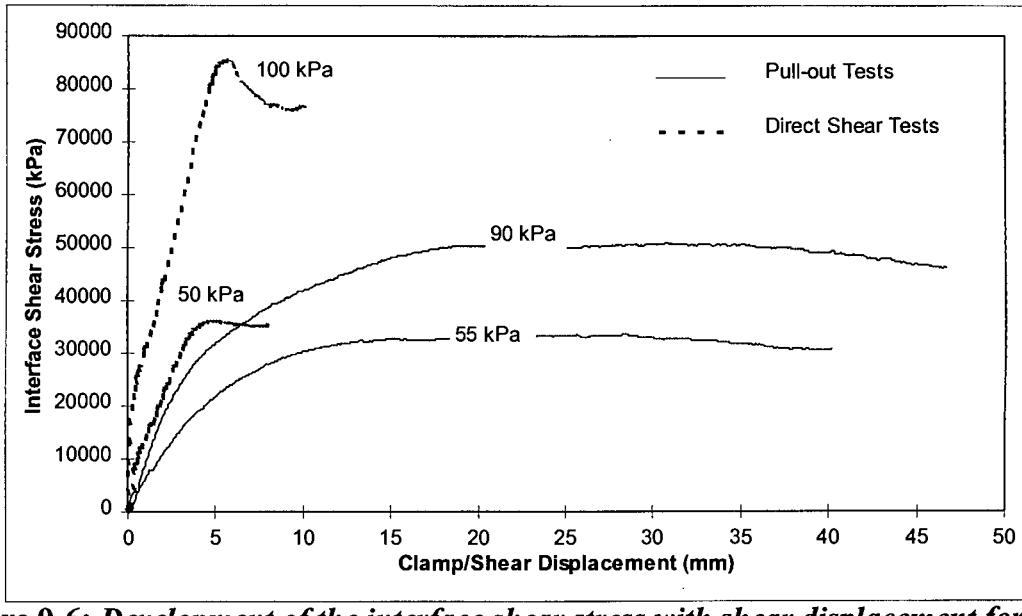

Figure 9-6: ***Development of the interface shear stress with shear displacement for pull-out and direct shear test***

In the direct shear tests, the interface shear stresses develop more rapidly with displacement compared to those in the pull-out tests. A clear peak dropping off to a residual shear stress can be detected for the direct shear test results, however, in the pull-out results, failure is approached gradually and no drop off to a residual stress is evident.

The pattern of development of the shear stress for the direct shear test corresponds well with that obtained by Makiuchi et al. (1988) (see Figure 3-14).

Another noteworthy comparison between the results of the two test approaches is shown in Figure 9-7 in terms of the relationship between maximum interface shear stress and confining pressure .

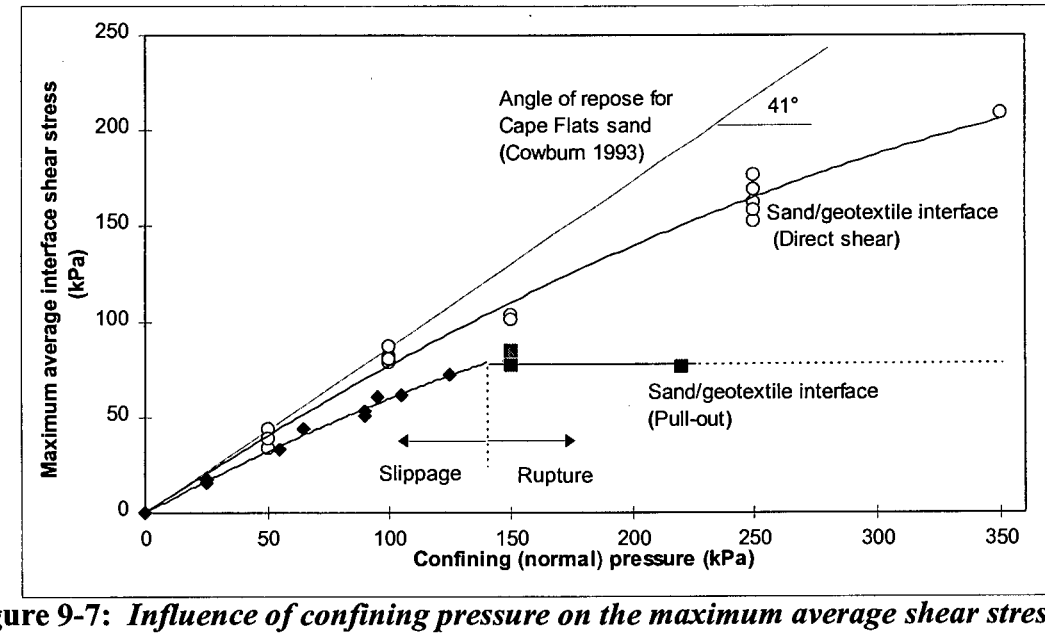

Figure 9-7: ***Influence of confining pressure on the maximum average shear stress at the sand/geotextile interface***

The maximum interface shear stresses obtained from direct shear tests is greater than those obtained in the pull-out tests. Depending on the confinement, this difference is between 25% and 40% for slippage failure. In the case of rupture failure this difference is as large as 100%. Both results are however lower than the soil-soil direct shear interface values, which is consistent with previous findings (Myles, 1982 and Makiuchi et al., 1988). The use of the direct shear test to determine the friction coefficient for design purposes must therefore be questioned as it appears to over-predict the shear strength of the sand/geotextile interface.

The front end displacement required to develop the maximum interface shear stress, obtained from both pullout and direct shear tests is shown in Figure 9-8.

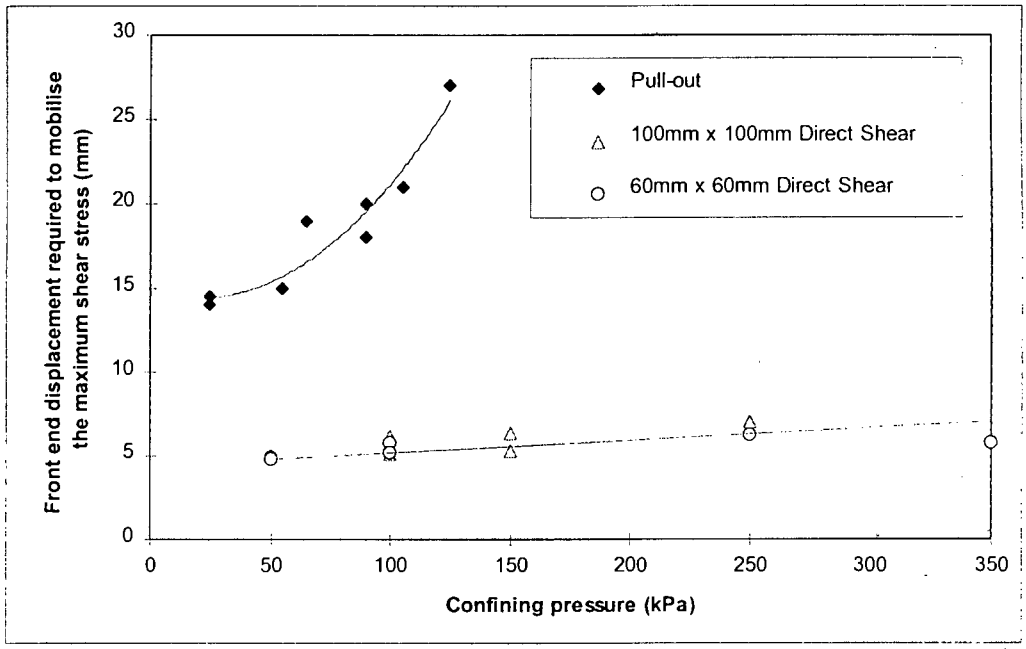

Figure 9-8: ***Front end displacement required to develop the maximum average shear stress for various confining pressures***

The graph is in support of the previous statements made that the direct shear test results are inadequate for design purposes. In terms of the front end displacement required to mobilise the maximum shear stress, the direct shear test greatly underestimates that experienced in the more representative pull-out tests.

Chapter 10
Conclusions

An experimental and numerical investigation into the shear interaction behaviour between a non-woven geotextile and Cape Flats sand has been presented. The conclusions that can be drawn from this research are presented here in terms of the initial objectives. The detailed results are summarised in Chapter 9 and it is thus not intended to repeat all the observations, but to present the major conclusions resulting from these findings.

Initially, a clamping method was developed for the in-isolation tensile tests of the non-woven geotextile, which greatly reduces the initial slip at the clamps during the tensile test. The in-isolation tensile tests indicated that the non-woven geotextile has a linear stress-strain relationship. Also, the in-isolation tensile strength and load-displacement modulus of the geotextile increases with sample thickness.

Pull-out tests were performed at confinements between 25 kPa and 225 kPa. An advancement in current understanding of the pull-out behaviour of a geotextile at high pressures (above 100 kPa) could thus be established. The confining pressures were measured at the sand/geotextile interface and not at the sand surface, which is a significant improvement compared with previous research. A solid foundation of experimental results of the geotextile interface behaviour problem was developed by means of the high precision measurements obtained in the pull-out apparatus which in turn was set-up in a highly controllable tensile testing machine.

Displacement and shear stress mechanisms

Insight into the displacement and shear mechanisms involved in the pull-out of a non-woven geotextile sheets from Cape Flats sand was obtained based on the pull-out test results and finite element analyses. During the laboratory tests, accurate displacement measurements were taken along the geotextile sample by means of extensometers which allowed for the determination of the displacement responses.

The displacement response patterns of individual positions on the geotextile sheet differ significantly for high confinement compared with low and medium confinements. These patterns in the displacement response to loading have been described and characterised.

The distribution of the displacement along the geotextile is non-linear and becomes more concentrated towards the front end with increased confinement.

The relationship between the tensile load and stretch of the geotextile is significantly different for a geotextile confined in sand compared with in-isolation test conditions. Therefore, the in-isolation load versus stretch relationship should not be employed in design procedures for geotextile reinforced soil structures.

The finite element method of analysis was found to be a useful interpretation tool in elaborating on the shear stress mechanisms during pull-out. Based on the analyses, the development of the interface shear stress initiates at the front end of

the sample and advances towards the free end with increasing clamp displacement until the entire sample is in a state of critical shear stress. The initial movement of the free end is reflected in an increase in the interface shear stress at the free end.

Although the finite element model adequately simulates the load transfer behaviour, it fails to satisfactorily predict the displacements of the geotextile because of a limitation in the interface model and the very high Young's Modulus which was employed for the geotextile. The limitation in the friction model was explained and an improved approach was suggested whereby a lag in the start of elastic slip should be incorporated. A smooth transition from elastic slip to real slip is also suggested. The implementing of these modifications was not considered within the scope of this project.

Confining pressure conditions defining the failure mode

The effect of confining pressure on the slippage and rupture failure was quantified from the pull-out experimental data. It is possible to predict whether rupture or slippage occurs since there is a specific confining pressure which separates the occurrence of the two failure modes. It appears that no transitional failure mode between slippage and rupture failure exists.

When designing a geotextile reinforced earth wall, it must be understood that there is a limiting tensile stress that can be applied to a geotextile sheet. At any confining pressure below this limiting value, the geotextile will fail in slippage and at any confinement above this value, the geotextile will tear at the confined rupture load, irrespective of the level of confinement. For the non-woven geotextile in Cape Flats sand, this limiting confinement was found to be 140 kPa. The confined tensile strength of the geotextile is 23% higher than the in-isolation tensile strength. The rupture of the geotextile sample occurs at the front end of the geotextile since the tensile load is highest at this point.

Three zones in the movement of the geotextile are evident from pull-out tests. These are defined by the displacement of the free end and are characterised by the amount of stretch and slip occurring along of the geotextile sample. In the first zone no slip of the geotextile takes place, with stretching only occurring at the front of the sample. In the second zone, both stretch and slip is observed. The finite element analysis showed that the slip in this zone is due to the sand and geotextile surfaces deforming in shear and is not due to relative displacement of geotextile sheet as a whole (real slip). The third zone is located after failure and is characterised predominantly by real slip.

Effect of confining pressure on the maximum average interface shear stress

A method which includes the geotextile slippage, but not the necking behaviour, was utilised to calculate the maximum average interface shear stress that can be sustained by the sand/geotextile interface. This maximum interface shear stress increases bi-linearly with increased confinement until a limiting confining pressure (140 kPa) is reached. Above this limiting confining pressure, the geotextile ruptures before slippage failure occurs.

In the design of a geotextile reinforced soil structure, it must be remembered that the pull-out or rupture failure load is attained only once the front end of the individual sheet has undergone a certain displacement. This required displacement was quantified using the pull-out test results.

Comparison between pull-out and direct shear tests

There is a significant difference in the shear stress development between the direct shear test and pull-out test. The direct shear test over predicts the maximum interface shear stress and under predicts the front end displacement required to develop the maximum interface shear stress. It was thus concluded that the direct shear test (in a modified direct shear apparatus) is not an adequate test procedure to accurately determine the friction parameters of geotextiles and backfill materials used in the design of a geotextile reinforced soil structure.

A comprehensive understanding into the displacement responses and associated shear stresses for a non-woven geotextile experiencing pull-out in sand has been achieved in this research and a reliable basis for further experimental and numerical investigations into a variety of geotextile reinforcement applications could be established. Ongoing research is currently being undertaken based on the findings of this work. Also, this research combined with existing knowledge and experience may enable the practising engineer to re-assess and modify the design procedures to improve the current design approach of geotextile reinforced soil structures.

Bibliography

Abramento, M. and Whittle, A.J. Analysis of Pullout Tests for Planar Reinforcements, *Journal of Geotechnical Engineering*, Vol. 121, No. 6, pp. 476-485, 1995.

Abramento, M. and Whittle, A.J. Experimental Evaluation of Pullout Analyses for Planar Reinforcements, *Journal of Geotechnical Engineering*, Vol. 121, No. 6, pp. 486-492, 1995.

ASTM Standard Method D1777-64, Standard Method for Measuring Thickness of Textile Materials, American Society for Testing Materials, 1975.

ASTM Standard Method D4595-86, Standard Method for Tensile Properties of Geotextiles with Wide Width Strip Method, American Society for Testing Materials, 1986.

Atmatzidis, D.K. and Athanasopoulos, G.A. Sand geotextile friction angle by direct shear testing, *Proceedings of the 13th International Conference on Soil Mechanics and Foundation Engineering*, Vol. 3, pp. 1273-1278, 1994.

Baudonnel, J., Giroud, J.P. and Gourc, J.P. Experimental and Theoretical Study of Tensile Behaviour of Nonwoven Geotextiles, *Proceedings of the 2nd International Conference on Geotextiles*, Las Vegas, USA, pp. 823-828, 1982.

Bonczkiewicz, C., Christopher, B.R. and Atmatzidis, D.K. Evaluation of Soil-Reinforcement Interaction by Large Scale Pull-out Tests, *Transportation Research Record*, No. 1188, pp. 1 - 18, 1988.

Bourdeau, Y., Gourc J.P., Gotteleland, P. and Perrier, H. Pull-out Behaviour-Experimental Study, *Proceedings of the 4th International Conference on Geotextiles, Geomembranes and Related Products*, The Hague, Netherlands, pp. 800, 1990.

British Standard BS 8006 Code of practice for strengthed/reinforced soils and other fills, June, 1994 Document No. 94/104108.

Cowburn, S. An experimental investigation of cyclically, axially loaded piles in sand, M.Sc. thesis, Civil Engineering Department, University of Cape Town, 1993.

Desai, C. S. and Christian, J.T. *Numerical Methods in Geotechnical Engineering*, (McGraw-Hill Publishers, USA), 1977.

El-Fermaoui, A. and Nowatzki, E. Effect of Confining Pressure on Performance of Geotextiles in Soils, *Proceedings of the 2nd International Conference on Geotextiles*, Las Vegas, USA, pp. 799-805, 1982.

El Mogahzy, Y. E., Gowayed, Y. and Elton, D. Theory of Soil/Geotextile Interaction. *Textile Research Journal*, Vol. 64, No. 12, PP. 744-755, 1994.

Forsman, J. and Slunga, E. The Interface Friction and Anchor Capacity of Synthetic Georeinforcements, *Proceedings of the 5th International Conference on Geotextiles, Geomembranes and Related Products*, Singapore, pp. 405-410, 1994.

Fourie, A.B. and Fabian, K.J. Laboratory Determination of Clay-Geotextile Interaction, *Geotextiles and Geomembranes*, Vol. 6, pp. 275-294, 1987.

Goodman, R.E., Taylor, R.L. and Brekke, T.L. A model for the mechanics of jointed rock, *Journal of Soil Mechanics and Foundation Engineering*, pp. 99, 1973.

Heath, A., Finite Element Analysis of Axially Loaded Pile Tests, B.Sc. thesis, Civil Engineering Department, University of Cape Town, 1994.

Handel, E., Schweiger H.F. and Yeo, K.C. A simple thin layer element to model soil-geotextile interaction, *Performance of reinforced soil structures*, British Geotechnical Society, pp. 317-321, 1990.

Hohberg, J.M. and Schweiger, H.F. On the penalty behaviour of thin-layer elements, *Proceedings of the International Reinforced Soil Conference,* Glasgow, Scotland, pp. 241-248, 1990.

Hibbitt, Karlsson and Sorenson, Inc. *ABAQUS/Standard User's Manual*, Vol. 1, 1995.

Ingold, T.S. A laboratory investigation of soil geotextile interaction, *Ground Engineering*, Vol. 22, pp. 21-28, 1985.

International Geosynthetics Society, *Milestones in the History of the IGS*, Internet Web site, http://geo.rmc.ca/igs/Highlights.html, 1994.

International Geosynthetics Society Secretariat, *Recommended Desciptions of Geosynthetics*, (IGS Secretariat, South Carolina, USA), pp 6, 1996.

Jianchao L. and Victor, N.K. Application of improved zero-thickness interface element to geosynthetically reinforced soil structures, Computer methods and Advances in Geomechanics, eds. Siriwardane and Zaman, (Balkema Press, Rotterdam), pp. 1367-1370, 1994.

Jones, C.J.F.P. *Soil Reinforcement and Earth Structures*, (Butterworth Publishers, London), pp 24 - 38, 1985.

Juran, I. and Chen, C.L. Soil-Geotextile Pull-Out Interaction Properties: Testing and Interpretation. *Transportation Research Record*, No. 1188, pp. 37 - 47, 1988.

Juran, I. and Christopher, B. Laboratory Model Study of Geosynthetic Reinforced Soil Retaining Walls, *Journal of Geotechnical Engineering*, Vol. 115, No. 7, pp 905-926, 1989.

Kaytech Industrial Fabrics, *Kaymat Material Specifications*, 1995.

Kharchafi, M and Dysli, M. Study of Soil-Geotextile Interaction by an X-Ray Method. *Geotextiles and Geomembranes*, Vol. 12, pp. 307-325, 1993.

Kokkalis, A. and Papacharisis, N. A Simple Laboratory Method to Estimate the In-Soil Behaviour of Geotexitles. *Geotextiles and Geomembranes*, Vol. 8, pp. 147-157, 1989.

Lai Sang, J. Tensile behaviour of geotextiles in soils, B.Sc. thesis, Civil Engineering Department, University of Cape Town, 1995.

Leshchinsky, D. and Field, D.A. In-Soil Load Elongation, Tensile Strength and Interface Friction of Nonwoven Geotextiles. *Proceedings of Geosynthetic '87 Conference*, New Orleans, USA, pp. 238-249, 1987.

Makiuchi, K. and Miyamori, T. Mobilization of Soil-Geofabric Interface Friction. *International Geotechnical Symposium on Theory and Practice of Earth Reinforcement,* Japan, pp. 129-134, 1988.

McGown, A., Andrawes, K.Z. and Kabir,M.H. Load-Extension Testing of Geotextiles Confined In-Soil. *Proceedings of the 2nd International Conference on Geotextiles*, Las Vegas, USA, pp. 793-798, 1982.

Murray, R.T. *Fabric reinforced earth walls: development of design equations*, Transport and Road research Laboratory, Supplementary report 496, 1981

Myles, B. Assessment if Soil Fabric Friction by Means of Shear, *Proceedings of the 2nd International Conference on Geotextiles*, Las Vegas, USA, pp. 787-791, 1982.

Palmeira, E.M. and Milligan, G.W.E. Large Scale Pull-out Tests on Geotextiles and Geogrids. *Proceedings of the 4th International Conference on Geotextiles, Geomembranes and Related Products*, The Hague, Netherlands, pp. 743-746, 1990.

Rowe, R.K. and Gnanendran, C.T. Geotextile Strain in a Full Scale Test Embankment, *Geotextiles and Geomembranes*, Vol. 13, pp 781-806, 1994.

Saxena, S.K. and Budiman, J.S. Interface Response of Geotextiles. *Proceedings of the 11th International Conference on Soil Mechanics and Foundation Engineering*, Vol. 5, pp. 1801-1804, 1985.

Shrestha, S.C. and Bell, J.R. A Wide Strip Tensile Test of Geotextiles. *Proceedings of the 2nd International Conference on Geotextiles*, Las Vegas, USA, pp. 739-743, 1982.

Solomone W.G., Boutrup, E., Holtz, R.D., Kovacs, W.D. and Sulton, C.D. Fabric Reinforcement Designed Against Pull-Out. *The use of Geotextiles for Soil Improvement*, ASCE, Portland, USA, pp. 80-117, 1980.

Steward J.R. Wiliiamson and Mohney, J. *Guidelines for Use of Fabrics in Construction and Maintenance of Low-Volume Roads*. USDA Forest Service, Portland, USA, 1977.

Thaum, B. Berechnung und Dimensionierung von Erdkonrpern mit Bewehorungseinlagen aus Geokeunststoffen, *Geotechnik*, DGGT, Essen, Vol. 20, No. 2, pp. 79-90, 1997.

Tzong, W.H. and Cheng-Kuang, S. Soil-Geotextile Interaction Mechanism in Pullout Test. *Proceedings of the Geosynthetics '87 Conference*, New Orleans, USA, pp. 250-259, 1987.

Vidal, H., La Terre Armée, *Annales ITBTP*, Paris, No.'s 223-229, pp. 888-938, 1966.

Wang, A., Zhang, B. and Lihua, L. Research of Infuence of Test Conditions on the Tensile Strength of Geotextile. *Proceedings of the 4th International Conference on Geotextiles, Geomembranes and Related Products*, The Hague, Netherlands, pp. 782 , 1990.

Wu, C.S. and Lin M.J. Mechanical behaviour of geotextile under confining stress. Computer methods and Advances in Geomechanics, eds. Siriwardane and Zaman, (Balkema Press, Rotterdam), pp. 1427-1432, 1994.

Yogarajah I., and Yeo K.C. Finite Element Modelling of Pull-Out Tests with Load and Strain Measurements, *Geotextiles and Geomembranes*, Vol. 8, pp. 43-54, 1993.

Zaman, M.M., Desai, C.S. and Faruque, M.O. An Algorithm for Determining Parameters for Cap Model from Raw Laboratory Test Data. *Proceedings of the 4th International Conference on Numerical Methods in Geomechanics*, Edmonton, pp. 275-285, 1982.